COMPOSITE AND CASE STUDY ANALYSES OF THE LARGE-SCALE ENVIRONMENTS ASSOCIATED WITH WEST PACIFIC POLAR AND SUBTROPICAL VERTICAL JET SUPERPOSITION EVENTS

By

Zachary J. Handlos

A dissertation submitted in partial fulfillment of

the requirements for the degree of

Doctor of Philosophy

(Atmospheric and Oceanic Sciences)

at the

UNIVERSITY OF WISCONSIN–MADISON

2016

Date of final oral examination: 4/25/2016

The dissertation is approved by the following members of the Final Oral Committee:
Jonathan E. Martin, Professor, Atmospheric and Oceanic Sciences
Michael C. Morgan, Professor, Atmospheric and Oceanic Sciences
Matthew H. Hitchman, Professor, Atmospheric and Oceanic Sciences
Daniel J. Vimont, Associate Professor, Atmospheric and Oceanic Sciences
Samuel N. Stechmann, Associate Professor, Mathematics

ACKNOWLEDGMENTS

If you would had told me 10 years ago when I started undergraduate school at the University of Wisconsin - Madison that, in 2016, I would be walking out of this University with a B.S., M.S. and Ph.D., I would have not believed you. Words cannot describe how incredible of a journey my experience has been here. The amount of knowledge that I have acquired from all of the classes I've taken and people I've either worked with or met cannot be quantified. I wish to use this space to thank several people that played an important role throughout the last few years as I've worked on completing my dissertation. If I for some reason did not include you, you likely still played an important role somewhere throughout this process.

First, I wish to thank my advisor Professor Jonathan Martin. Working with Jon since August 2013 has been an absolute joy, as he has provided me countless insight and advice regarding the research that I discuss within this dissertation. You provided me the opportunity to not only pursue my research interests, but also allowed me to continue to teach and develop my instructional ability during this time. Most importantly, you provided me the support and confidence to re-take the Ph.D. qualifying exam and to not give up in pursuing a Ph.D. If it were not for the conversation we had after my unfortunate result the first time around in 2012, I would not have reached this point in my career. Thank you.

Second, I want to thank my Ph.D. dissertation committee (Professors Jonathan Martin, Michael Morgan, Matthew Hitchman, Daniel Vimont and Samuel Stechmann). Thank you for all of the advice that you provided throughout my dissertation research, especially for the questions and comments that intellectually challenged the philosophy behind my research. These questions helped me to think more deeply about why I was doing the research I was doing as well as how best to approach addressing my research questions critically and constructively. Lastly, thank you all for being phenomenal instructors and providing me an outstanding educational experience.

Actually, thank you to all of the faculty in the AOS department at UW-Madison, as you have all helped to make this experience the best possible for me. I want to thank Professor Larissa Back as well for providing me my first opportunity at research in graduate school and for all of her research advice throughout the completion of my M.S. degree.

I am not the strongest person when it comes to computing besides the programming skills that I have used to conduct graduate level research. Therefore, I especially want to thank Pete Pokrandt for all of his technological help, both during graduate school as well as during my undergraduate years in the AOS department. If you ever retire or leave your position, the department might crumble; that is how valuable you are to everyone here.

I also want to thank of my graduate student colleagues that I have worked with over the years. I want to especially thank Andrew Winters, Croix Christenson, Kyle Griffin and Melissa Breeden for being unbelievably fantastic friends to work and socialize with. If there was a way for us to be able to work together as a group regardless of our career paths for many more years, I would happily accept such an offer. I also want to thank the newer members of the lab group: Maria Madsen, Simran Raju, Jessica Taheri and Connor Dacey. You were all very supportive, energetic and friendly lab-mates, and I'm confident that you will all be very successful in your careers post-graduate school. Also, as a general comment for the entire lab group, I had a blast working with you all, I'm going to miss our serious research "brainstorming" sessions during our lab group meetings and during "Flick Football," "Top Cuts 2K16" and "Pass the Pigs" events.

Thank you also to all of the other graduate students from other lab groups, including (but certainly not limited to) Darren Pilcher, Alexis Ritzer, Elena Wilmont, Alex Goldstein, Sean Ridge and Lucas Gloege for all of their support as well. Without graduate student friends, I don't know how I would have survived graduate school. Thank you for all of the great memories, which includes trips to Pizza Hut Buffet, Vitense Golf, Applebee's for half-off appetizers, and many other events/places that I could list for another full paragraph.

Oh, and even though I haven't worked with these people since undergraduate school, I want to thank Croix Christenson, Ryan Collins, Sam Ahrendt, Jake Goldberg and Nick Lorenz, who were all awesome classmates throughout the advanced-level AOS courses I took junior and senior year. I don't know how we actually graduated with our degrees, especially those nights where we would watch basketball in room 1411, go to Taco Bell at 2 AM, or just simply talk about everything else besides our actual homework/lab assignments, but we figured out how to get through it and all become successful in life. Hope you are all doing well!

While not a member of my lab group, I want to thank Michael Morgan for being a great office neighbor over the last year. You have provided me so much advice regarding research, teaching and career questions that I have had, and I cannot thank you enough for this. I also had a blast being able to talk about both the topics I've listed as well as other topics related to food, current events and the importance of humans drinking milk products. I hope to meet with you often post-graduation, especially after winds and seas subside.

Arguably the most underappreciated people in the AOSS building are the academic staff. These people work very hard to keep our department in-line from an administrative perspective, helping all of the students and faculty with any logistical questions or issues that arise. I want to thank all of the office staff over the years for everything that they have done to help me make sure that my graduate school experience was as smooth as possible. Specifically, I want to thank Toni-Sumner Bebe, Sonja Johnson, Kathy Kruger, Sue Foldy, and especially Debbie Weber. Debbie, thank you for all of the help that you have provided with regards to tax form questions, health insurance issues, payroll, and everything in-between. Thank you also Debbie for all of your support and encouragement throughout graduate school as well; I will miss visiting you and your visits up to my office. I hope that you enjoy your retirement and get the chance to do the things in life that you always wanted to. If you ever want to talk about Wisconsin sporting events, feel free to contact me.

Outside of my dissertation research, I want to thank Professor Steve Ackerman, Margaret Mooney and Professor Dominique Brossard for the opportunity to pursue my recently developed interest in science education research. Also, you all provided me extensive research, teaching and career advice as well, and I am very thankful for this. I want to thank Don Gillian-Daniel from the Delta Program for all of his help and advice throughout my Delta journey; the skills that I learned through Delta were also applicable in many situations while completing my Ph.D. in Atmospheric and Oceanic Sciences.

With respect to my outreach experiences, I want to thank Professor Galen McKinley for letting me borrow the rotating tank dozens of times for outreach events. That tank is very popular, and all of the kids these days love seeing the demonstrations throughout the Madison, WI community. I want to thank Dolly Ledin as well for helping me become involved within outreach events throughout the community. As for the book groups I led on campus, I thank Lillian Tong for these opportunities as well as Fred Boehm for being a great co-facilitator with me.

Finally, I wish to thank the most supportive group of people that I know: my friends and family. I have met so many incredible people throughout my entire UW-Madison experience and have developed so many great memories with them. There are too many people for me to list in this document, but I know that if you are my friend and reading this, you know that I'm talking about you. As for my family, I want to thank my Mom, Dad and sister Amanda for always encouraging me to dream big and give everything I do the fullest effort. Thank you for everything you have done to be supportive not only throughout this process, but also throughout my life. I also want to thank my extended family members for their support; I'm pretty sure I have the best extended family ever. Furthermore, I want to thank my new family members in-law as well (Phil, Terri, Rachel, Gary, Emma, Noah); I am lucky to have married someone who has an amazing family.

This brings me to the last person I want to thank, my wife Hannah Sievers. Thank you for always being there for me, letting me talk about weather all the time (even if you are sick of hearing about it) and for supporting me through both the good and tough times over the past several years. This was not always easy for me, and even when I was really stressed out and not the most fun person to talk to, you supported me anyway. I am a very lucky man because of this, and I can't wait to start the post-graduate school chapter of my life with you.

Oh, and one word of advice for anyone who actually checked this out from the library and read this entire Acknowledgments section: I was advised after failing the Ph.D. qualifying exam the

first time several years ago that I should not consider taking the exam again, which is required in order to pursue a Ph.D. Well, that statement was inconsistent with my goals, so I didn't listen, and here I am thanking people about this dissertation that I just completed for my Ph.D. Long story short: don't give up on your dreams, and don't let anyone stop you from doing what you are most passionate about in your life.

Make sure though to take full advantage of any opportunities to accomplish your goals; you only get one shot at life. In other words, and as best summarized by Shawshank Redemption character Andy Dufresne, "I guess it comes down to a simple choice, really. Get busy living or get busy dying."

TABLE OF CONTENTS

Page

Appendix

Page

LIST OF TABLES

LIST OF FIGURES

Appendix
Figure — Page

Appendix
Figure Page

Appendix
Figure | Page

Appendix
Figure Page

Appendix
Figure | Page

Appendix
Figure Page

Appendix
Figure | Page

ABSTRACT

Though considerable research attention has been devoted to examination of the Northern Hemispheric polar and subtropical jet streams, relatively little has been directed toward understanding the circumstances that conspire to produce the relatively rare vertical superposition of these usually separate features. This dissertation investigates the structure and evolution of large-scale environments associated with jet superposition events in the northwest Pacific.

An objective identification scheme, using NCEP/NCAR Reanalysis 1 data, is employed to identify all jet superpositions in the west Pacific (30-40°N, 135-175°E) for boreal winters (DJF) between 1979/80 - 2009/10. The analysis reveals that environments conducive to west Pacific jet superposition share several large-scale features usually associated with East Asian Winter Monsoon (EAWM) northerly cold surges, including the presence of an enhanced Hadley Cell-like circulation within the jet entrance region. It is further demonstrated that several EAWM indices are statistically significantly correlated with jet superposition frequency in the west Pacific.

The life cycle of EAWM cold surges promotes interaction between tropical convection and internal jet dynamics. Low potential vorticity (PV), high θ_e tropical boundary layer air, exhausted by anomalous convection in the west Pacific lower latitudes, is advected poleward towards the equatorward side of the jet in upper tropospheric isentropic layers resulting in anomalous anticyclonic wind shear that accelerates the jet. This, along with geostrophic cold air advection in the left jet entrance region that drives the polar tropopause downward through the jet core, promotes the

development of the deep, vertical PV wall characteristic of superposed jets. West Pacific jet superpositions preferentially form within an environment favoring the aforementioned characteristics regardless of EAWM seasonal strength.

Post-superposition, it is shown that the west Pacific jet extends eastward and is associated with an upper tropospheric cyclonic (anticyclonic) anomaly in its left (right) exit region. A downstream ridge is present over northwest Canada, and within the strong EAWM environment, a wavier flow over North America is observed relative to the neutral EAWM environment. Preliminary investigation of the two weak EAWM season superpositions reveals a Kona Low type feature post-superposition. This is associated with anomalous convection reminiscent of an atmospheric river southwest of Mexico.

Chapter 1

Introduction

1.1 Polar, Subtropical and Vertically Superposed Jet Streams

Northern Hemisphere middle latitude weather is strongly governed by the position and magnitude of narrow but rapidly moving currents of tropopause-level air known as jet streams. Despite the fact that jet streams are narrow in width, their length can span the entire hemisphere. Furthermore, there are regions embedded within the jet steam, known as jet streaks, in which air accelerates, reaches a maximum wind speed, and then deaccelerates downstream of the maximum. While the definition of a jet stream is simple in concept, these features are associated with circulations that play a role in both the development of synoptic-scale weather phenomena as well as the large-scale general circulation of the atmosphere.

There are three types of jet streams that reside in the Northern Hemisphere. The subtropical jet stream (STJ) resides at lower latitudes relative to the other two jet streams. Located on the poleward side of the Hadley Cell circulation (Krishnamurti, 1961), the STJ persists in accord with angular momentum conservation. The polar jet stream (PJ) is found poleward of the STJ within the middle latitudes, residing in regions of strong lower and middle tropospheric baroclinicity in accord with thermal wind balance (Reiter, 1963). While the STJ is also associated with horizontal temperature gradients, such baroclinicity is generally weaker relative to the PJ and is confined to the upper troposphere. A third jet stream known as the Arctic jet stream resides in the higher latitudes near the North Pole (Shapiro et al., 1987; Shapiro and Keyser, 1990). This dissertation will focus on the PJ and STJ. Several decades of inquiry have been directed toward understanding the dynamics driving the maintenence of these jet streams as well as their effects on the development and propagation of weather systems. The topics of these studies range from observational studies of the jet stream (e.g., Loewe and Radok, 1950a,b; Yeh, 1950; Mohri, 1953; Defant and Taba, 1957; Krishnamurti, 1961; Riehl, 1962; Shapiro and Keyser, 1990) to theoretical considerations of the formation of jet streams and their associated ageostrophic secondary circulations (e.g., Koetswaram, 1953; Koetswaram and Parthasarathy, 1954; Newton, 1954; Sutcliffe and Bannon, 1954; Reiter, 1963; Palmén and Newton, 1969; Keyser and Shapiro, 1986; Shapiro and Keyser, 1990).

The wind speed maxima associated with the PJ and STJ are associated with strong gradients in tropopause height, which can be demonstrated from consideration of the quasi-geostrophic potential vorticity (QGPV) equation, written as

$$q = \frac{1}{f_0}\nabla^2\phi + f + \frac{\partial}{\partial p}(\frac{f_0 \partial\phi}{\sigma\partial p}) = \Lambda(\phi) + f \qquad [1.1]$$

where ϕ is geopotential, f is the coriolis parameter, f_0 is a constant, σ is the static stability parameter and Λ is the second order linear differential operator $\Lambda = \frac{1}{f_0}\nabla^2 + \frac{\partial}{\partial p}(\frac{f_0}{\sigma})\frac{\partial}{\partial p} + \frac{f_0}{\sigma}\frac{\partial^2}{\partial p^2}$ (Cunningham and Keyser, 2004). The across-flow gradient of QGPV ($\frac{\partial q}{\partial n}$) is largest where the geostrophic wind (V_g) is largest since, from (1) and assuming f is constant,

$$\frac{\partial q}{\partial n} = \Lambda(\frac{\partial\phi}{\partial n}) = \Lambda(-fV_g). \qquad [1.2]$$

Defant and Taba (1957), were among the first to recognize this physical relationship. They identified three tropopause "steps" in the Northern Hemisphere: "tropical," "subtropical" and "polar" (Fig. 1.1). Both the PJ and STJ reside where the magnitude of the meridional gradient of tropopause height is large (Fig. 1.1b, recreated from Defant and Taba, 1957). The analysis of Defant and Taba (1957) made it clear that there is often a separation in both altitude (Fig. 1.1a) and latitude (Fig. 1.1b) between the two jet species.

While relatively rare, there are instances in which both the PJ and STJ become vertically superposed to form a single jet stream entity characterized by a deep tropopause wall that is bounded by two (rather than three) tropopause steps. In this study, such an occurrence is defined as a vertical jet superposition event. An example of this "superposition" of the PJ and STJ can be seen in the North Atlantic Ocean in Fig. 1.1b as well as in the West Pacific region near Japan (Defant and Taba, 1957). It is clear that the subtropical tropopause step is essentially non-existent within these two regions, and thus a single jet separates the tropical tropopause from the polar tropopause. An unusually large horizontal gradient in tropopause height (and thus a strong wind maximum relative to the PJ and STJ as single entities), along with the presence of a deep, nearly vertical tropopause wall, are the primary structural features associated with a superposed jet.

Very few prior studies have considered jet superposition events. One of the first studies to investigate a vertically superposed jet was that of Mohri (1953), who considered such a feature in the West Pacific. Figure 1.2 shows Mohri's conceptual model summarizing how the jet superposition event during the week of 8-12 December 1953 formed and dissipated. Prior to superposition occurrence, the STJ and PJ ("J_1" and "J_2" or "J_3" respectively) are well separated meridionally, with the STJ (PJ) associated with upper (lower and middle) tropospheric baroclinicity (stage 1 of Fig. 1.2). Over time, the PJ moves equatorward and approaches the relatively stationary STJ (stage 2). Upon the PJ and STJ vertically aligning with each other, the PJ baroclinity merges with that of the STJ and the intermediate tropopause step between the tropical and polar tropopause is eliminated. At the time of jet superposition, a region of strong baroclinicity sits below the now singular vertically superposed jet, with the jet residing between the tropical and polar tropopause steps (stage 3). In the final stage (i.e., stage 4), Mohri (1953) writes that the polar air sinks and moves equatorward and "new temperate air masses occupy gradually the space between the subsiding polar air and the sloping subtropical front." In the end, the PJ and STJ once again become separate entities, and their structures are similar to those observed in stage 1.

One of the limitations of the Mohri (1953) study is that the results of this work were based on limited obserational data. Despite this, no study since Mohri (1953) has considered the investigation of jet superposition events specifically within the West Pacific. Furthermore, no study has even reconsidered such an investigation using any of the more detailed observational or reanalysis datasets now available.

During the 1960's, Reiter (1961) and Reiter (1963) mention the possibility of PJ/STJ merger via vertical superposition of one jet stream on the other, stating that the characteristics of such jets are different than that of the PJ or STJ as single features. Several years later, Reiter and Whitney (1969) conducted a case study analysis of a jet superposition event over the eastern United States (U.S.). An example of two cross sections investigating the PJ and STJ versus the PJ/STJ superposition on 20 November 1962 is shown as Fig. 1.3. The authors conclude that while the STJ in the region where the PJ and STJ approach each other appears to be located "at a present level (ca. 200 mb) normally assigned to the STJ," significant baroclinicity is present below the jet, which was not consistent with the expected confinement of this baroclinicity within the upper troposphere. The combined baroclinicity between the two jets is consistent with Mohri's observations, the only difference being the geographical region in which Reiter and Whitney (1969) investigates this phenomena.

No known studies have investigated vertical jet superposition events between the late 1960's and the 2010's. However, within this 40-year time period, a few significant middle latitude weather events investigated within the literature have occurred within large-scale enviornments where a vertical jet superposition event was likely present. For example, Hoskins and Berrisford (1988) consider a cross-section through a jet associated with a storm near the United Kingdom on 15-16 October 1987 (Fig. 1.4). It is clear that a single jet is present (Fig. 1.4a) and is associated with a PV wall that extends from 8-9 km to $\sim$ 17 km above sea level (Fig. 1.4b). These observed characteristics are similar to those of superposed jet features shown in both Christenson (2013) and Winters and Martin (2014) and to be discussed in Chapter 2. As another example, the late-January 1988 rapid cyclogenesis event along the east coast of the U.S. discussed in Shapiro and Keyser (1990) was associated with a 90 m s^{-1} "polar jet" that may have actually been a superposed jet event (not shown).

Recently, Winters and Martin (2016) consider the interaction between the internal jet dynamics and tropical convection in inducing a vertical jet superposition event during both the Nashville Flood of May 2010 as well as a significant blizzard over the mid-Atlantic region of the U.S. on 18-20 December 2009. These studies, as well as the possible association of jet superposition with significant weather in the studies discussed above, provide extensive support for the notion that jet superposition events can, at times, be associated with extreme weather events. Given the impact of extreme weather on society, understanding the frequency, magnitude and distribution of vertical jet superposition events is a worthwhile endeavor.

The first research studies to officially acknowledge and subsequently investigate the role of a jet superposition event with respect to extreme weather were that of Christenson (2013), Winters and Martin (2014) and Winters and Martin (2016). Christenson (2013) discusses the role that a West Pacific jet superposition event played with respect to the April 2011 severe weather outbreak over the southeastern U.S. The first known climatology of such events (Christenson, 2013) using an innovative objective jet identification (ID) scheme (explained in Ch. 2) found that while superpositions are extrememly rare in the Northern Hemisphere, the maximum frequency of occurrence of superpositions hemispherically occurs during boreal winter (i.e., DJF: December, January and February). These events occur primarily within three regions: 1) the West Pacific within the region of the West Pacific jet, 2) the southern continental U.S., and 3) northern Africa. Jet superposition events are most frequent in the West Pacific relative to the other two regional maxima.

Winters and Martin (2014) were the first study to discuss the role of a jet superposition during a signficant flood event - the record setting Nashville flood of May 2010. The authors show that the superposition of the PJ and STJ over the central U.S. was a result of a combination of diabatic heating via tropical convection in concert with internal jet dynamics (Fig. 1.5). Outflow associated with lower latitude convection acts to erode PV such that the tropical tropopause step increases in altitude, and the tropopause fold associated with the STJ tilts into a more vertical orientation. Subsidence as a result of internal jet dynamics eliminates the PV trough that exists between the PJ and STJ prior to superposition, helping to bring high-PV values from the stratosphere to lower altitudes as well as eliminate the subtropical tropopause step between the two jets. As a result, the final superposed jet exists along the deep PV wall characteristic of the two-step tropopause associated with a vertical jet superposition.

The recent research discussed above has improved our understanding of the distribution of jet superposition events in the Northern Hemisphere and the physical mechansims driving superpositions within the U.S. region. However, none of these studies specifically focus on investigating the physical mechanisms and/or large-scale environments conducive to PJ/STJ superposition in the West Pacific outside of Mohri's single West Pacific superposition case study. With the superposition events occurring most often within the West Pacific during boreal winter, it seems valuable to explore why this region exhibits such a maximum. Furthermore, since the West Pacific jet is associated with the large-scale circulation of the Northern Hemisphere, developing a stronger understanding of West Pacific vertical jet superposition will help to further understand this relationship.

1.2 East Asian Winter Monsoon and its Relationship to the West Pacific Jet Stream

One large-scale phenomenon that can directly influence the strength of the West Pacific jet is the East Asian Winter Monsoon (EAWM). The EAWM is a large-scale circulation boreal winter phenomenon that is strongly driven by the strength and location of the Siberian-Mongolian high (SMH) pressure system. This feature exists due to subsidence over the Tibetian Plateau along with strong radiative cooling resulting from reflection of incoming solar radiation by snow cover on the plateau back to space (Chan and Li, 2004). The presence of the SMH allows for cold air residing over Siberia to be advected equatorward on its eastern side by the system's northerly winds, inducing events known as Northerly Cold Surge Events. Such cold air can be advected as far south as the South China Sea, resulting in cold air outbreak events that have negative consequences for large population centers such as Hong Kong (Chin, 1969; Morrice, 1973; Chang et al., 1979; Chang and Lau, 1980; Chan and Li, 2004). Easterly cold surge events can also occur, though such events receive less attention relative to northerly cold surges in the literature. This is because easterly surges are more localized over the east coast of China, whereas northerly surges affect East and South China, including the South China Sea (Chan and Li, 2004).

Cold surges tied to the EAWM have been investigated extensively over the last several decades, as summarized (for example) in Boyle and Chen (1987) and Chan and Li (2004). The earliest study acknowledging the existence of any monsoon flow over eastern Asia is that of Halley (1686) with respect to the discussion of trade wind observations near the equator. Two of the earliest known studies considering cold surges associated specifically with the EAWM are Haude (1930) and Lu (1930). Figure 1.6 shows examples of cold surge "tracks" identified by Lu (1930). The majority of tracks show cold air being advected southward on the east or southeast side of the SMH.

Chin's (1969) summary of lectures presented at the Royal Observatory of Hong Kong on 24 November 1967 reviewing what was then known about EAWM cold surges represented one of the earliest comprehensive summaries of EAWM research. The author discusses the work of a few research studies that investigated the frontal structure associated with cold surges as they moved equatorward (e.g., Gherzi, 1951; Chyou, 1957; Koo et al., 1958) as well as studies that had investigated the climatological distribution of cold surge features (e.g., Lu, 1954; Cheng, 1955; Heywood, 1957). Dao (1957) performed a case-study analysis on a cold wave event associated with the breakdown of a block over Eurasia and the Atlantic region. He found that the cold air surge was associated with a significant change in the Northern Hemispheric general circulation upon breakdown of the Ural High, a poleward shift of the "westerly wind belt" (Chin, 1969) a reduction in wavenumber across the hemisphere, and finally the development of the PJ and STJ near 125°E. Hsu and Wang (1958) showed that for some cold surge events, the surge begins when the SMH is observed to exceed a mean sea level pressure of 1054 hPa.

Chin's (1969) summary also describes efforts to measure and predict cold surge events, using observed data at Hong Kong, for example, to describe cold surge events that reach as far south as the South China sea. The author writes how such cold air events are associated with "depressions" that form in eastern China and move towards Japan. Also, it is mentioned that the STJ shifts southward along with the cold surge, likely implying the movement of the West Pacific jet equatorward given the frequent presence of a singular jet in this region during boreal winter. Morrice (1973) writes a comprehensive technical report discussing properties associated with northerly and easterly cold surges, including discussion on forecasting such events within the Hong Kong region.

Chang et al. (1979) and Chang and Lau (1980) use pre-Winter Monsoon Experiment (pre-MONEX) data to investigate four December 1974 cold surge events and their relationship to large-scale phenomena within the Maritime Contient region as well as the West Pacific. Figure 1.7 shows a conceptual model from Chang et al. (1979) summarizing the role of northerly winds associated with cold surges influencing lower tropospheric convection in the West Pacific. They found that cold surge events act to enhance surface convergence within regions where tropical convection is present. This acts to further enhance the tropical convection by increasing vertical motion via surface convergence. With the enhanced convection, the local Hadley Cell circulation over the West Pacific becomes enhanced (Fig. 1.8; see Chang and Lau (1980) for more details). This, in turn, strengthens the West Pacific jet stream, as enhanced poleward flow aloft turns westerly due to the effect of the Coriolis force.

Some more recent studies have continued to focus on investigating the physical mechanisms associated with EAWM cold surge events. For example, Wu and Chan (1995) show that easterly cold surges are associated with a coastal Kelvin wave along the east coast of China. Several studies have investigated the impacts of the EAWM on the Northern Hemisphere storm track and planetary waves (e.g., Takaya and Nakamura, 2013). Shoji et al. (2014) investigated the temporal evolution of cold air outbreaks over East Asia, finding that such events account for a significant portion of cold air mass flux over the Northern Hemisphere, and that these events are strongly associated with the magnitude of the zonal pressure gradient force generated by the presence of a strong SMH and Aleutian Low.

However, relative to earlier studies on EAWM cold surge events, many recent studies have shifted the focus of EAWM research from understanding the physical mechanisms associated with the EAWM towards measuring and forecasting its strength. While this is a very difficult task given the complexity of this phenomenon, such studies attempt to measure the seasonal strength of the EAWM by constructing EAWM indices. Wang and Chen (2010) assessed the ability of 18 indices in measuring the seasonal strength of the EAWM (Table 1 of Wang et al., 2010). The authors show that the indices considered can be classified into four index categories based on how the index calculates EAWM strength. For example, one category of indices considers the magnitude of zonal wind associated with the West Pacific jet relative to other regions within East Asia and the West Pacific (e.g., Jhun and Lee, 2004). Another considers the magnitude of meridional wind in the lower troposphere within the region in which cold air surges occur (e.g., Yang et al., 2002), while a third considers differences in mean sea level pressure given the significance of the SMH and Aleutian Low. The fourth category considers 500 hPa geopotential height variations near Japan, as such a feature is common during EAWM cold surge events (e.g., Wang et al., 2009).

Using any (or a combination) of the indices from previous research, it is possible to composite boreal winter seasons into "strong" versus "weak" EAWM seasons and compare/contrast the large-scale environments present within each. This is done by Wang and Chen (2010), for example, and Fig. 1.9 shows an example of the results from such a consideration for one of the indices analyzed in their study. The figure shows, within strong EAWM seasons relative to weak seasons, greater sea level pressure in the region of the SMH and reduced sea level pressure near Japan (Fig. 1.9a), a stronger trough (i.e., negative geopotential height) near Japan at 500 hPa (Fig. 1.9b), a stronger zonal wind tied to the West Pacific jet (Fig. 1.9c), and colder air east of China (Fig. 1.9d). Other figures in Wang and Chen (2010) comparing strong and weak EAWM seasons using other indices show similar results. All of the highlighted features are consistent with what is expected during seasons where the EAWM and subsequent cold surges are stronger in magnitude. Note that the same type of composite analysis is performed in some of the index studies cited by Wang and Chen (2010). For example, Jhun and Lee (2004) arrive at similar findings in compositing strong versus weak EAWM seasons using their 300 hPa zonal wind-based index.

The EAWM and associated northerly cold surge events are components of the large-scale environment in this part of the globe and are therefore also tied to the behavior of the West Pacific jet. Therefore, it seems reasonable to consider the relationship between the EAWM and jet superposition events in the West Pacific. This has not been considered in prior research. Thus, this dissertation aims to examine the nature of the physical connection between the EAWM and West Pacific jet, particularly focusing on the role of EAWM circulation features in promoting vertical superposition of the separate PJ and STJ in the West Pacific region.

1.3 Research Goals and Questions

This dissertation is motivated by the lack of significant research regarding jet superposition events in the West Pacific, the role that the EAWM plays in influencing the West Pacific jet stream and the consequences that the West Pacific jet can have on the Northern Hemisphere large-scale circulation. The connection between jet superposition events in the Northern Hemisphere to some extreme weather events also motivates this research, because such events have a significant impact on society.

A comprehensive analysis of West Pacific vertical jet superposition events, including investigation of the life cycle of superpositions, the large-scale environments conducive to superposition, the evolution of all key features considered after superposition and their effect on the large-scale circulation of the Northern Hemisphere is presented in this dissertation. Specifically, the following research questions (RQ) will be considered:

> *RQ1: What are the large-scale environments conducive to West Pacific PJ/STJ superposition, and how does the EAWM relate to these events?*

> *RQ2: How do the large-scale environments identified in the context of RQ1 compare/contrast for West Pacific vertical jet superposition events within strong, neutral and weak EAWM environments?*

> *RQ3: How do West Pacific vertical jet superposition events and their associated large-scale environments evolve after superposition, and how does this evolution affect the large-scale circulation of the Northern Hemisphere?*

The foregoing trio of research questions will be considered by first identifying West Pacific vertical jet superposition events using an innovative jet ID scheme and then applying both composite and case-study analysis methods towards addressing RQ1-3. Chapter 2 will discuss the data and methodologies used to address all research questions. Chapter 3 will explore RQ1 via composite analysis of West Pacific vertical jet superposition events. Chapter 4 extends the investigation in Chapter 3 by considering the same superposition events partitioned based on EAWM seasonal strength. Chapter 5 investigates the evolution of West Pacific superposition and all relevant large-scale features after the time of superposition, including discussion regarding significant features that develop throughout the Northern Hemisphere. Chapter 6 summarizes the key findings pertaining to each RQ and discusses applications of this knowledge towards future research endeavors.

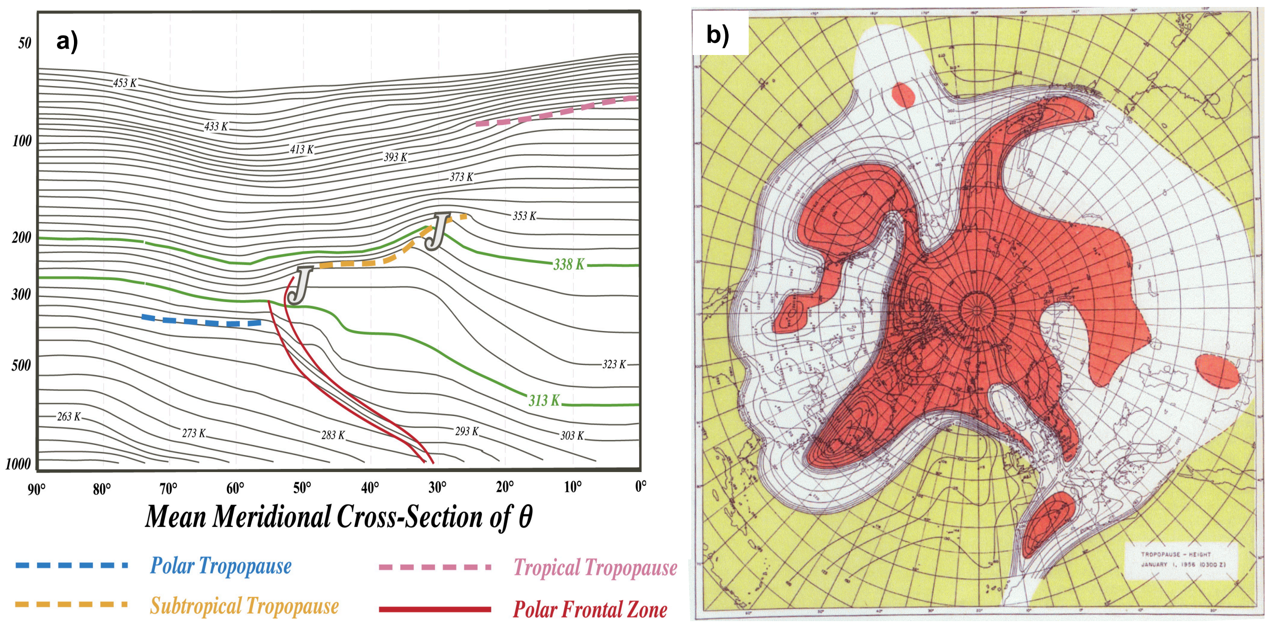

Figure 1.1 a) From Winters and Martin (2014), color-enhanced mean meridional cross section of isentropic (θ) surfaces (units K, solid black lines) along with labeled jet stream locations ("J" symbols) and the tropical, subtropical and polar tropopause steps (dashed contours, see legend at bottom of figure). The polar frontal zone is also labeled (solid red contour). b) From Defant and Taba (1957), tropopause height (hPa) over the Northern Hemisphere at 0300 UTC on 1 January 1956. The yellow regions represent the tropical tropopause height region, white regions represent the subtropical tropopause height and red regions represent the polar tropopause height. The PJ (STJ) approximately resides along the strong concentrations in isolines bordering between the red and white (yellow and white) regions.

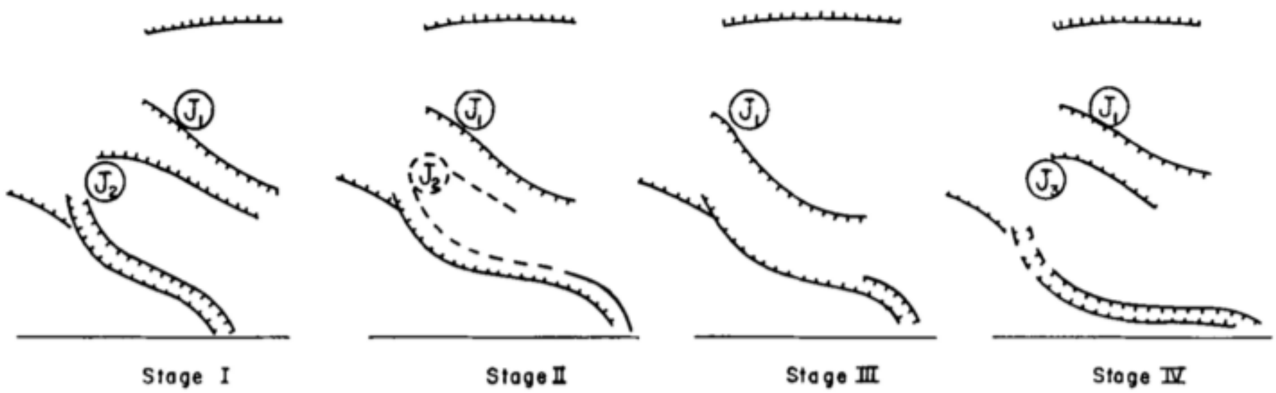

Figure 1.2 From Mohri (1953) (Figure 21 of original study): conceptual model of the development of a West Pacific vertical jet superposition event. "J_1" ("J_2 or J_3") indicates the STJ (PJ) with baroclinic regions associated with each jet marked with frontal boundaries. See text for more details.

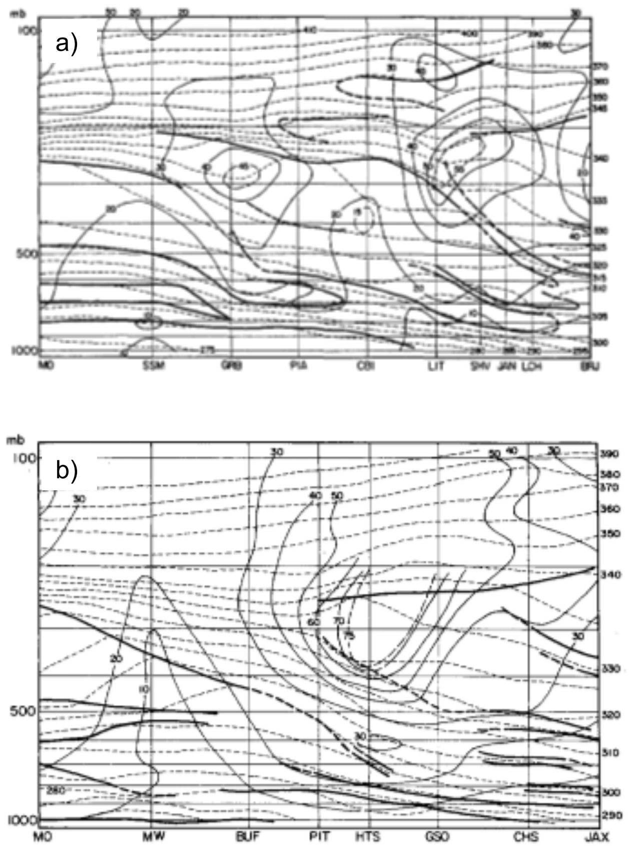

Figure 1.3 From Reiter and Whitney (1969): a) cross-section from Moosonee, Ontario through Burrwood, Louisiana on 20 November 1962 1200 UTC through separate PJ and STJ features, and b) cross-section from Moosonee, Ontario through Jacksonville, Florida on 20 November 1962 1200 UTC through a possible superposed PJ/STJ. Isotachs (thin solid lines, units m s^{-1}), potential temperature (thin dashed lines, units K), stable layers and tropopauses (thick solid lines) are plotted.

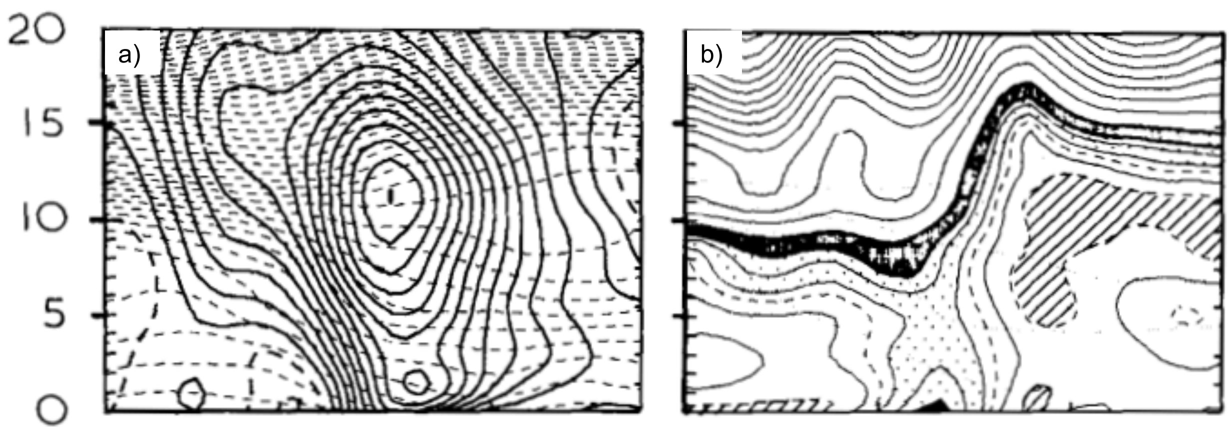

Figure 1.4 From Hoskins and Berrisford (1988): Vertical cross section through potential vertical jet superposition event associated with the 16 October 1987 storm near the United Kingdom. Plotted in each panel are a) isotachs (solid lines every 5 m s^{-1}) and isentropes (dashed lines every 5 K) and b) potential vorticity contours drawn at 0.25 (dashed), 0.5, 0.75 (dashed), 1, 1.5, 2-3 (filled in black), and $\geq$ 5 PVU (1 PVU = 10^{-6} m^2 kg^{-1} K s^{-1}) contoured every 2 PVU. Any regions $<$ 0.25 PVU are hatched, and regions between 1-2 PVU are stippled.

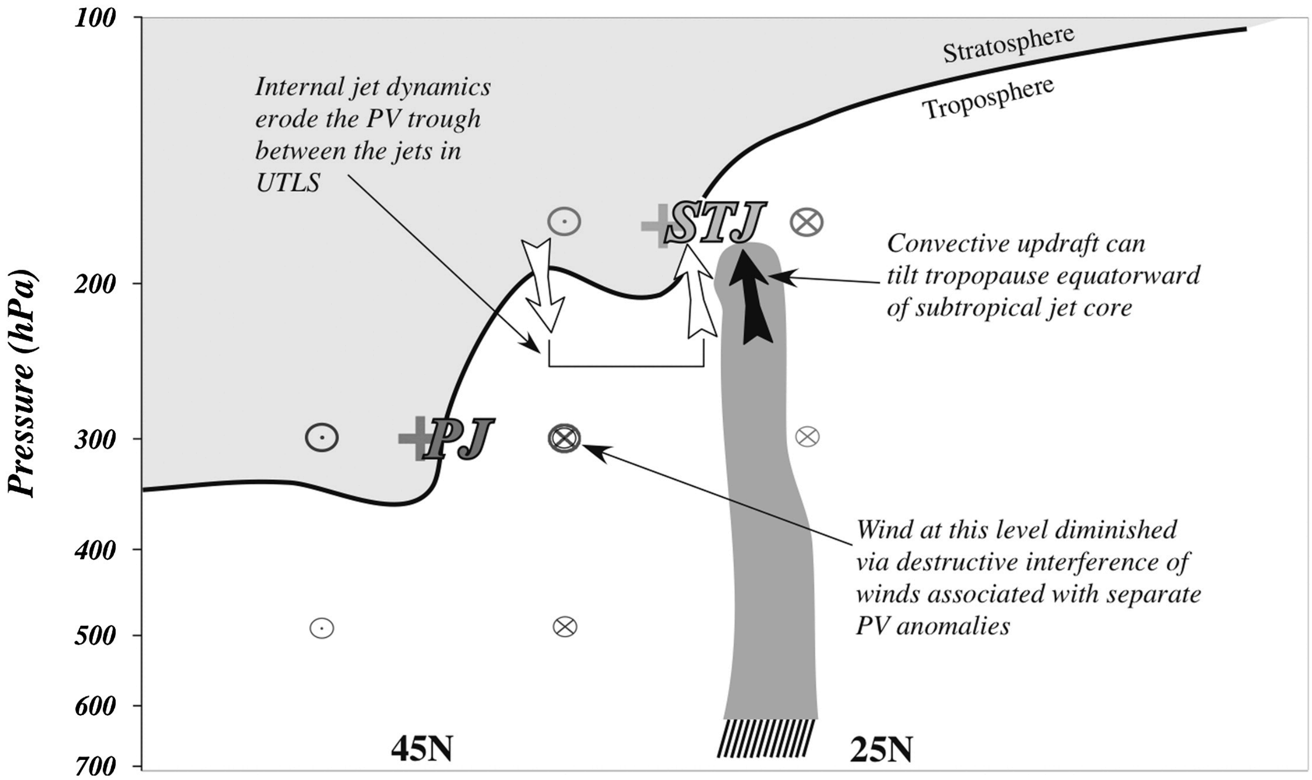

Figure 1.5 From Winters and Martin (2014): Conceptual model describing processes associated with the vertical superposition of the PJ and STJ. Marked on this model are the tropopause (black solid line), PJ/STJ features wind flow along the axis of each jet (circles with "X" (dot) indicate flow into (out of) the figure), convection (dark gray shaded area equatorward of the STJ), convective updraft (black arrow), and the ageostrophic secondary flow associated with the jets (white arrows). See text for details.

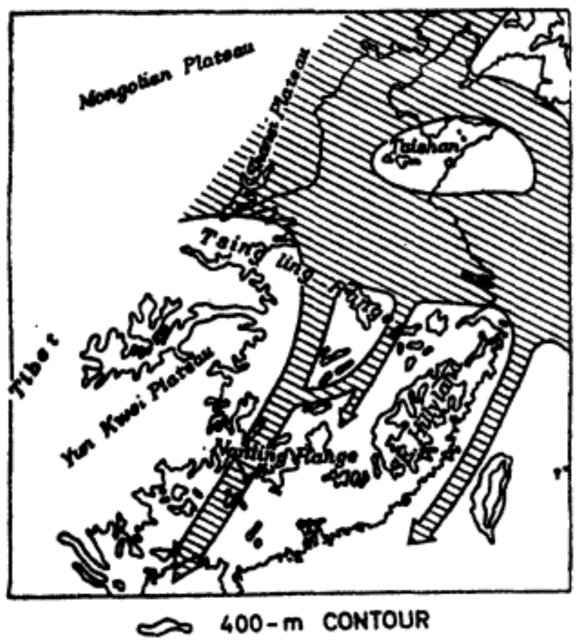

Figure 1.6 From Chin (1969) (who adopted the figure from Lu, 1930): example cold air surge tracks over eastern China.

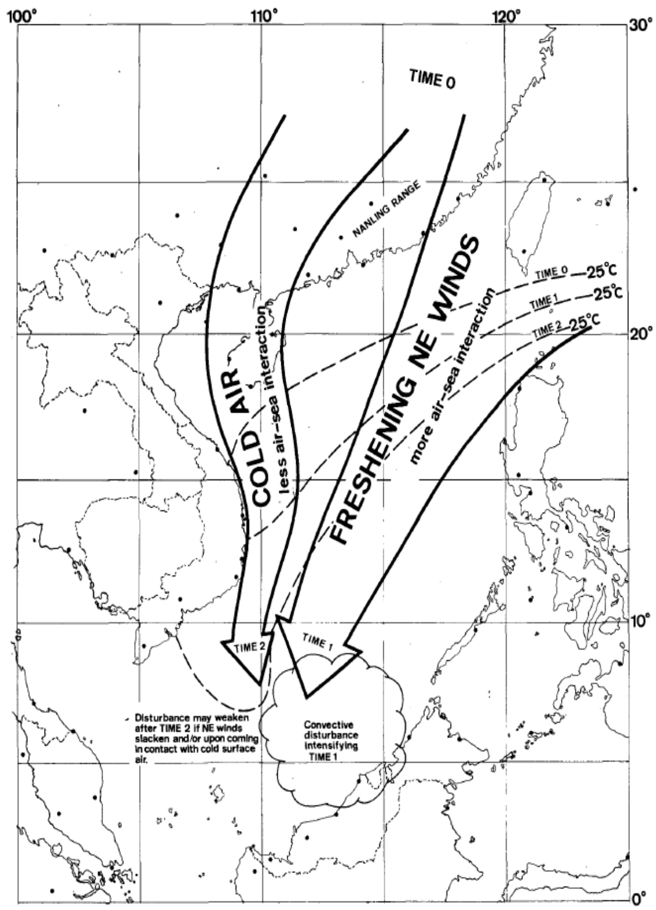

Figure 1.7 From Chang et al. (1979): Conceptual model demonstrating the role northerly winds associated with an EAWM northerly cold surge play in strengthening (and weakening) convection in the lower latitudes of the Maritime Continent region. See text for more details.

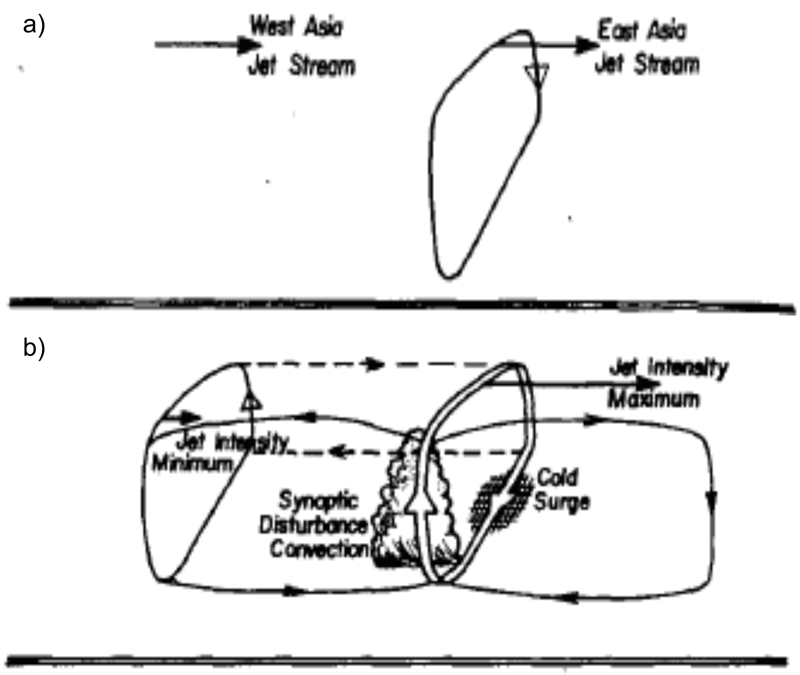

Figure 1.8 From Chang and Lau (1980): Conceptual model demonstrating the influence of an EAWM cold surge event on the local Hadley Cell circulation over the West Pacific. a) Local Hadley Cell circulation (thin solid line with white arrow) and the West and East Asian jet streams (black arrows) and b) Cold surge (shaded area) and its influence on lower latitude convection (cloud symbol), the Hadley Cell (thick white circulation), the Walker cell (thin solid lines perpendicular to Hadley Cell), and the intensity of the West and East Asian jet streams (black arrows, where longer arrows indicate faster winds). See text for details.

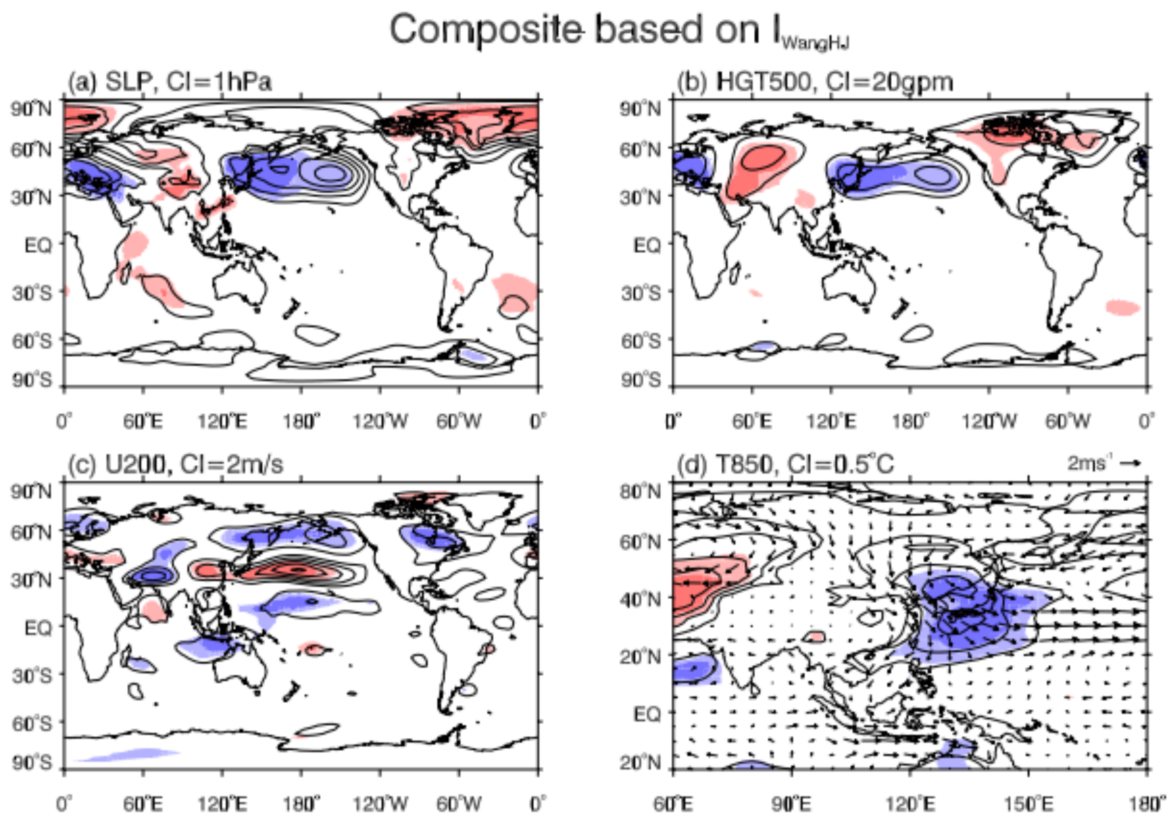

Figure 1.9 From Wang and Chen (2010): Composite strong minus weak EAWM season a) sea level pressure (contoured every 1 hPa), b) 500 hPa geopotential height (contoured every 20 gpm), c) 200 hPa zonal wind (contoured every 2 m s^{-1}), and d) 850 hPa temperature (contoured every 0.5°C) and winds (2 m s^{-1} reference arrow included). Statistically significant regions at the 95% (99%) level are shaded as light (dark) red and blue colors for positive and negative values, respectively.

Chapter 2

Data and Methodology

2.1 Data

The NCEP/NCAR Reanalysis 1 data (Kalnay et al., 1996) are employed for all variables and calculations utilized in this study. The data have a 2.5° horizontal grid spacing and 6-hourly temporal resolution. Data on both isobaric (unevenly spaced between 100-1000 hPa) and isentropic surfaces (interpolated every 5 K and examined in the 315-330 K and 340-355 K layers) are used. We focus on the months of December, January and February (DJF) for all winters 1979/80 - 2009/10 (31 winters; leap days excluded); data from the months of November and March are used for any lead/lag plots shown in later chapters for cases in which the dates are close to the edge of our boreal winter temporal domain.

2.2 Jet Superposition Identification Scheme

The jet identification scheme used in Christenson (2013) and Winters and Martin (2014) is adopted. The scheme is described with the aid of Fig. 2.1 which illustrates aspects of two different cases over the Pacific. It is clear in Fig. 2.1a that separate PJ and STJ features are present in plan view. Figure 2.1b shows a vertical cross section through both jet cores. The polar jet core, located at approximately 300 hPa, is largely contained within the 315-330K isentropic layer while the subtropical jet core, located at approximately 200 hPa, occupies the 340-355K layer (Fig. 2.1b). Both the subtropical and polar jet cores lie at the low potential vorticity (PV) edge of the strong horizontal PV gradient that separates the upper troposphere from the lower stratosphere.

The ID scheme evaluates characteristics of the PV and wind speed distributions in each grid column. Within the 315-330K (340-355K) layer, whenever $|\nabla PV|$ within the 1-3 PVU channel exceeds or is equal to a threshold value[1] and the integrated wind speed in the 400-100 hPa layer $\geq$ 30 m s^{-1}, we identify a polar (subtropical) jet in that grid column. The occurrence of both polar and subtropical jet characteristics in a single grid column identifies a jet superposition event at that time in that grid column. An example vertical cross section through an identified jet superposition[2] (Fig. 2.1c) is shown in Fig. 2.1d. Notice the steepness of the dynamic tropopause - a nearly vertical PV wall extends from $\sim$ 550 hPa to $\sim$ 150 hPa - illustrating the leading structural characteristic of a jet superposition.

2.3 Composite of Robust Jet Superposition Cases

Figure 2.2 shows the frequency of occurrence of vertical jet superposition events over the Northern Hemisphere for boreal winters 1979/80 - 2009/10 using the objective ID scheme. A distinct maximum in these events resides over the West Pacific within the same region where the near juxtaposition of the tropical and polar tropopauses was evident in the DT57 analysis (Fig. 1.1). Though there are also local maxima in jet superposition frequency over the southern U.S. and northern Africa (Christenson, 2013), the frequency maximum in Fig. 2.2 is, by far, the largest. As stated in Chapter 1, it is this maximum (along with the lack of research on these events in the West Pacific) that motivate the investigation of West Pacific vertical jet superposition events. Specifically, superposition events that occur within the boxed region in Fig. 2.2 (30-40°N, 135-175°E), enclosing the maximum frequency of occurrence of Northern Hemisphere superposition ID frequency, are specifically to be considered.

To investigate the large-scale environments associated with the development of vertical jet superpositions in the West Pacific in general, a composite analysis of robust West Pacific superposition events is conducted. The compositing procedure starts by identifying 6-hourly times in which superpositions occur in the boxed region in Fig. 2.2. A robust vertical superposition event

[1] The threshold values are 0.64 x 10^{-2} PVU km^{-1} for both the 315-330K and 340-355K layers.

[2] Real-time identifications of the PJ, STJ, and jet superpositions using this identification scheme are available at http://marrella.aos.wisc.edu/JET/jet.html.

is identified if the following criteria are satisfied: 1) at least 7 or more vertical jet superposition ID's occur simultaneously within the interest region, 2) during the 6-hourly time period before superposition, fewer ID's occur than at the time of superposition, and 3) during the 6-hourly time period after the time of superposition, no more than the number of ID's identified at the time of superposition occur within the box. The choice of a minimum ID threshold of 7 to define "robust" superposition events is motivated by the fact that such events are above the 99^{th} percentile of all 6-hourly times we consider (Table 2.1).

After identifying all 6-hourly times meeting the above requirements, meteorological quantities of interest are averaged over all cases identified in this analysis to construct composite maps of robust West Pacific superposition events. Anomalous or standardized anomalous quantities of interest are constructed as follows:

$$X_{std.anom.} = \frac{X_{supj} - X_{climo}}{X_{stdclimo}} \qquad [2.1]$$

where $X_{std.anom.}$ is the standardized anomalous variable for a superposition event, X_{supj} is the variable measured at the point of interest at the time of the vertical jet superposition event, X_{climo} is the climatological value of the variable[3], and $X_{stdclimo}$ is the standard deviation of the 31-winter climatology of variable X. Composite maps of such quantities are then analyzed.

From this composite analysis methodology, 44 6-hourly robust jet superposition cases are identified (Table 2.2). Chapter 3 discusses the results of this composite analysis, focusing on the large-scale features present at the time of composite jet superposition (T = 0) as well as the evolution of the large-scale environments present at times 72, 48 and 24 hours prior to jet superposition (i.e., T-n, where $1 \leq$ n ≤ 3 represents days after time of composite jet superposition occurrence). Since it will be shown in Chapter 3 that the frequency of occurrence of West Pacific vertical jet superposition events is strongly correlated to the seasonal strength of the EAWM, Chapter 4 repeats the analysis of Chapter 3 after partitioning the robust superposition events into cases occurring in

[3]The climatological value of X is the 31 winter average (i.e., 1979/80 - 2009/10) of variable X for that specific 6-hourly time in the reanalysis. For example, if a robust superposition occurred on 0000 UTC 14 February 2008, X_{climo} would be the 31 winter average of variable X at 0000 UTC 14 February.

strong, neutral and weak EAWM seasons. Differences in the large-scale environments for robust jet superposition cases within each of these EAWM seasonal environments are explored via composite and case-study analysis. Finally, in order to explore connections between West Pacific vertical jet superposition events and their relationship to the large-scale flow of the Northern Hemisphere, Chapter 5 explores the evolution of West Pacific jet superpositions and their associated large-scale environments after time of jet superposition occurrence (i.e., times T+n, where $n > 0$).

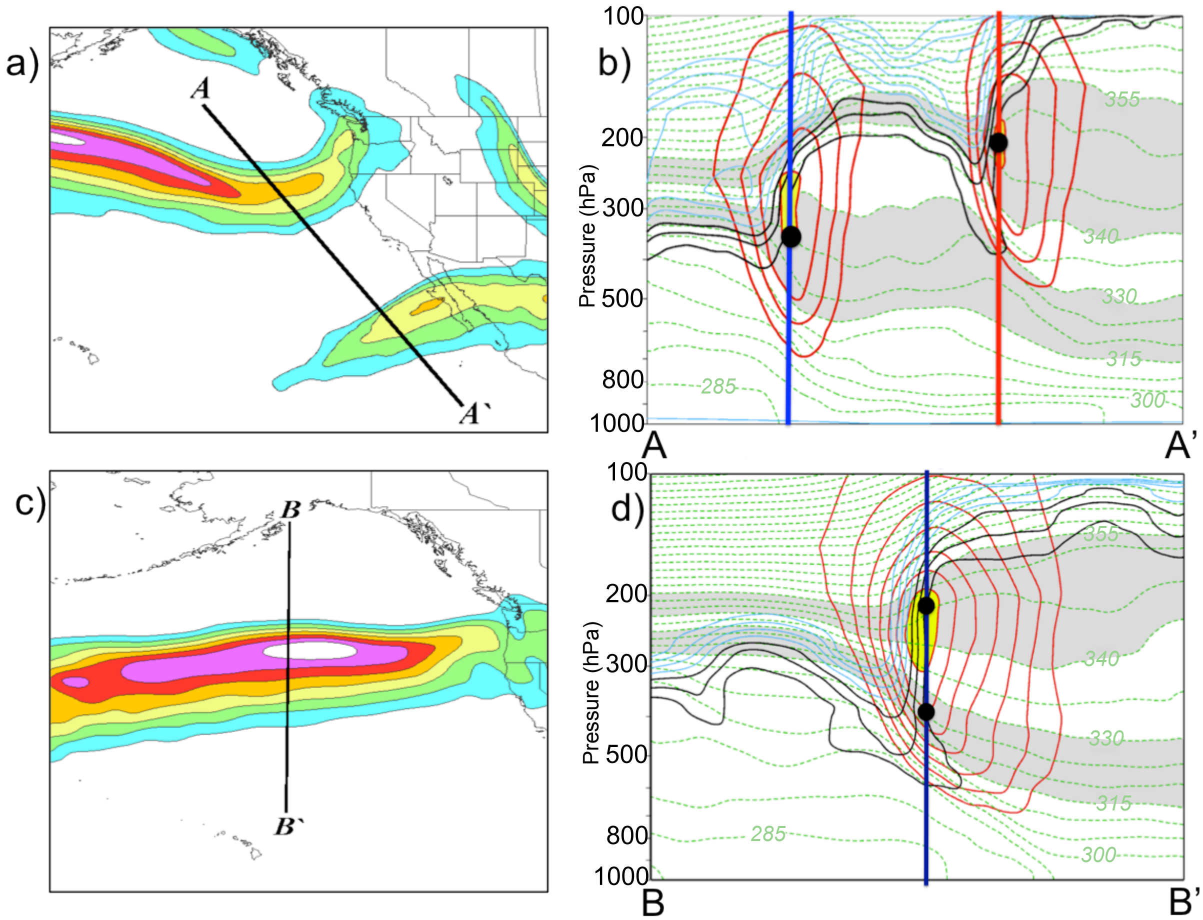

Figure 2.1 From Winters and Martin (2014): a) 300-hPa isotachs shaded every 10 m s^{1} starting at 30 m s^{1} showing separate polar and subtropical jets near the west coast of the U.S. at 0000 UTC 27 April 2010. b) Cross section A-A through both the polar and subtropical jet cores from panel a) with 1-, 2-, and 3-PVU surfaces contoured in black, 4-, 5-, 6-, 7-, 8-, and 9-PVU surfaces contoured in light blue, potential temperature contoured every 5 K in dashed green, and isotachs (red) every 10 m s^{1} starting at 30 m s^{1}. The PJ and STJ jet cores are shaded in yellow and the 315-330 and 340-355K isentropic layers (i.e., PJ and STJ isentropic layers, respectively), are shaded in grey. The blue (red) lines through a grid column with a black dot repesent the identification of a polar (subtropical) jet. c) Same as panel a) but for a vertical jet superposition event at 0000 UTC 24 Oct 2010. d) Same as panel b) but for the cross section B-B in panel c), with the PJ and STJ identifications (black dots) occurring within the same grid column indicating a jet superposition.

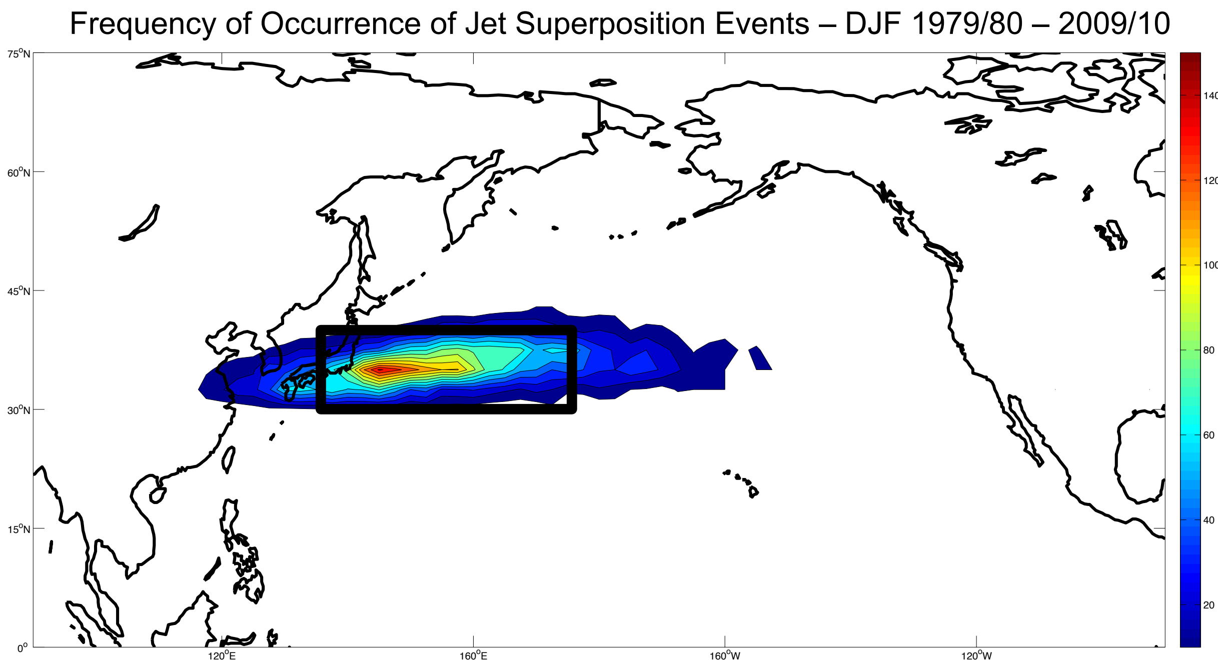

Figure 2.2 Frequency of occurrence of vertical jet superposition events over the Pacific Ocean in the Northern Hemisphere during boreal winters 1979/80 - 2009/10. The black box region represents the region of interest in our study.

Table 2.1 Number of 6-hourly times where "X" number of vertical jet superposition ID's are found in the West Pacific region of interest (boxed in Figure 2.2), where "X" is the value in column 1 of this table.

X	Number of Times with X ID's	Percent of 6-hourly times with X or more ID's
1	1451	13.0%
2	862	7.72%
3	532	4.77%
4	309	2.77%
5	184	1.65%
6	114	1.02%
7	66	0.591%
8	36	0.323%
9	22	0.197%
10	13	0.117%

Table 2.2 List of 44 robust West Pacific vertical jet superposition events considered thoughout all research studies presented.

Robust Event Date/Time	Robust Event Date/Time
07 February 1980 (0000 UTC)	14 February 1999 (1200 UTC)
29 December 1980 (0600 UTC)	23 December 1999 (0000 UTC)
11 January 1981 (0600 UTC)	31 January 2000 (0600 UTC)
29 January 1981 (1200 UTC)	16 February 2000 (1200 UTC)
14 December 1981 (1800 UTC)	17 February 2000 (0000 UTC)
15 December 1981 (1800 UTC)	11 December 2000 (0600 UTC)
04 February 1987 (0600 UTC)	04 January 2001 (0000 UTC)
10 January 1988 (0000 UTC)	04 January 2001 (1200 UTC)
23 February 1991 (1200 UTC)	15 January 2001 (0000 UTC)
24 February 1991 (1800 UTC)	15 January 2001 (1200 UTC)
25 February 1991 (1200 UTC)	16 January 2001 (0000 UTC)
24 February 1993 (1800 UTC)	19 February 2002 (1800 UTC)
25 December 1995 (0000 UTC)	21 December 2003 (0000 UTC)
25 December 1995 (1800 UTC)	26 December 2003 (1800 UTC)
01 February 1996 (0000 UTC)	07 February 2004 (0600 UTC)
02 February 1996 (1200 UTC)	27 December 2005 (1800 UTC)
01 December 1996 (0000 UTC)	10 January 2007 (0000 UTC)
01 December 1996 (1200 UTC)	15 February 2008 (0000 UTC)
02 December 1996 (0000 UTC)	16 February 2008 (0000 UTC)
09 January 1999 (1200 UTC)	16 February 2008 (1800 UTC)
12 January 1999 (1200 UTC)	08 January 2010 (1200 UTC)
13 February 1999 (0000 UTC)	15 January 2010 (1200 UTC)

Chapter 3

Composite Environments Conducive to Polar/Subtropical West Pacific Jet Superposition

3.1 Introduction

Recall from Chapter 1, that very few research studies have investigated vertical jet superposition events in the Northern Hemisphere, with only one such study (to the author's knowledge) even considering such an event in the West Pacific (Mohri, 1953). While Mohri (1953) developed a conceptual model summarizing the genesis and decay of a West Pacific jet superposition event, this model is based on a single case study using the quite limited observational data available at the time. Therefore, it is worthwhile to revisit West Pacific jet superposition events given the available contemporary reanalysis data products available. Furthermore, as with any atmospheric phenomena, each superposition event is likely to differ in some way from all others given the spatio-temporal variability of the PJ and STJ features in the West Pacific. Thus, in order to develop an understanding of West Pacific superpositions overall (rather than a single case), a goal of the research in this chapter is to investigate multiple jet superposition events rather than single cases to develop a more extensive and accurate conceptual model of the formation of jet superpositions in this region.

The composite analysis methods outlined in Section 2.3 will be used for this investigation. The remainder of this chapter is organized as follows: Section 3.2 focuses on discussion of features that are associated with West Pacific vertical jet superpositions. In Section 3.3, the evolution of those synoptic features and how their interactions lead to jet superposition is discussed. A summary and discussion of the results are offered in Section 3.4.

3.2 Results

3.2.1 *Large-Scale Environments Associated with Composite Vertical Jet Superposition*

Figure 3.1 shows various standardized anomalous quantities that characterize the environment associated with jet superpositions. The composite analysis reveals several key features that are also present during East Asian Winter Monsoon (EAWM) northerly cold surge events in the West Pacific during boreal winter. The $\vec{v}_{250,std.anom}$ in Fig. 3.1a shows a very strong West Pacific jet stream relative to climatology, with maximum wind speed in the jet core (located $\sim$ 160°E longitude) reaching speeds $\geq$ 90 m s^{-1}. Such speeds in the composite jet core exceed climatology by greater than 1.5σ while flanking anomalies north and south of the jet core are more than 1σ below climatology. This implies that the composite vertically superposed jet is not only faster but also narrower than the climatological West Pacific jet.

Figure 3.1b shows standardized anomalous geopotential height at 250 hPa ($\phi_{250,std.anom}$). An anomalous ϕ maximum (minimum) is present on the anticyclonic (cyclonic) shear side of the composite jet. There is also an anomalous ϕ maximum of $\geq$ 0.5σ in northern Russia. At 500 hPa (Fig. 3.1c), an anomalous trough feature resides just to the east of Japan, with $\phi_{500,std.anom.} <$ -1σ. An anomalous anticyclonic feature in northern Russia exists at this level as well. An anomalous maximum in 500 hPa ϕ also exists to the southeast of the trough (though it does not exceed 0.5σ).

Lastly, Fig. 3.1d shows 925 hPa standardized anomalous temperature ($T_{925,std.anom.}$). The combination of anomalous cold air and anomalous northerly winds over the East and South China Sea regions suggests that anomalous cold air advection is occurring there. Anomalously warm temperatures are present on the eastern side of the anomalous cyclonic flow to the east of the "northerly cold surge" feature.

3.2.2 *Frequency of Occurrence of EAWM-Like Features from Composite Maps*

One of the disadvantages of performing a composite analysis is that large-scale synoptic features prominent within individual cases may be smoothed out within composite results. Alternatively, a large magnitude feature appearing in a single case (or even a few cases) can exact an undue influence in the resulting composite. In order to minimize any associated misinterpretation of the composite results, the number of times at which, for each grid point, values of the standardized variables in Fig. 3.1 were greater than or less than 0.5σ from the mean were determined. That number was converted to a percentage of the 44 events in the composite. The results of this analysis are shown in Fig. 3.2.

Figure 3.2a shows that within the core of the composite jet (Fig. 3.1a), $\geq$ 90% of the superposition events have $|\vec{u}_{250,std.anom.}| \geq 0.5\sigma$, with $\geq 70\%$ of cases exhibiting $|\vec{u}_{250,std.anom.}| \leq$ -0.5σ in the flanking regions of reduced wind speed illustrated in Fig. 3.1a. Figure 3.2b shows that for $\geq$ 50% of superposition cases, many of the grid points on the anticyclonic shear side of the composite jet are associated with $\phi_{250,std.anom.} \geq 0.5\sigma$. At the center of this feature, $\geq 80\%$ of cases meet this criterion. The minimum in $\phi_{250,std.anom.}$ ($\leq$ -0.5σ) near Japan is equally present in as many as 70-80% of cases. Within the region where the composite trough feature at 500 hPa is present, $\phi_{500hPa} \leq$ -0.5σ for $\geq$ 80-90% of superposition cases (Fig. 3.2c). This feature is present more consistently relative to the upper-tropospheric ridge and trough features indicated by $\phi_{250,std.anom.}$ in Fig. 3.2b. Interestingly, the anomamlous geopotential height feature in the mid- to upper troposphere over northern Russia is only present within $\geq$ 50-60% of the cases within a very localized region northeast (east) of Lake Baikal at 250 hPa (500 hPa).

As for the lower tropospheric "northerly cold surge" feature, Fig. 3.2d shows that in the East and South China Sea regions, $T_{925hPa} \leq$ -0.5σ for $\geq$ 80-90% of the superposition cases. Furthermore, the frequency of occurrence of $v_{925,std.anom.}$ in this region is $\leq$ -0.5σ for $\geq$ 50-80% of cases or greater (not shown). Thus, it is clear that the features highlighted in Fig. 3.1 are quite common elements of the 44 cases that comprise the composite jet superposition (Fig. 3.2). Accordingly, we conclude that the majority of cases constituting the composite are associated with a cold surge feature east off the coast of China. The implications of the association of such events with this cold surge are discussed in the next subsection.

3.2.3 *East Asian Winter Monsoon Cold Surges and Jet Superpositions*

As discussed in Chapter 1, the EAWM is a boreal winter large-scale circulation phenomenon that is strongly a function of the strength of the Siberian-Mongolian surface high (SMH) pressure system (Chan and Li, 2004). Northerly cold surge events associated with the SMH occur on its eastern side, as the northerly winds associated with the SMH advect cold air as far south as the South China Sea region, leading to significant cold air outbreak events (Chin, 1969; Morrice, 1973; Chang et al., 1979; Chang and Lau, 1980; Chan and Li, 2004). A recent study by Wang and Chen (2014) utilizes a seasonal EAWM index based on normalized mean sea level pressure (MSLP) over Siberia, the North Pacific Ocean and the Maritime Continent to determine large-scale features that are associated with strong and weak EAWM winters. In their Figure 3, they showed that strong (weak) EAWM winters are associated with negative (positive) 500 hPa ϕ anomalies east of Japan, stronger (weaker) 200 hPa zonal winds near the jet entrance region of the West Pacific jet, and anomalous northerly (southerly) wind at 850 hPa. The composite West Pacific jet superposition is also characterized by a strong wind speed along with a minimum in ϕ_{500} over Japan and anomalous northerly winds in the lower troposphere. Other studies such as Jhun and Lee (2004) and Wang and Chen (2010), using other EAWM indices, show that strong EAWM winters are characterized by the presence of similar large-scale features. Additionally, Lee et al. (2010) show that the subtropical Pacific jet is stronger (weaker) during strong (weak) EAWM winters.

The studies described above in conjunction with the results of the composite analysis presented thus far suggest that West Pacific vertical jet superposition events may be a component of the large-scale circulation associated with EAWM northerly cold surge events. To further explore this possible relationship, the time series of total number of cold season superposition ID's in the box are compared to time series of several EAWM indices used in previous studies (Fig. 3.3). Four indices are selected from the list of 18 considered by Wang and Chen (2010). The EAWM index from Wang and Chen (2014) is also correlated with ID frequency of occurrence.

Figure 3.3 shows that the time series of the total number of West Pacific superposition ID's is similar to that of the various EAWM indices plotted. For the u_{300} index (Jhun and Lee, 2004), the number of superposition events increases with increased zonal wind speed. The region where the data was averaged is where the West Pacific jet in boreal winter frequently resides, implying a stronger (weaker) West Pacific jet magnitude during strong (weak) EAWM winters. Since a vertically superposed jet is associated with anomalously higher wind speed (Fig. 3.1a), the increase (decrease) in jet superposition ID's during strong (weak) EAWM winters is consistent with the composite results.

A negative correlation exists between ID counts and the Wang et al. (2009) EAWM index (based on using the first principal component extracted from a principal component analysis on ϕ_{500}), where negative (positive) index values indicate strong (weak) EAWM winters. The correlation implies more (less) jet superposition ID's with lower (higher) geopotential heights in the West Pacific region where mid-tropospheric trough features develop and progress north of the location of the composite jet. Given that an anomalous 500 hPa trough is observed north of the composite jet (Fig. 3.1c), the presence of anomalously negative ϕ_{500} values in this region during seasons with more jet superposition events in the West Pacific is in line with the composite environment at 500 hPa.

There is a negative correlation between ID counts and the v_{850} index (Yang et al., 2002), indicating that a stronger northerly wind is associated with a higher superposition ID frequency of occurrence and vice versa. Stronger northerly (southerly) winds imply a stronger (weaker) cold surge event pattern at 850 hPa and are thus associated with strong (weak) EAWM seasons. Given that a cold anomaly associated with composite anomalous northerly winds is observed in our composite analysis at 925 hPa (Fig. 3.1a) as well as at 850 hPa (not shown), the Fig. 3.1d result supports the correlation between jet superposition ID's and the Yang et al. (2002) index.

Finally, a positive corrleation exists between the normalized MSLP index (Wang and Chen, 2014) and superposition ID counts. Strong (weak) EAWM winters have been shown to be associated with a stronger gradient in MSLP between the Siberian High and Aleutian Low. Since the composite illustrates a strong MSLP gradient between the approximate location of the SMH and

Aleutian Low (not shown), the observation of higher (lower) jet superposition ID counts in the West Pacific with a higher (lower) index value is consistent with the composite results.

All correlations are statistically significant at least at the 95% confidence level. The v_{850} and normalized MSLP indices (i.e., Yang et al. (2002) and Wang and Chen (2014), respectively) are both significant at the 99% confidence level. In all cases, the sign of the correlation is such that more vertical jet superposition counts occur during stronger EAWM winters, and vice versa. Based on these simple correlations, we find a robust statistical relationship between the frequency of West Pacific superposition events and the strength of the EAWM.

3.2.4 *Composite Cross Section Results*

The compositing methodology is next extended to the construction of composite cross-sections that illuminate the vertical structure associated with West Pacific jet composite superposition. Figure 3.4 shows both the climatological (Fig. 3.4a) and the superposition composite (Fig. 3.4b) vertical cross section along 155°E (line C-C' in Fig. 3.1a) approximately through the composite jet core. Both the climatological and composite cross-sections are characterized by a "two-step" tropopause, which is not surprising given that the West Pacific is typically associated with the singular West Pacific jet. However, note that the composite cross section exhibits a deep tropopause wall stretching from $\sim$ 500 to 150 hPa and a jet core at $\sim$ 250 hPa. This PV "wall" is much stronger in magnitude (i.e., $|\nabla PV|$) and more vertically oriented in the composite superposition environment relative to climatology, as indicated by the region of negative (positive) anomalous PV located both equatorward (poleward) of and above (below) the composite jet core (Fig. 3.4b). The negative (positive) anomalous PV is associated with anomalously weak (strong) static stability on the equatorward (poleward) side of the composite jet within the STJ (PJ) isentropic layer (i.e., 340-355K and 315-330K, respectively). Finally, the jet core has a stronger wind speed maximum in the superposed composite than the climatology; this along with the enhanced "PV wall" are features characteristic of a vertical jet superposition (Fig. 2.1).

Since vertical jet superposition events in the West Pacific appear to be associated with strong EAWM winters and cold surges, cross sections of the composite jet entrance region circulation

($120^{\circ}E$ longitude) were considered in order to determine whether or not the jet entrance region circulation is enhanced relative to climatology (Fig. 3.5). The analysis is motivated by observational studies such as Chang et al. (1979), Chang and Lau (1980), Wu and Chan (1997) and Yen and Chen (2002) that show an enhancement of the West Pacific jet as well as the "local Hadley Cell circulation" spanning the Maritime Continent and East China regions during EAWM cold surge events. An enhanced jet entrance region circulation should be characterized by enhanced rising (sinking) motions equatorward (poleward) of the composite jet, with enhanced upper-tropospheric divergence (convergence) and vice versa at the surface.

Figure 3.5a shows anomalous divergence (convergence) in the upper troposphere equatorward (poleward) of the composite jet. Near the surface below each of these anomalies, the reverse occurs, with anomalous convergence (divergence) equatorward (near or poleward) of the jet. In fact, the anomalous jet entrance region circulation is displaced such that subsidence occurs beneath the jet core. Via mass continuity, anomalous upward (downward) vertical motion is present in the air column equatorward of (within) the jet core (Fig. 3.5b), representing an anomalous enhancement of the jet entrance region circulation.

While the analysis thus far reveals that the composite possesses the structural and dynamical characteristics of a superposed jet, nothing has been shown regarding the evolution of the environment that eventually produces such a jet. These issues are examined in the next section.

3.3 Lagged Composite Map Analysis of West Pacific Vertical Jet Superposition

3.3.1 *Evolution of Large-Scale Features Associated with Composite West Pacific Superposition*

To further investigate the physical mechanisms involved in the production of West Pacific jet superpositions, we construct composite maps at a series of times prior to the time of superposition (Figs. 3.6-3.8). At T-3 days, (where T is the is the date/time of jet superposition), the core of the West Pacific jet resides just south of Japan, with maximum 250 hPa wind speeds over 70 m s^{-1} (Fig. 3.6a). Unlike the composite shown in Fig. 3.1a, the anomalous flow on the anticyclonic shear side of the composite jet in Fig. 3.6a is near zero. However, an anomalous upper tropospheric anticyclone with $\phi_{250,std.anom.} > 0.5\sigma$ is present near the right jet entrance region of the composite jet while a minimum in $\phi_{250,std.anom}$ is present on the cyclonic shear side of the jet. There is also a region of $\phi_{250,std.anom.} > 0.5\sigma$ in northern Russia associated with anomalous anticyclonic flow.

At 500 hPa at this time (Fig. 3.6b), an anomalous trough-like feature is centered near Korea with $\phi_{500,std.anom.} <$ -0.5 σ. A weak anomalous anticyclonic feature near the jet entrance region is also present, and the anomalous anticyclone observed in northern Russia at 250 hPa also exhibits a magnitude $> 0.5\sigma$ at 500 hPa. At 925 hPa (Fig. 3.6c), anomalous cyclonic flow near Korea and Japan suggest (along with Figs. 3.6a and 3.6b) the barotropic nature of the trough feature at this time. Anomalous cold air associated with strong anomalous northerly winds west of Korea along with weaker anomalous northerly winds over the South China Sea are also evident. Note that anomalous anticyclonic flow is also present in northern Russia with a slight tilt eastward as altitude decreases. Finally, Fig. 3.6d shows anomalous negative OLR values over the Maritime continent, with the strongest values (in magnitude) confined to $\sim$ 10°N, 130°E. To first order, negative OLR anomalies indicate regions of high cloud tops, likely resulting from composite anomalous convection.

By T-2 days, the magnitude of the West Pacific jet has intensified with its core now centered east of southern Japan (Fig. 3.7a). The $\phi_{250,std.anom.}$ minimum along the cyclonic shear side of the composite jet has strengthened by this time, contributing to the enhancement of the composite jet speed. The composite trough at 500 hPa (Fig. 3.7b) has remained stationary while also intensifying. The anticyclonic flow southwest of the trough observed in Figs. 3.7a and 3.7b also remains stationary. The anomalous anticyclone in northern Russia in the middle-to-upper troposphere moves eastward and strengthens.

The anomalous cold air and northerly winds associated with the composite cold surge over eastern China at 925 hPa (Fig. 3.7c) have increased in magnitude while progressing southward at time T-2 days. Attendant with the advance of the lower-tropospheric cold air, the near-surface anomalous northerly winds at this time extend equatorward from the East China Sea, leading to an increase in near-surface anomalous convergence (not shown). This convergence, in turn, contributes to forcing of anomalous upward vertical motion. Given that this convergence and upward vertical motion (not shown) occurs within the region in which negative anomalous OLR is observed near Indonesia (Fig. 3.7d), it is likely that this convergence aids in sustaining this anomalous convection.

Finally, by T-1 day, the composite jet is even stronger with jet core wind speeds exceeding 90 m s^{-1} (Fig. 3.8a). A $\phi_{250,std.anom}$ maximum that was barely discernible to the south of the jet core at T-2 days has grown in strength and areal coverage by this time. The composite $\phi_{250,std.anom}$ minimum near Japan continues its slow eastward propagation, while the $\phi_{250,std.anom.}$ maximum in northern Russia shifts slightly southward and weakens. The anomalous trough feature at 500 hPa (i.e., $\phi_{500,std.anom.}$ minimum) continues to move eastward as well while the $\phi_{500,std.anom.}$ maximum in northern Russia evolves in a similar fashion to that observed at 250 hPa.

At 925 hPa, the composite cold surge feature and associated anomalous northerly winds continue to move equatorward as the anomalous cyclonic feature east of Japan continues to strengthen (Fig. 3.8c). The continued equatorward advection of cold air continues to fuel near-surface anomalous convergence which maintains anomalous upward vertical motion and the associated convection in the lower latitudes (Fig. 3.8d). Note that this convection also spreads poleward at this time. The resulting enhancement of the rising branch of the local meridional overturning circulation plays a role in enhancing the entire composite jet entrance region circulation over the West Pacific, as shown in Fig. 3.5b.

3.3.2 *Evolution of Deep, Vertical PV Wall Associated with Composite Jet*

While Figs. 3.6-3.8 provide some insight regarding the evolution of the key synoptic features in the composites, they offer little explanation of how the deep PV wall structure associated with a negative (positive) PV anomaly on the anticyclonic (cyclonic) shear side of the composite jet develops. In this subsection, the physical mechanisms that reduce (increase) the magnitude of PV equatorward (poleward) of the jet are investigated.

First, to better understand the mechanisms responsible for the reduction in Ertel PV on the equatorward side of the composite superposed jet, anomalous isentropic pressure depth within the 340-355K isentropic layer, which houses the STJ, is computed. Figures 3.9 and 3.10 show plots of anomalous potential vorticity and anomalous pressure depth within the STJ isentropic layer, respectively, with the panels ordered from T-3 days to composite superposition T = 0. Also plotted are the composite 1, 2 and 3 PVU contours as a guide to the tropopause location relative to the anomalous features of interest.

Figure 3.9 shows a negative PV anomaly that develops on the anticyclonic shear side of the composite jet core over the time period. Associated with this feature is a positive pressure depth anomaly (Fig. 3.10), which also propagates eastward and stengthens over time. The negative PV anomaly at T-3 days (Fig. 3.9a) elongates and stretches eastward along the equatorward edge of the jet by T-2 days (Fig. 3.9b). Subsequently, this feature becomes more intense and slightly more isotropic by T-1 day (Fig. 3.9c) - a trend that continues through to the time of jet superposition (Fig. 3.9d). The singular negative PV anomaly becomes more negative throughout the 72 hour period in association with an increase in magnitude of the positive pressure depth anomaly (Fig. 3.10).

The eastward propogation and strengthening of the pressure depth anomaly equatorward of the composite jet has two effects on the composite jet core that play a significant role in inducing vertical jet superposition. First, increasing the pressure depth within the STJ layer on the anticyclonic shear side of the composite jet enhances the anomalous anticyclonic flow in that layer in accord with the isentropic thermal wind equation:

$$\frac{\partial \vec{v_g}}{\partial \theta} = \frac{1}{f\rho\theta}\vec{k} \times \nabla p \qquad [3.1]$$

where ρ is the density of air. Thus, the expansion and intensification of the pressure depth anomaly on the equatorward side of the jet seen in Fig. 3.10 is associated with an anomalous anticyclonic vertical wind shear that is associated with the anomalous wind speed in the jet core.

Secondly, the coincidence of the negative PV anomalies in Fig. 3.9 with the positive perturbation pressure depths in Fig. 3.10 is a function of the fact that the air that fills the STJ layer originates in the tropical/subtropical boundary layer where θ_e is large and PV is small. To illustrate this connection, a Lagrangian perspective is adopted in order to investigate air parcel back-trajectories generated using the Air Resources Laboratory (ARL) Hybrid Single Particle Lagrangian Integrated Trajectory (HYSPLIT) model (Draxler and Hess, 1997, 1998; Draxler, 1999; Draxler and Rolph, 2015; Rolph, 2015). Specifically, back-trajectories from the location of the center of the positive pressure depth anomaly maximum at the time of composite superposition (Fig. 3.10d) for all robust superposition cases are computed.

The results of this analysis are shown in Fig. 3.11, which shows single air parcel back-trajectories in plan view for each case calculated starting at 32.5°N, 160°E. Parcel trajectories starting at altitudes of 10 and 12 km are shown in blue and red, respectively. Figure 3.11b shows the potential temperature (θ) associated with each trajectory, and Fig. 3.11c the altitude associated with each parcel over a 120-hour period. It is clear that the majority of the air parcels came from lower latitudes within the vicinity of the negative anomalous OLR observed in Figs. 3.6d, 3.7d and 3.8d, with a few back-trajectories extending westward past the prime meridian. Nearly all of the parcels remain within the middle to upper troposphere between T-5 days and T=0 days (Fig. 3.11c), tracing the anomalous anticyclonic flow observed in this region (Figs. 3.1a and 3.1b). The θ-values associated with these trajectories (Fig. 3.11b) demonstrate that the majority of air parcels remain within the STJ layer throughout the period. Several of these air parcels increased their θ value diabatically over time and ultimately ended up within the STJ layer (Figs. 3.11b and 3.11c).

Thus we suggest that upper tropospheric exhaust from convection in the South China Sea systematically exports low-PV, high-θ_e boundary layer air poleward and eastward into the STJ layer on the anticyclonic shear side of the West Pacific jet. This process results not only in an enhancement of the jet core wind speed (via anomalous geostrophic vertical shear associated with the deposition of mass on the south side of the jet), but also accounts for the importation of the negative PV anomaly on that side of the jet that contributes to steepening the PV wall characteristic of a superposed jet. Enhancement of this convection during an EAWM cold surge event thus increases the likelihood of the development of a jet superposition.

Poleward of the jet, a positive PV anomaly within the PJ isentropic layer (associated with the upper tropospheric anomalous trough) propogates eastward over the 72 hour period (Fig. 3.12). At the time of superposition, the positive PV anomaly resides on the poleward side of the composite jet to the northwest of the composite negative PV anomaly within the STJ layer. This feature is responsible for the positive PV anomaly observed in Fig. 3.4b, and therefore also plays a role in strengthening the PV wall associated with the superposed jet.

Recall from Fig. 3.5b that the jet entrance region circulation associated with the composite superposed jet is both anomalously strong and shifted equatorward. This equatorward shift places the region of anomalous subsidence directly beneath the composite jet core. Such a distribution promotes downward extrusion of stratospheric air into the upper troposphere and is dynamically related to the presence of geostrophic cold air advection in cyclonic shear (e.g., Eliassen, 1962; Shapiro, 1982; Keyser and Pecnick, 1985; Martin, 2014).

Figure 3.13 shows composite geostrophic temperature advection and vertical motion at 300 hPa (the isobaric level at which the PJ approximately resides) at times T-3, T-2 and T-1 prior to composite jet superposition (Figs. 3.13a, 3.13b and 3.13c respectively) as well as at time T = 0 (Fig. 3.13d). It is clear that geostrophic cold air advection is present on the cyclonic shear side of the jet, and the regions of composite cold air advection are associated with composite subsidence. It appears that this subsidence through the jet core in its entrance region accounts for the intensification of the positive PV anomaly and thus plays a central role in creating the anomalous positive PV feature found on the poleward side of the composite superposed jet (Fig. 3.4b). Thus, the juxtaposition of opposing PV anomalies across the composite superposed jet (portrayed in Fig. 3.4b) is a result of internal jet dynamics lowering the polar tropopause on its cyclonic shear side acting in concert with a raising of the subtropical tropopause on its anticyclonic shear side through transport of low-PV, high-θ_e boundary layer air to the STJ level via convection.

3.4 Discussion and Conclusions

An investigation of the structure and evolution of the large-scale features most commonly associated with wintertime vertical jet superposition events in the West Pacific has been presented within this chapter, focusing specifically on the composite analysis of the 44 robust vertical jet superposition events identified over 31 winters using the NCEP/NCAR Reanalysis 1 Dataset. The analysis reveals that the most robust synoptic features associated with West Pacific jet superposition events are: 1) A single, strong and latitudinally narrow composite West Pacific jet stream with a wind speed maximum of $\geq$ 90 m s^{-1}, 2) a positive/negative couplet of $\phi_{250,std.anom.}$ anomaly straddling the composite West Pacific jet, 3) an anomalous trough ($\phi_{500,std.anom.}$ minimum) on the cyclonic shear side of the composite jet and 4) a negative $T_{925,std.anom.}$ feature that resembles a "cold surge" type of event that occurs during strong EAWM winters (Fig. 3.1). All of these features are shown to occur within the majority of the superposition events selected for the analysis (Fig. 3.2).

The simultaneous presence of a strong jet along with middle tropospheric trough and cold surge anomalies are also characteristic features of EAWM cold surge events, suggesting that West Pacific jet superposition events may be preferentially tied to the cold surges of strong EAWM winters. Statistical support for this suggestion arises from the fact that several EAWM indices are significantly correlated with the number of jet superposition ID's that occur in the West Pacific analysis region (Fig. 3.3). Future work will include further exploration of this suggested relationship.

Cross sections through the composite jet core (Fig. 3.4) show a two-step tropopause and a deep PV wall through the jet; both the stronger winds and deeper PV wall relative to climatology are features characteristic of West Pacific jet superpositions (Fig. 2.1d). Also, negative (positive) anomalous Ertel PV equatorward (poleward) of the jet core is present (Fig. 3.4b) associated with weak (strong) static stability within the STJ isentropic layer (Fig. 3.4b). The jet entrance region circulation associated with the composite superposed jet is also stronger relative to climatology (Fig. 3.5), and is shifted equatorward such that subsidence occurs beneath the jet core in its entrance region.

To better understand the evolution of key synoptic features that lead to robust West Pacific jet superposition, composite maps at times 1-3 days prior to composite jet superposition were constructed. The relationship between these key features and their respective evolutions is summarized in a conceptual model (Fig. 3.14). A near surface cold air anomaly is located in northeastern China 3 days prior to composite jet superposition (Fig. 3.14a). Anomalous convection in the tropical West Pacific (cloud symbols in Fig. 3.14a) is also present. As the cold pool moves equatorward over time, the associated anomalous northerly winds (purple arrows in Fig. 3.14) produce and/or maintain anomalous near-surface convergence in the tropical West Pacific, which fuels anomalous upward vertical motions (dot over the cloud symbols in Fig. 3.14b) that sustain the anomalous convection. This leads to anomalous divergence aloft (red shaded oval with black dot in center in Fig. 3.14b). An attendant region of anomalous convergence aloft poleward and above the region of cold air is also present, associated with anomalous subsidence (blue circle with "X" in Fig. 3.14b).

High-θ_e, low-PV convective outflow on the equatorward side of the jet is advected by the anomalous anticyclonic flow east of the anomalous convection (brown arrows with "H" in Fig. 3.14c). Given that this air has $\theta_e \approx 350$ K, as it is advected poleward, it is locally exhausted within the STJ isentropic layer on the equatorward side of the composite jet (jet symbol with black contour in Fig. 3.14c). The movement of this air into the STJ layer on the anticyclonic shear side of the jet increases the anomalous pressure depth. This not only induces anomalous anticyclonic shear equatorward of the jet, enhancing the anomalous wind speed within the jet core, but also acts to reduce the PV on the equatorward side of the jet core such that the PV gradient (i.e., in the 1-3 PVU channel) associated with the jet becomes stronger and more vertically orientated (Fig. 3.14d).

On the cyclonic shear side of the composite jet, geostrophic cold air advection drives subsidence through the jet core in its entrance region, transporting high-PV air downward and thus increasing the strength of the positive PV anomaly poleward of the jet core (Figs. 3.12 and 3.13). This positive PV anomaly plays a role in increasing the magnitude of the 1-3 PVU gradient as well as in shaping the PV wall into a more vertical orientation. The increase in anomalous wind speed coincident with the development of a deep and vertical PV wall are the hallmarks of a West Pacific vertical jet superposition.

This conceptual model shows many elements of the various conceptual models and results from Chang et al. (1979), Chang and Lau (1980) and Wu and Chan (1997). For example, as shown in Figure 14 of Chang and Lau (1980), as cold air on the eastern side of the Siberian-Mongolian High (SMH) is advected equatorward, the associated strong northerly winds may lead to enhanced surface convergence in the West Pacific equatorial region. This convergence enhances upward vertical motions associated with pre-existing tropical convection in the equatorial West Pacific which, in turn, enhances the local Hadley cell circulation (Chang and Lau, 1980; Wu and Chan, 1997). Enhanced poleward flow associated with the invigorated Hadley cell induces a stronger West Pacific jet via enhanced angular momentum transport. While the results from this study focus on the the enhancement of the jet via tropical convection, a similar process is described in Rowe and Hitchman (2015) and Rowe and Hitchman (2016) regarding the enhancement (and poleward shift) of the polar jet in the mid-latitudes due to convection associated with thunderstorm activity.

In Chang et al. (1979) and Chang and Lau (1980), it was shown that EAWM cold surge events induce enhanced surface convergence in the West Pacific equatorial region, which helps to intensify the local Hadley Cell circulation in the region and subsequently enhance the speed of the West Pacific jet. While the present analysis shows an enhancement of the jet in this region due to the presence of a cold surge, it appears in Fig. 3.14 as a component of the larger scale evolution of an environment that produces a vertical superposition of the usually separate polar and subtropical jets. Those physical mechanisms associated with EAWM cold surges that strengthen the West Pacific jet appear to be vital elements in the development of West Pacific superposition events.

It is interesting to note that even within the climatological cross section through the jet core (Fig. 3.4a), only two steps in the tropopause are evident, implying that the West Pacific jet borders on a superposed structure rather frequently as suggested by Christenson (2013). The foregoing analysis, however, makes clear that, despite the temptation to consider the West Pacific jet as a single monolithic feature, only the collection of large-scale environments described in this chapter can foster production of the relatively rare vertical jet superposition. It appears that cold surge events, associated as they are with an increase in the strength of the West Pacific jet entrance region circulation, the transport of tropical boundary layer air into the STJ isentropic layer and the occurrence of geostrophic cold air advection in the jet entrance region, are key physical mechanisms that help to induce robust vertical jet superposition.

A number of additional research questions remain to be explored in the wake of the foregoing analysis. For example, while the cold surges in our composite results play a key role leading up to jet superposition, understanding the mechanisms triggering the cold surge events prior to superposition would aid in refining the developing conception of the life-cycle of West Pacific jet superpositions. It would also be beneficial to investigate the downstream effects of West Pacific jet superpositions on weather events throughout the Northern Hemisphere. For example, this topic can be investigated using the same composite analysis technique we use in our methodology, investigating times up to several days after composite jet superposition (i.e., composite analysis at times T+1, T+2, ..., T+5 days). This would provide further understanding of any relationship that these events have with other large-scale Northern Hemisphere teleconnections, and this could also help to improve understanding and prediction of significant weather events that derive from West Pacific jet superpositions. Such an analysis is considered in Chapter 5. Finally, given the significant correlation between various EAWM indices and the number of jet superposition ID's in our West Pacific interest region, it is of interest to compare and contrast the physical processes leading to jet superposition within strong versus weak EAWM seasons. This will be considered in the next chapter.

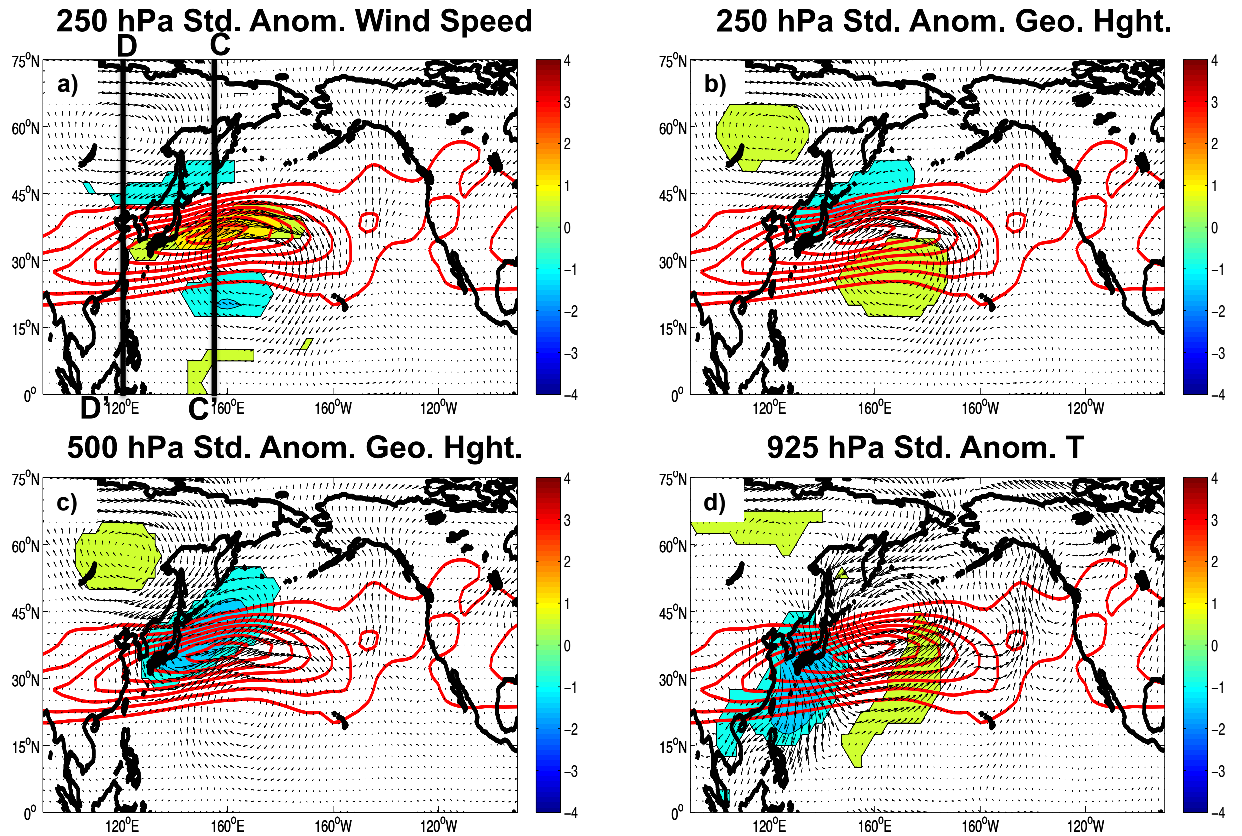

Figure 3.1 Composite maps over the North Pacific ocean. a) $\vec{v}_{250,std.anom.}$ (fill; yellow (blue) colors represent values $\geq$ ($\leq$) 0.5σ from climatology), b) $\phi_{250,std.anom.}$ (same fill pattern conventions as panel a), c) $\phi_{500,std.anom.}$ (same fill pattern conventions as panel a) and d) $T_{925,std.anom.}$ (same fill pattern conventions as panel a). On all maps, anomalous wind speeds at the level specified are plotted as vectors, and composite wind speed at 250 hPa is plotted as solid red contours every 10 m s^{-1} starting at 30 m s^{-1}. All maps are composite at the time of West Pacific vertical jet superposition. The cross section lines C-C' and D-D' are relevant for Figs. 3.4 and 3.5, respectively.

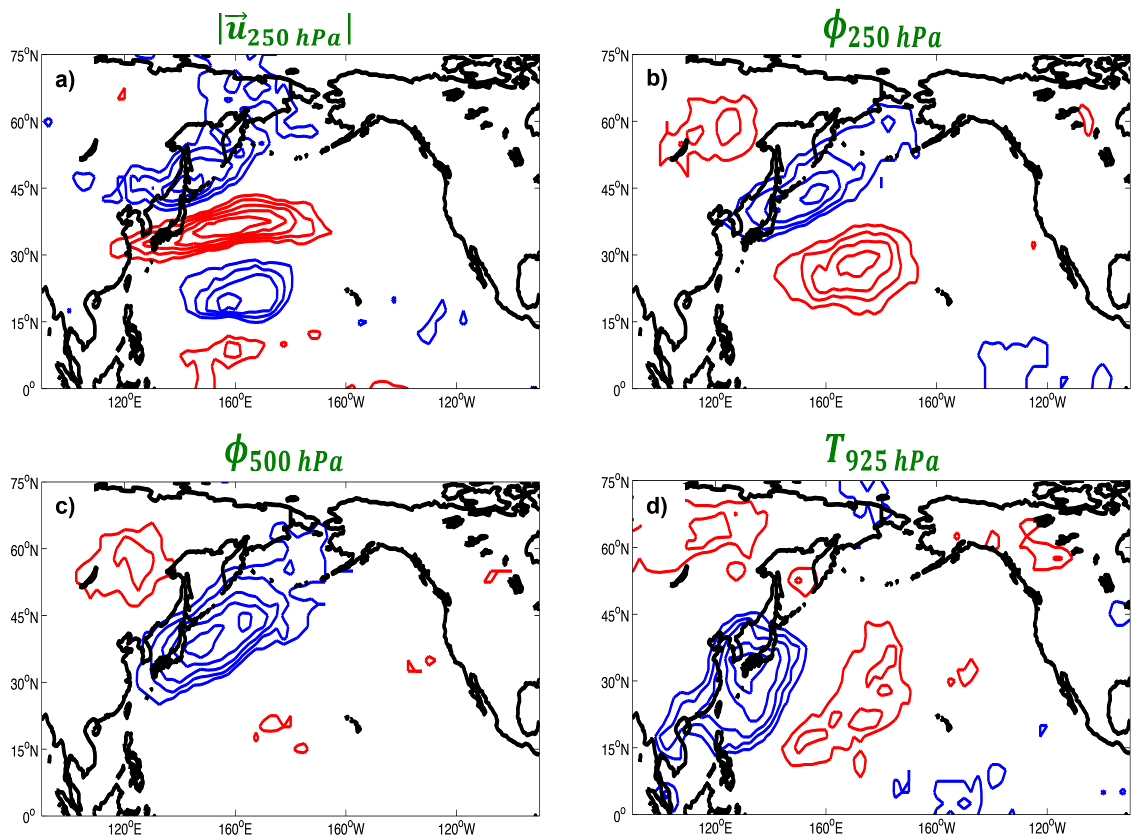

Figure 3.2 Percent occurrence of each of the standardized variables in Fig. 3.1 for all 44 cases used in the composite. Red (blue) contours indicate regions where variable of interest with standardized value $\geq 0.5\sigma$ ($\leq -0.5\sigma$) occurs in at least 50% of cases contoured every 10%. Variables in each panel match those of Fig. 3.1.

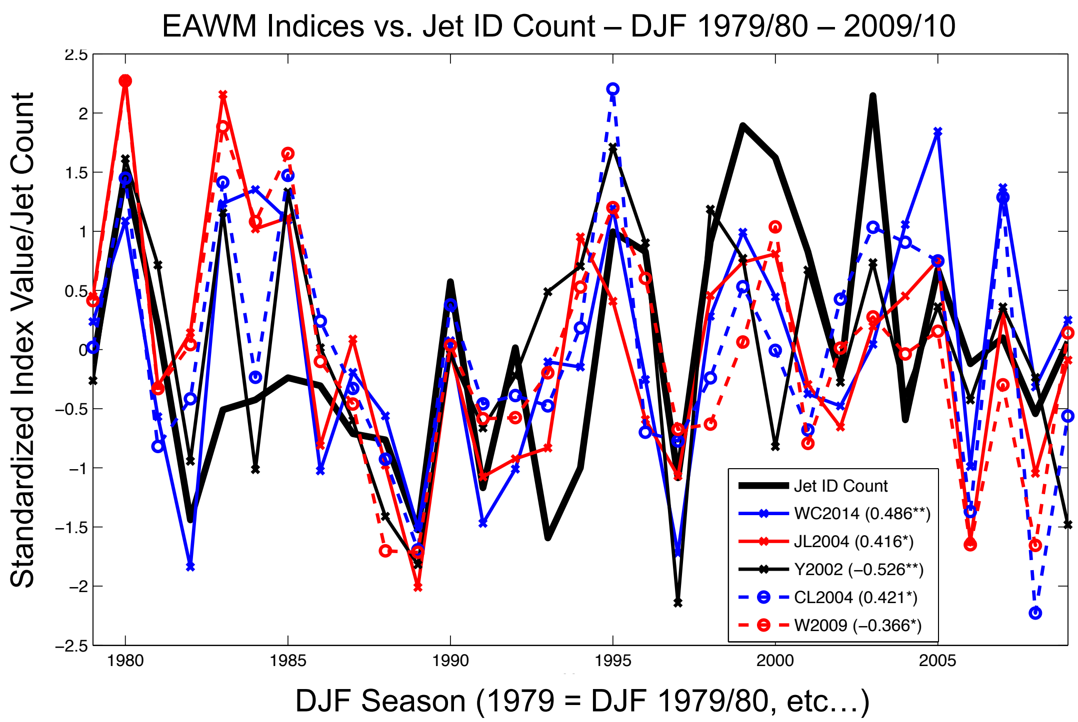

Figure 3.3 Time Series of boreal winter season standardized jet superposition ID frequency in the West Pacific interest region (thick black solid line) along with 5 standardized EAWM indices for winters 1979/80 - 2009/10. Note that for the Yang et al. (2002) and Wang et al. (2009) time series plots, the time series were multiplied by -1 so that for all indices shown, positive (negative) values imply strong (weak) EAWM winters. Also included are the correlation coefficients between each EAWMI and superposition ID frequency, where values with a single (double) asterisk are significant at the 95% (99%) level (note that it is assumed that each winter season is independent of the others such that the number of degrees of freedom = N-2, with N = 31).

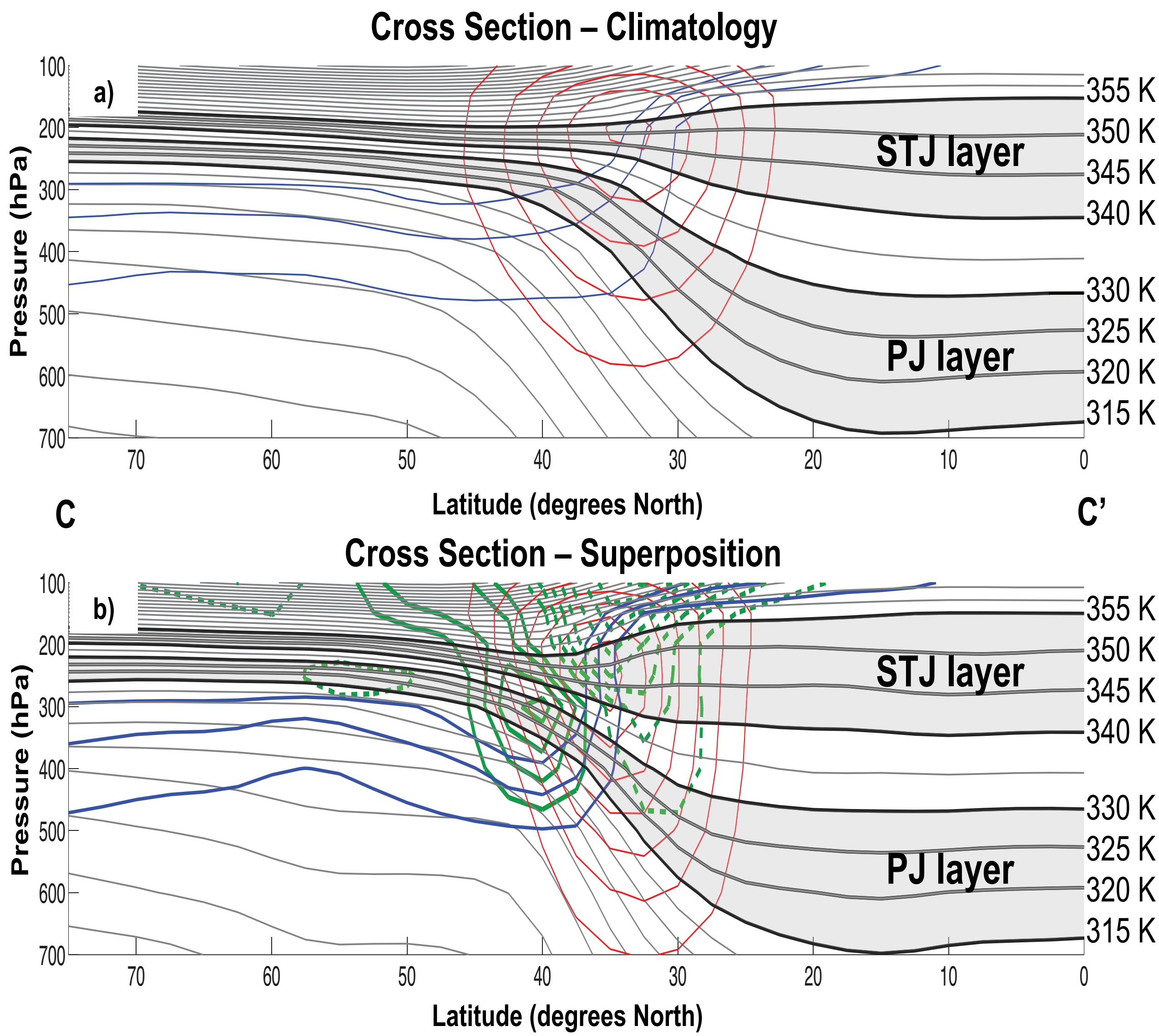

Figure 3.4 a) Climatological composite cross section taken along 155°E longitude (C-C' line from Fig. 4a) of wind speed (solid red contour; 10 m s^{-1} intervals starting at 30 m s^{-1}), isentropic surfaces (solid gray contour every 5K with levels within 315-330K and 340-355K layers in thicker black contour, labeled and shaded in light gray) and the 1-3 PVU channel in the upper troposphere (solid blue contour; units PVU). b) Same as Fig. 3.4a but for the composite superposition data, including anomalous Ertel PV (solid (dashed) green contour every 0.5 PVU starting at + (-) 0.5 PVU). Note that the climatological composite cross section is computed by averaging together the climatological data for all 44 dates/times considered in this study, with the climatology for each date/time being the 31-year average at that particular time.

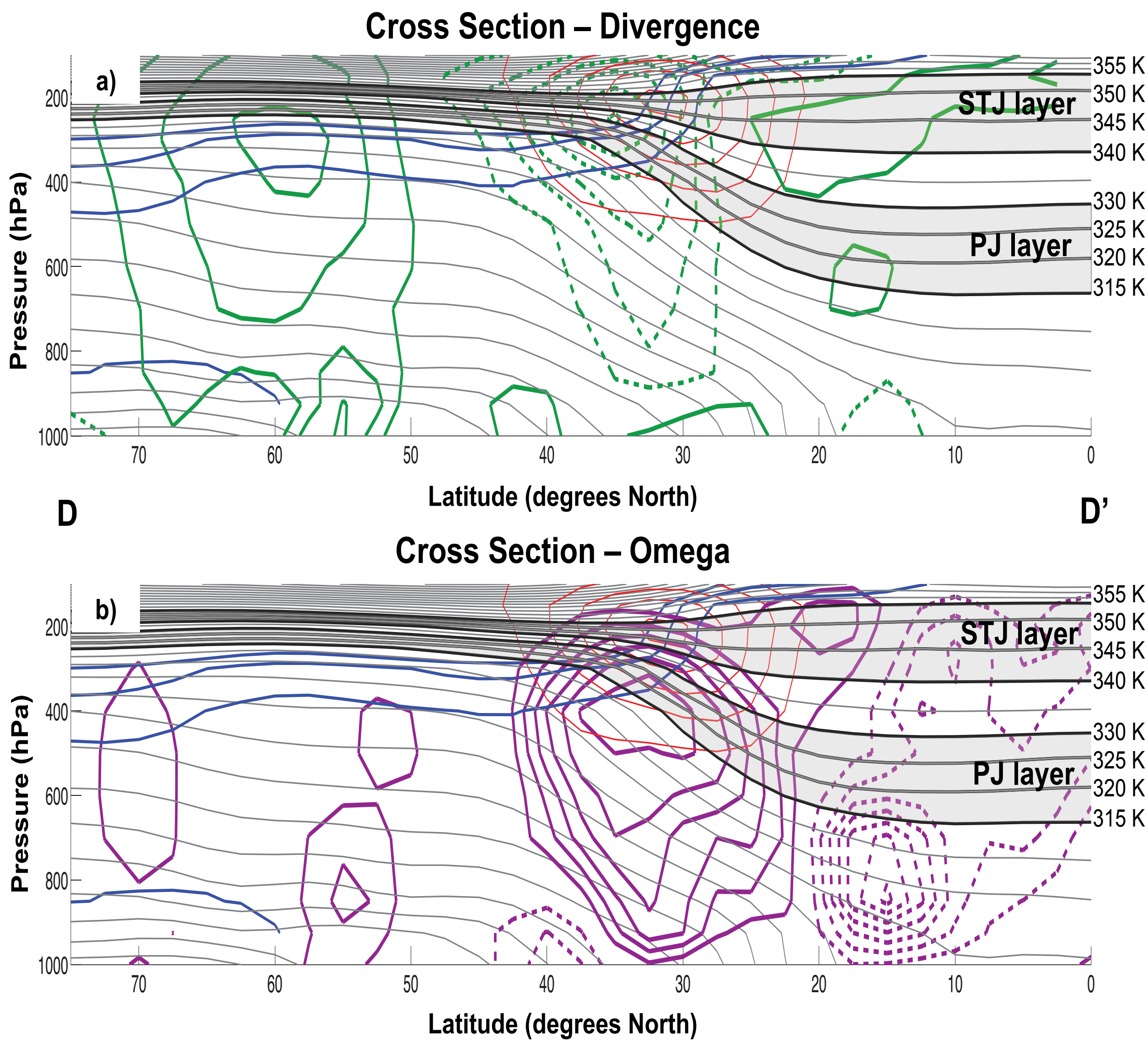

Figure 3.5 Cross sections taken along 120°E longitude (D-D' line from Fig. 3.1a). All conventions are the same as that of Fig. 3.4 except that the solid (dashed) green contour represents anomalous divergence (convergence) every 0.5 x 10^{-6} s^{-1} starting at + (-) 0.5 x 10^{-6} s^{-1} in panel a and the solid (dashed) purple contour represents anomalous downward (upward) vertical motion every 1.0 x 10^{-2} Pa s^{-1} starting at + (-) 1.0 x 10^{-2} Pa s^{-1} in panel b.

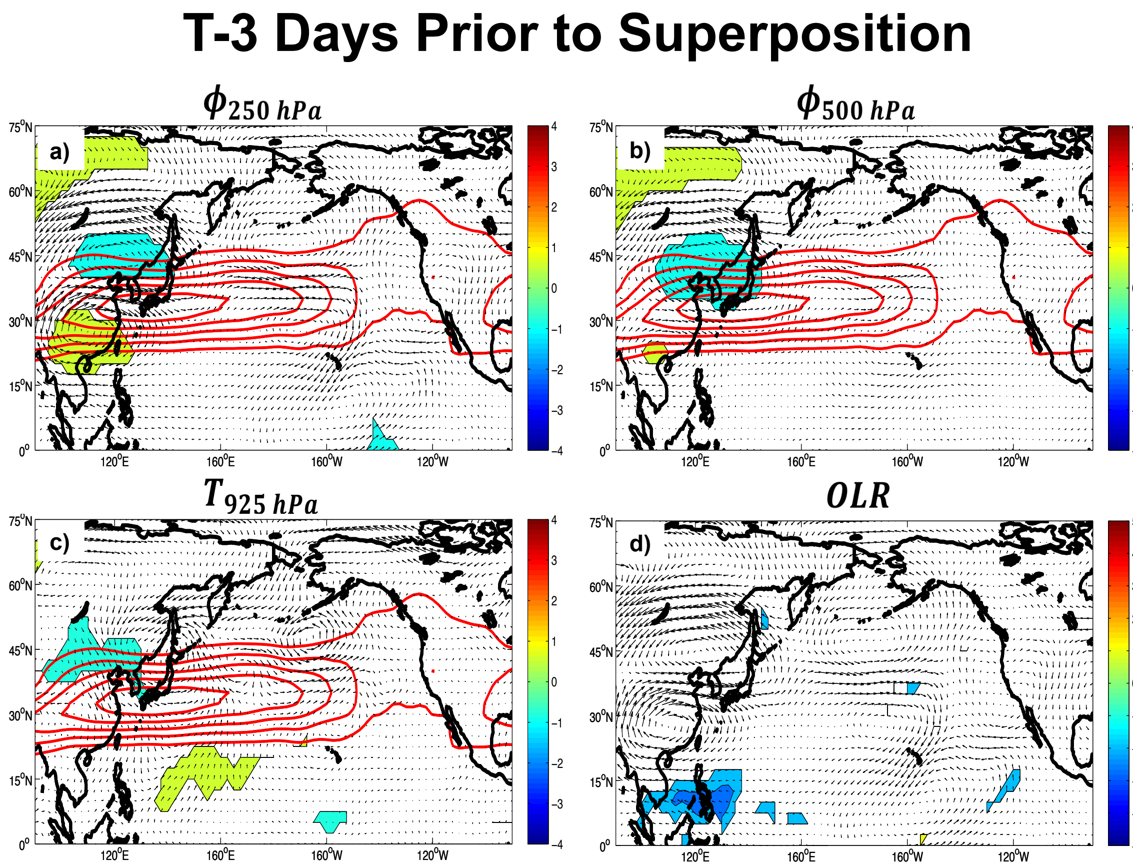

Figure 3.6 Composite maps of a) $\phi_{250,std.anom.}$, b) $\phi_{500,std.anom.}$, c) $T_{925,std.anom.}$ and d) daily-averaged anomalous interpolated Outgoing Longwave Radiation (OLR) 3 days prior to composite West Pacific vertical jet superposition. Conventions are the same as Fig. 3.1 except for the OLR plots, where the anomalous OLR values are contoured every 10 W m^{-2} starting at $\pm$ 10 W m^{-2}, and wind vectors represent 250 hPa anomalous wind (m s^{-1}).

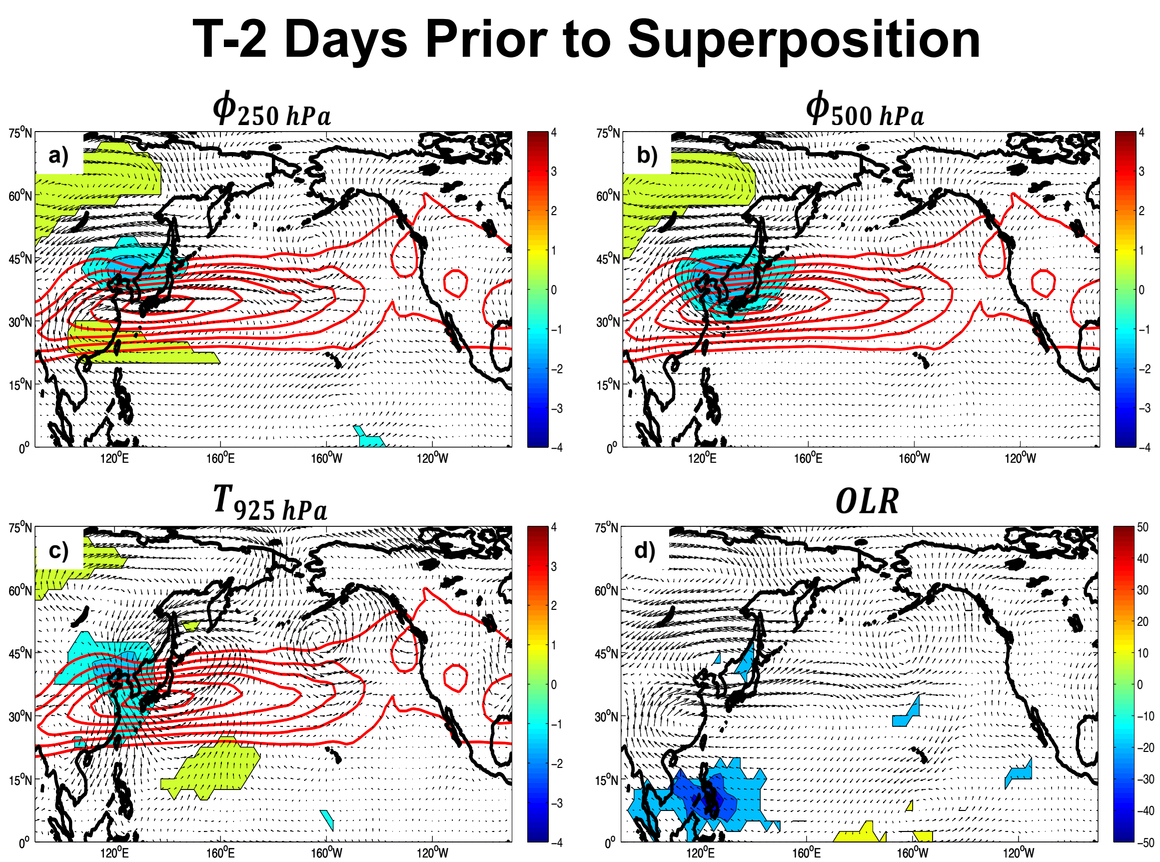

Figure 3.7 Same as Fig. 3.6 except at time T-2 (2 days prior to jet superposition).

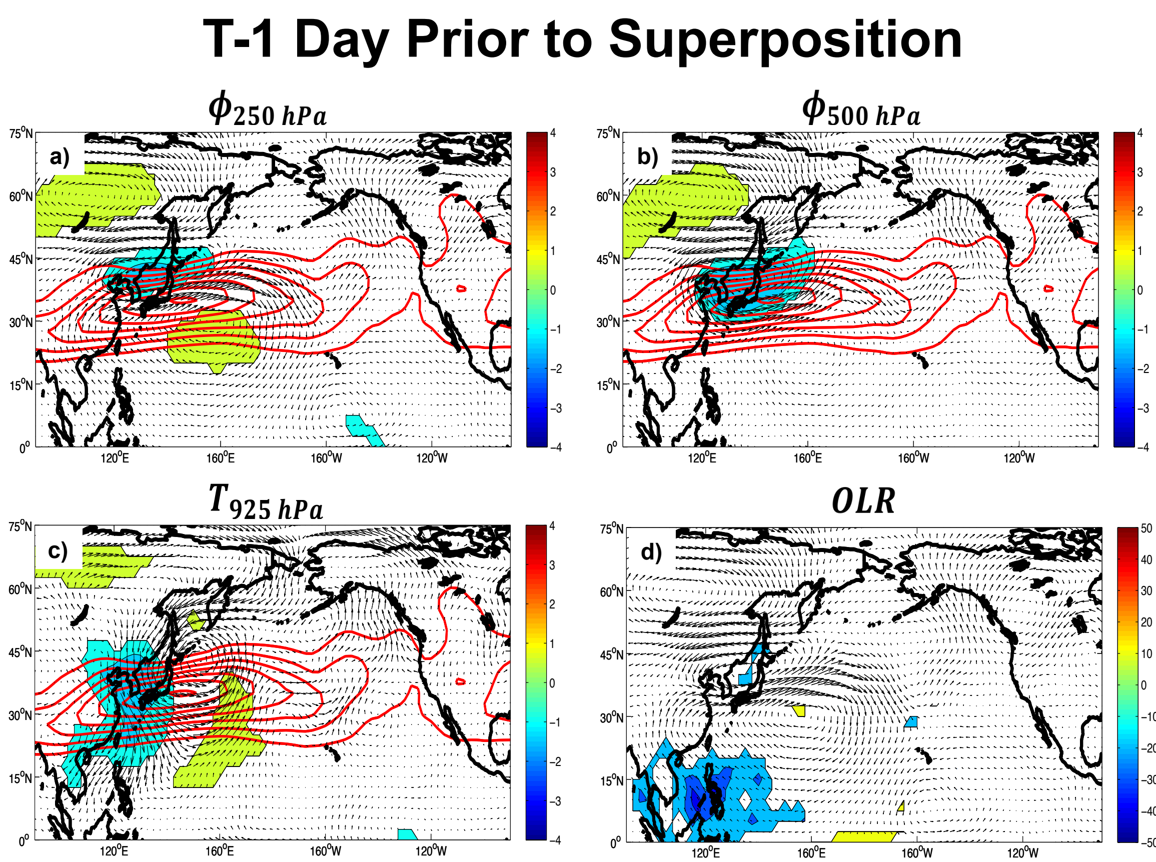

Figure 3.8 Same as Fig. 3.6 except at time T-1 (1 day prior to jet superposition).

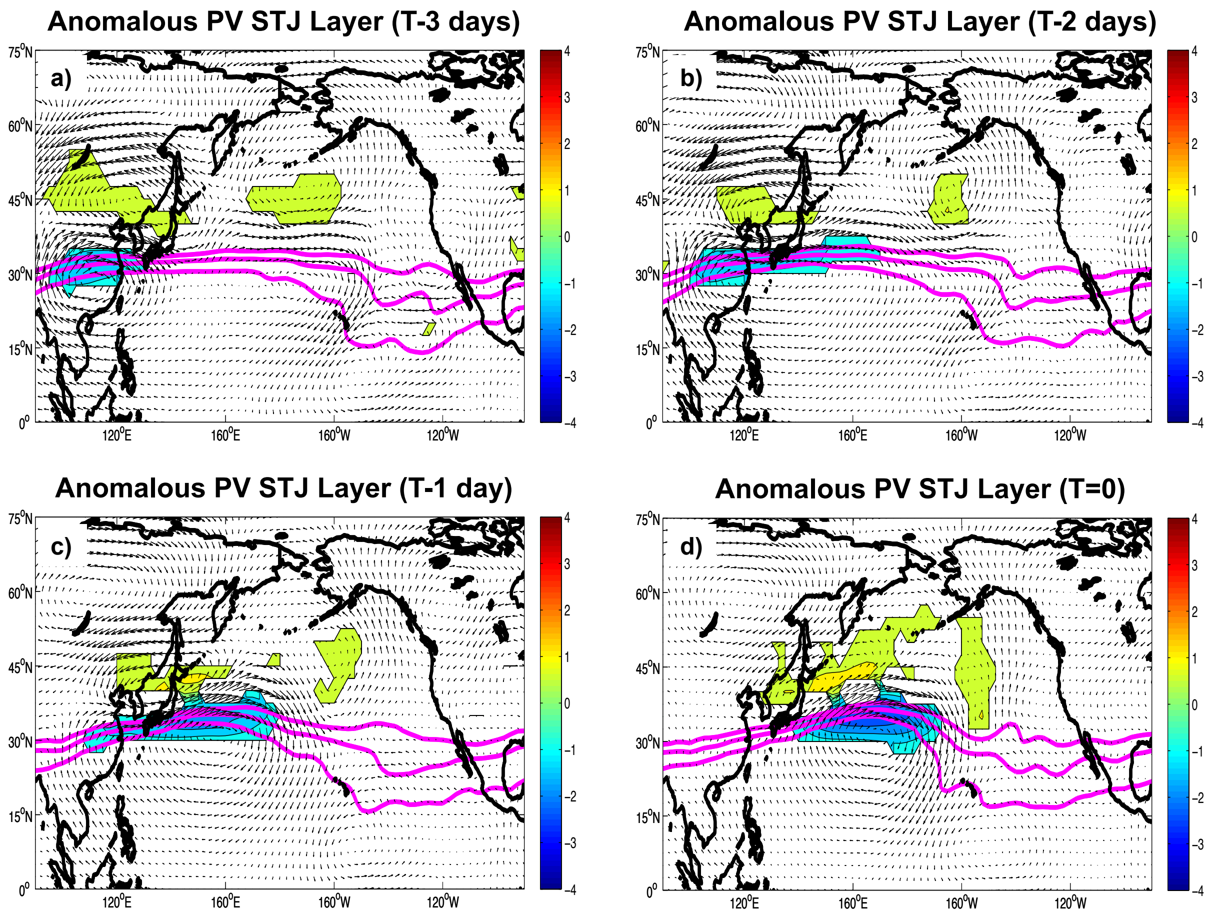

Figure 3.9 Anomalous PV (PV units) within the STJ (340-355K) isentropic layer (fill pattern) a) 3 days prior to composite superposition, b) 2 days prior to composite superposition, c) 1 day prior to composite superpositon and d) at the time of composite superposition. The 1-3 PVU surfaces are contoured in solid purple. Anomalous winds within the STJ layer are shown as vectors.

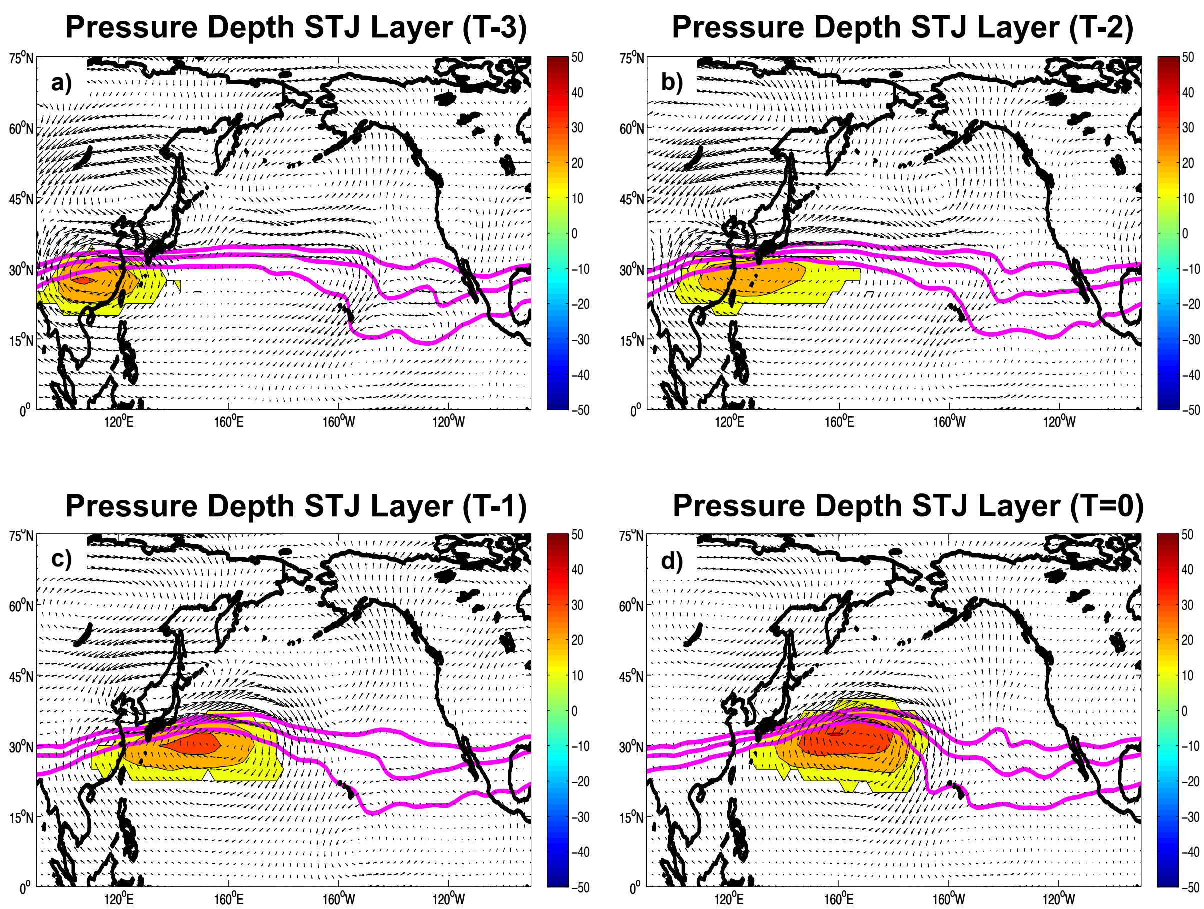

Figure 3.10 Composite anomalous pressure depth within the STJ (340-355K) isentropic layer (fill pattern) a) 3 days prior to composite superposition, b) 2 days prior to composite superposition, c) 1 day prior to composite superpositon and d) at the time of composite superposition. Note that $dp = p_{340K}$ - p_{355K} for the 340-355K isentropic layer. 1-3 PVU surfaces are contoured in solid purple. Anomalous winds within the STJ layer are shown as vectors.

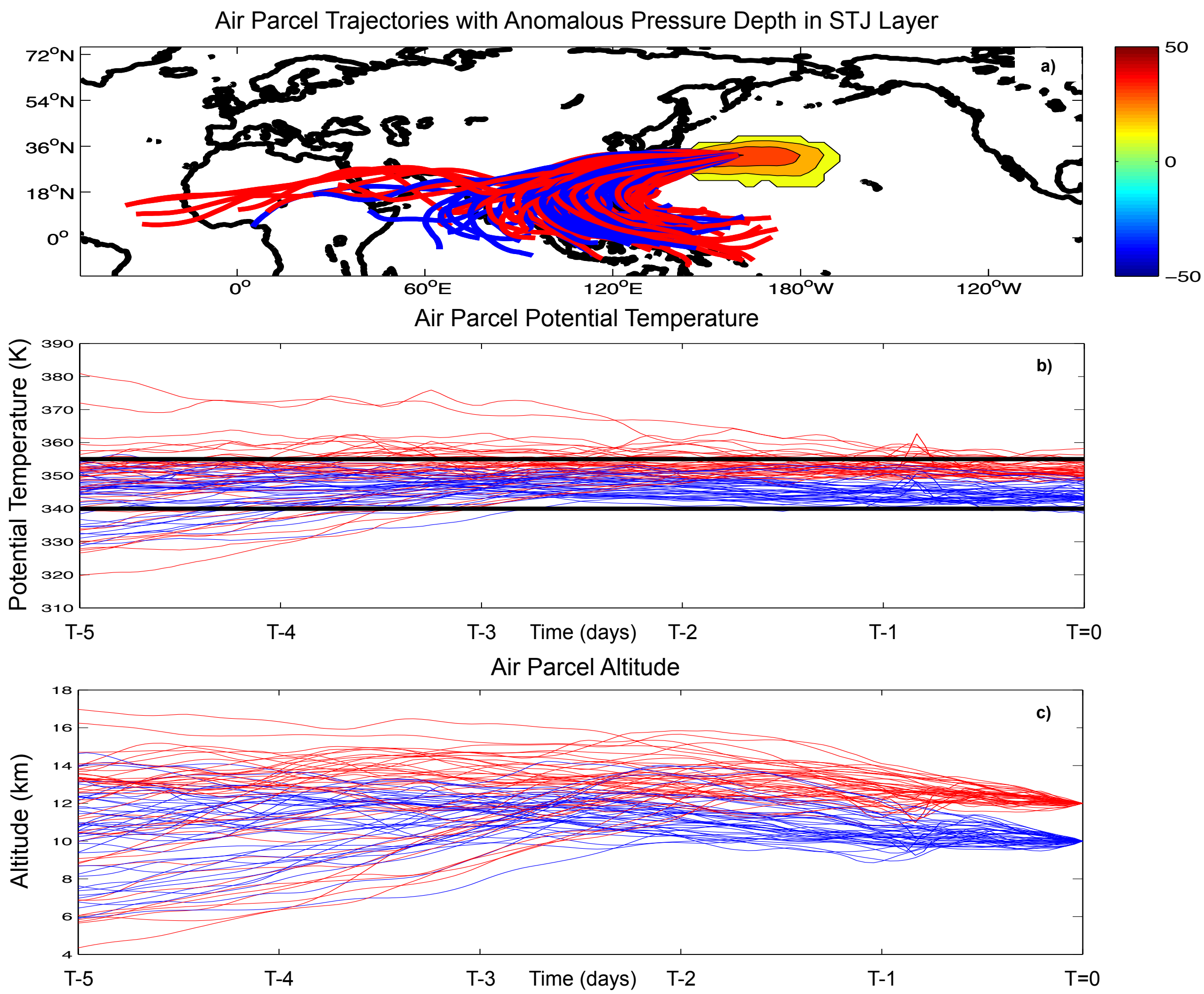

Figure 3.11 a) Same as Fig. 3.10d, but included are ARL HYSPLIT 120 hour back-trajectories for air parcels, where the trajectories begin at the center of the anomalous pressure depth feature within the STJ isentropic layer (32.5°N, 160°E). Trajectories colored in blue (red) represent parcels with back-trajectories starting at 10 km (12 km). b) Time series of θ (K) associated with each parcel back-trajectory shown in panel a. Color conventions for the time series are same as that of the trajectories from panel a. The STJ isentropic layer lies between the solid black lines (340-355K). c) Time series of altitude (km) associated with each parcel back-trajectory shown in panel a. The color conventions are the same as panel b.

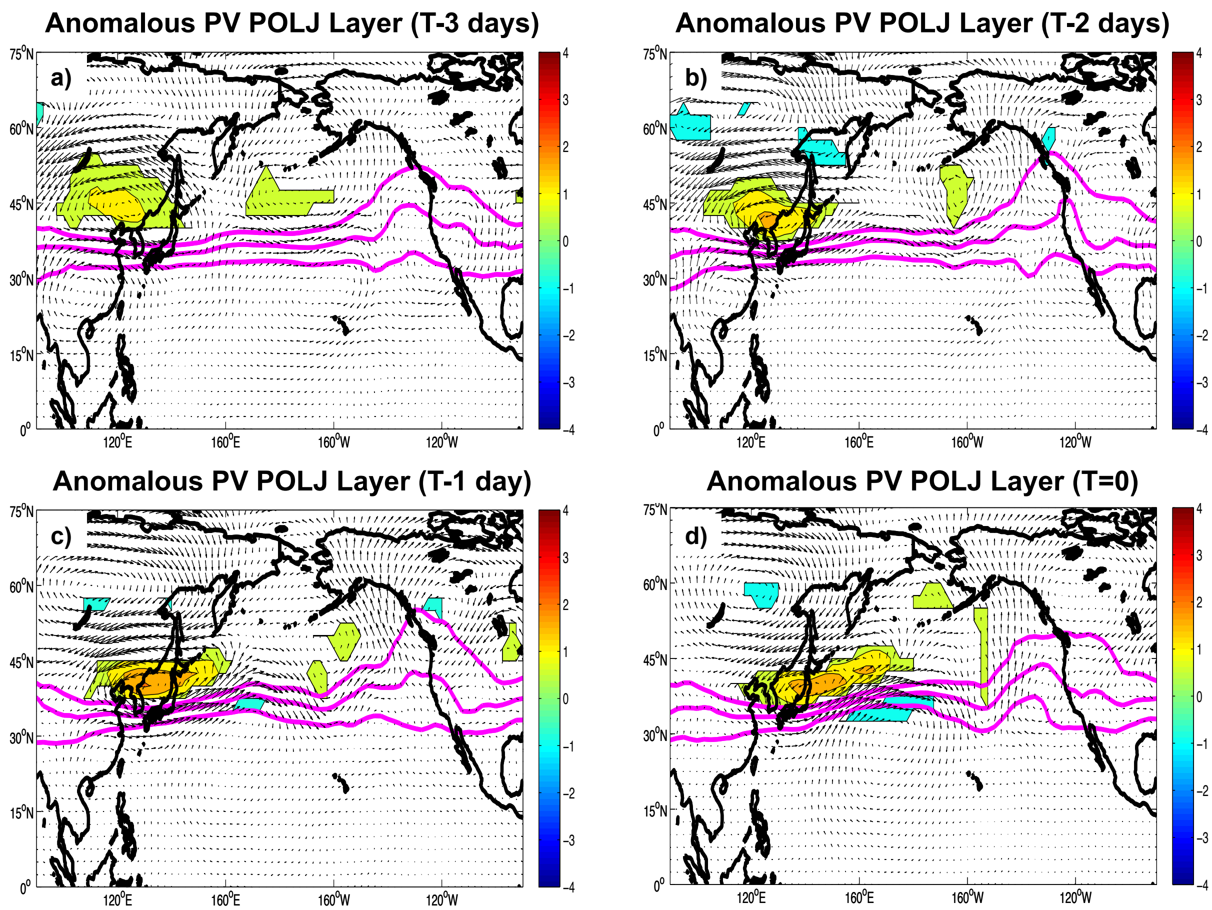

Figure 3.12 Anomalous PV (PV units) within the PJ (315-330K) isentropic layer (fill pattern) a) 3 days prior to composite superposition, b) 2 days prior to composite superposition, c) 1 day prior to composite superpositon and d) at the time of composite superposition. The 1-3 PVU surfaces are contoured in solid purple. Anomalous winds within the PJ layer are shown as vectors.

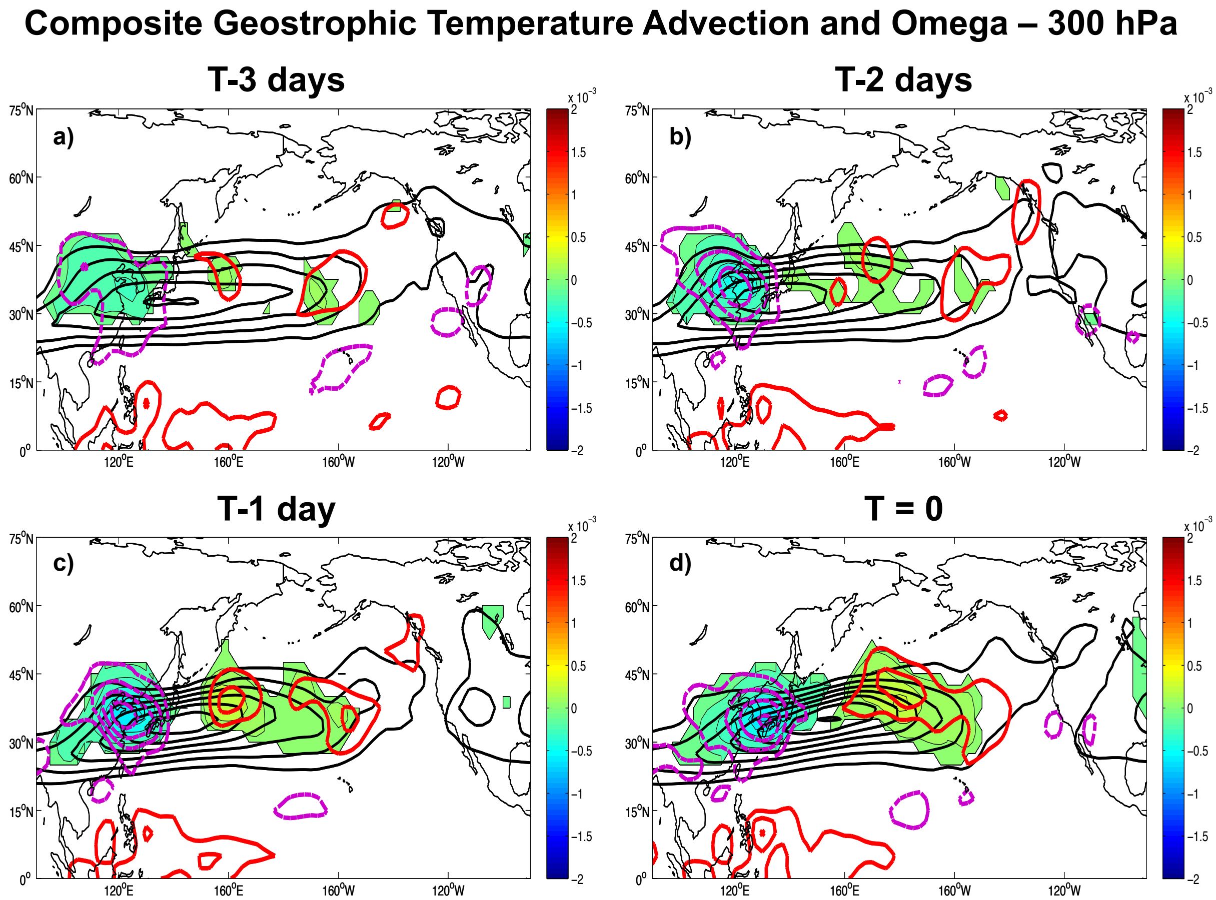

Figure 3.13 300 hPa composite geostrophic temperature advection (fill pattern; units K s^{-1}) and vertical motion (red (purple) solid (dashed) contour indicates upward (downward) vertical motion) contoured every 0.05 Pa s^{-1} starting at + (-) 0.05 Pa s^{-1} for times a) 3 days prior to jet superposition, b) 2 days prior to jet superposition, c) 1 day prior to jet superposition, and d) at time of jet superosition. Also plotted on all panels are 300 hPa composite wind speed (black solid contour) every 10 m s^{-1} starting at 30 m s^{-1}.

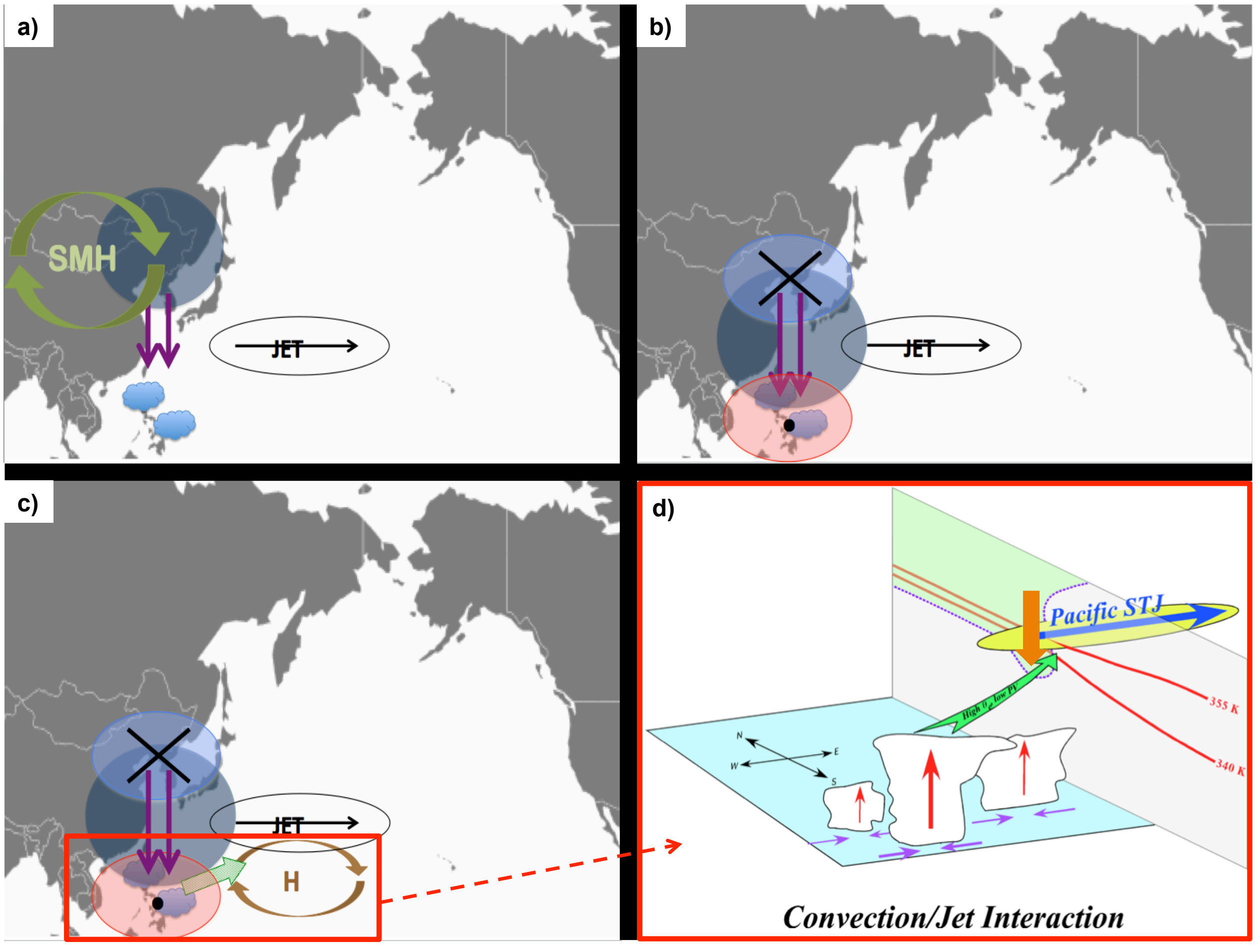

Figure 3.14 Conceptual model outlining the role of tropical forcing with respect to onset of robust vertical jet superposition events in the West Pacific. In panel a, the green arrows with the abbreviation “SMH” represent the Siberian-Mongolian High, the purple arrows represent near-surface anomalous northerly winds, the blue cloud symbols represent anomalous tropical convection and the black thin circle with the westerly vector represents the approximate position of the composite West Pacific jet. All features in panel a are present 3 days prior to composite vertical jet superposition. In panel b, the blue (red) circle indicates the region of anomalous upper tropospheric convergence (divergence), with the “x” (dot) symbol representing anomalous downward (upward) vertical motion within the air column. In panel c, the brown arrows with the “H” in the center represents the anomalous geopotential height maximum feature on the antiyclonic shear side of the jet that develops 48 hours prior to composite jet superposition. The hatched green arrow represents the direction of transport of high-θ_e, low-PV air mass from the tropics towards the region where the anomalous anticyclone develops equatorward of the jet. Panel d shows the relationship between tropical convective outflow and the transport of this tropical air into the STJ (340-355K) isentropic layer in more detail. The orange arrow represents subsidence within the jet entrance region that plays a role in the development of the deep, vertical PV wall associated with the composite superposed jet. See text for further explanation.

Chapter 4

Comparison of Large-Scale Environments Conducive to West Pacific Jet Superposition within Strong, Neutral and Weak EAWM Environments

4.1 Introduction

In the previous chapter, it was found that several key large-scale features associated with the EAWM are tied to West Pacific vertical jet superposition events. Similar to the case examined by Winters and Martin (2014), the interaction of internal jet dynamics with tropical convective outflow associated with enhanced convection tied to an EAWM northerly cold surge event induce anomalously stronger wind speeds in the jet core and the development of a deep, vertical PV "wall," two features that characterize superposed jets. Furthermore, the conceptual model demonstrating such interactions (shown as Fig. 3.17 in the previous chapter), incorporates elements present in the conceptual models of the Chang et al. (1979) and Chang and Lau (1980) shown in Figs. 1.7 and 1.8. What is observed to be the strengthening of the West Pacific jet entrance region circulation prior to jet superposition is analogous to the observed strengthening of the local Hadley Cell circulation in these earlier studies, with both situations resulting in the strengthening of the West Pacific jet wind speed. One primary difference between the Chang et al. (1979) and Chang and Lau (1980) studies and the results from Chapter 3 is that the research presented in Chapter 3 is the most recent research that has investigated the relationship between the EAWM and West Pacific jet from the superposition perspective.

It was discussed in Chapter 1 that many recent studies have explored the seasonal predictability of the EAWM by constructing an EAWM "index." It is shown in Chapter 3 that the frequency of West Pacific superposition events are statistically significantly correlated with several of these indices (Fig. 3.3). While the above information provides some initial insight as to how the West Pacific jet may vary within these two distinct seasonal scenarios, no study has specifically investigated the evolution of West Pacific vertical jet superposition events and their associated large-scale environments within strong versus weak EAWM seasons. Accordingly, this chapter seeks to acheive the following research goals: 1) Understand why vertical jet superposition events occur more often during strong EAWM seasons compared to weak EAWM seasons, and 2) investigate the differences in the large-scale environments conducive to the formation of vertical jet superposition events in the West Pacific between strong, neutral and weak EAWM winter environments. The remainder of this chapter is outlined as follows: Section 4.2 explains methodologies used in exploring these research topics, Section 4.3 discusses statistical differences between strong and weak EAWM winters with respect to vertical jet superposiiton events, Section 4.4 explores jet superposition events within strong and neutral EAWM seasonal environments, Section 4.5 explores two superposition events that occurred during weak EAWM winters, and Section 4.6 summarizes the results and conclusions of this research.

4.2 Methodology

4.2.1 *Identifying Strong, Neutral and Weak EAWM Winter Seasons*

NCEP/NCAR Reanalysis 1 data is again used for all analysis in this chapter. In determining the seasonal strength of the EAWM, a composite seasonal EAWM index is used, which is constructed from the five EAWM indices considered in Chapter 3. Figure 4.1 shows the the same seasonal time series from Chapter 3 along with the composite EAWM index (olive-colored time series). Note that the EAWM composite index is highly correlated with each EAWM index as well as the frequency of occurrence of West Pacific jet superposition ID's (i.e., all correlations are statistically significant at the 99$\%$ level).

The EAWM composite index ($EAWM_{comp}$) is used to define strong, neutral and weak EAWM seasons. A strong (weak) EAWM season is defined as a season where $EAWM_{comp} \geq$ ($\leq$) 0.5σ. "Neutral" EAWM seasons are defined as winters where -0.5$\sigma \leq EAWM_{comp} \leq 0.5\sigma$. Table 4.1

shows a list of the strong, neutral and weak winter seasons identified in this manner. 10 (8) strong (weak) EAWM seasons are identified, with 13 winters falling within the "neutral" season category. The use of 0.5σ as a threshold value is consistent with that used in other EAWM index studies that consider differences between strong and weak EAWM seasonal environments, such as Wang et al. (2009) and Wang and Chen (2014), for example. Although Jhun and Lee (2004) use a more strict threshold of $\pm$ 0.9σ to define each type of season, the choice of a 0.5σ is such that the seasons identified as strong and weak include those from their study.

4.2.2 *Selecting Jet Superposition Events within Strong vs. Weak EAWM Winter Seasons*

The 44 "robust" vertical jet superposition events from Chapter 3 are partitioned in this study based on the seasonal strength of the EAWM in which the event occurred. 18 of these robust superposition events occurred during a strong EAWM season, 24 cases occurred during a neutral EAWM season, while only 2 cases occurred during a weak EAWM season (Table 4.1). While it is not surprising that fewer robust jet superposition events occur during weak EAWM seasons, it is striking that only two weak EAWM superpositions are observed throughout all 6-hourly times within the 31-winter period.

4.2.3 *Analysis Methods for Investigating Strong, Neutral and Weak EAWM Seasonal Environments*

The large-scale environments associated with the 18 strong EAWM cases are investigated using the same composite analysis technique as employed in Chapter 3. Recall that, in using composite analysis, meteorological quantities of interest are averaged over all strong EAWM cases to construct composite maps of West Pacific superposition events at the time of jet superposition as well as at times prior to and after superposition occurrence. This same analysis is also repeated for the 24 neutral EAWM season cases. To compare the differences between the strong and neutral enviornments, difference maps of the variables considered in a composite sense are computed, including calculation of regions of statistically significant differences between the two scenarios using a two-tailed difference in means student t-test.[1]

While desirable to compare the weak EAWM composite environment to those of the strong and neutral environments, due to the small sample size of weak EAWM season cases, the evolution of large-scale features conducive to superposition during weak EAWM seasons are considered individually within a case-study analysis framework. This includes a detailed analysis of the evolution of these environments as well as the West Pacific jet itself. The same variables will be considered in the analysis of these weak EAWM cases in order to facilitate a qualitative assessment of the similarities and differences between these cases and the composite scenarios.

4.3 PJ, STJ and Jet Superposition Frequency of Occurrence - Strong vs. Weak EAWM Seasons

Figure 4.2a shows the difference in the number of jet superposition ID's per winter season between the strong and weak EAWM seasons. There are more jet superposition ID's in the West Pacific during strong EAWM seasons relative to weak seasons. This is consistent with what is expected based on the correlation between the $EAWM_{comp}$ and jet superposition frequency from Fig. 4.1. However, within the southern United States, more jet superposition ID's occur per season on average during weak EAWM winters than in strong EAWM winters. Thus, unlike the West Pacific, the large-scale forcing necessary for the PJ and STJ to vertically superpose in this region is present more often during weak EAWM seasons.

Figure 4.2b shows the difference in the frequency of occurrence (per winter season) of PJ ID's at each grid point. The analysis reveals that PJ's are more common during strong EAWM seasons south of 35°N latitude in the West Pacific, as well as within northern China. The PJ is also more common over the southern U.S. and North Africa during strong EAWM seasons, suggesting that during such winters, the PJ characteristically extends to lower latitudes. During

[1]For all t-test calculations, it is assumed that each winter season is independent of the other season such that the number of degrees of freedom considered is N-2, where N represents the number of seasons used within each of the strong and neutral composites. Also, it is assumed that the variances between the two composite environments are unequal.

weak seasons, more PJ's are observed at higher latitudes over the western Pacific (i.e., $40 - 55°N$). In strong EAWM seasons the STJ (Fig. 4.2c) is observed more frequently in the 30-40°N latitude band extending from northern China through southeastern Japan out into the North-Central Pacific ocean. This narrow swath is meridionally flanked by regions where the STJ is more frequent during weak EAWM seasons, especially in the eastern Pacific. This suggests that the Pacific STJ is more zonally oriented during strong EAWM seasons, while its meridional position is more variable during weak EAWM seasons. This interpretation is consistent with the composite 300 hPa zonal wind analysis in Jhun and Lee (2004) as well as 200 hPa zonal wind in Wang and Chen (2010) and Wang and Chen (2014), as these studies show anomalous strong (weak) zonal wind flanked by anomalously weak (strong) winds within the vicinity of the West Pacific interest region during strong (weak) EAWM seasons.

In sum, Fig. 4.2 suggests that the greater frequency of jet superposition events during strong EAWM seasons may be a function of a characteristically southward shifted PJ coincident with a rigidly zonal STJ within the West Pacific region of interest. During seasons associated with a northward-shifted PJ and/or a "wavier" STJ (e.g., weak EAWM seasons), the PJ and STJ are more likely to be sufficiently separated from one another meridionally as to inhibit their vertical superposition. Thus, the development of a jet superposition event during a weak EAWM season would appear to require some mechanism that shifts the PJ equatorward. Whether or not this occurs in the two weak EAWM environment superposition events identified earlier is considered in Section 4.5.

4.4 Composite Analysis of Strong and Neutral EAWM Winter Vertical Jet Superposition Events

Figure 4.3 shows standardized anomalous variables of interest for the composite vertically superposed jet within strong EAWM winter seasons. Qualitatively, the composite environments look very similar to that of the overall 44-case composite from Chapter 3 (Fig. 3.4). The composite jet in the strong EAWM environment is associated with positive (negative) anomalous ϕ and anomalous anticyclonic (cyclonic) flow in the middle and upper troposphere equatorward (poleward) of the jet

(Figs. 4.3a and 4.3b). Anomalous anticyclonic flow associated with a positive ϕ anomaly is also observed over Russia at these levels. In the lower troposphere, anomalous cold air and northerly winds over the East and South China seas are observed (Fig. 4.3c), matching the observed composite cold surge feature from the 44-case composite (Fig. 3.4d). This is not surprising given that cold surge events are more significant during strong EAWM seasons (e.g., Wang and Chen, 2010) and have been shown to be associated with the strenghtening of the West Pacific jet (Chang et al., 1979; Chang and Lau, 1980; Chan and Li, 2004).

Figure 4.3d shows composite daily averaged anomalous (non-standardized) outgoing longwave radiation (OLR). A negative OLR anomaly $\sim$ -40 W m^{-2} is present over the South China Sea and Malaysia. Such a feature has been shown to be integral to the formation of robust jet superposition events in Chapter 3. Given that an anomalous cold surge feature is also observed within the strong EAWM environment, and that this feature enhances convection within the Maritime Continent region, it is no surprise that anomalous negative OLR values are observed.

Dynamically, the neutral EAWM season composite environment is similar to that of the strong EAWM seasonal environment (Fig. 4.4). In this composite, a significant positive ϕ anomaly equatorward of the jet core at 250 hPa (Fig. 4.4a), anomalous trough at 500 hPa (Fig. 4.4b), cold air anomaly with anomalous northerly winds at 925 hPa (Fig. 4.4c) and anomalous negative OLR (Fig. 4.4d) are all present, though the OLR anomaly in the Maritime Continent region is much weaker relative to the strong EAWM season composite. These similarities are further supported by subtracting the neutral EAWM composite analyses from the strong (Fig. 4.5). While some differences between the two composite environments exist, the majority of these differences are not statistically significant at the 95% level. The anomalous negative ϕ equatorward of the composite jet at 250 and 500 hPa is greater in magnitude during the neutral seasons relative to the strong EAWM seasons (Figs. 4.5a and 4.5b). However, these differences are only statistically significant on the southern edge of this feature. While the strong EAWM composite exhibits a slightly "wavier" pattern (indicated by alternating anomalous negative/positive ϕ features in the eastern Pacific), these differences are not statistically significant. Note too that no differences exist within the region of the anomalous composite trough in the mid- to upper troposphere near Japan.

There are also no significant differences between the anomalous cold surge features present within each composite environment over the Maritime Continent region (Fig. 4.5c). Only near 30°N, 160°E, the region where the mid- to upper-tropospheric anticyclonic ϕ anomaly resides, are significantly warmer temperatures observed in the neutral EAWM seasons relative to the strong EAWM seasons. Some regions exhibit statistically significant differences in OLR magnitude within lower latitudes of the Maritime Continent region, where OLR values are more negative within the strong EAWM season composite (Fig. 4.5d). However, similar to the other observed differences, the majority of grid points within the Maritime Continent region do not possess statistical significance.

Figure 4.5 reinforces our findings suggesting that the large-scale environments associated with strong EAWM season jet superposition events are similar to that of robust superpositions occuring during neutral EAWM seasons. Given this similarity, it is not surprising that the evolution of the above highlighted large-scale environments from 72 hours prior to superposition up to the time of composite superposition are also quite similar (not shown). Therefore, it seems that robust vertical jet superposition events preferentially form within an environment that includes a combination of upper tropospheric anomalous anticylonic flow (i.e., positive pressure depth anomaly) equatorward of the jet core, a middle tropospheric trough poleward of the jet and a northerly cold surge type of event. The same conceptual model regarding the evolution of jet superpositions within the 44-case composite (i.e., Fig. 3.14) also applies to the strong and neutral composite environments. The EAWM-related processes listed in this paragraph enhance convection in the Maritime Continent region such that the convective outflow grows a positive pressure depth anomaly that acts to increase the jet wind speed and play a role in the development of a deep, vertical PV wall.

While the strong and neutral composite environments conducive to West Pacific vertical jet superposition are similar to that of the 44-case composite of Chapter 3, the two superposition cases observed during weak EAWM seasons still require investigation. The goal of the next section is to explore these two robust vertical jet superposition cases using a case-study analysis approach to compare/contrast their superposition environments to those observed within strong/neutral EAWM seasons.

4.5 Case Study Analysis of Weak EAWM Winter Vertical Jet Superposition Events

4.5.1 *24 February 1993 Case*

Figure 4.6 shows the evolution of the 250 hPa wind speed and mean sea level pressure (MSLP) for dates 21-24 February 1993 (all at 1800 UTC), with 24 February 1993 1800 UTC being the time of robust jet superposition. Grid points where a jet superposition event was recorded are marked with white "0" symbols. On 21 February 1993 (Fig. 4.6a), two jet stream features are observed east of Japan $\sim$ 160°E longitude, with a single jet over eastern China associated with only STJ charactersitics as determined using the ID scheme described in Chapter 2 (ID's not shown). The Siberian-Mongolian High (SMH) is centered south of Lake Baikal with a maximum MSLP $\sim$ 1048 hPa, and within the left jet exit region of the West Pacific jet over Japan, a closed 996 hPa contour indicates the presence of a surface cyclone. On 22 February 1993 (Fig. 4.6b), the jet over China moves eastward and increases in magnitude over 20 m s^{-1}, now associated with maximum wind speeds at this level $>$ 80 m s^{-1}. This feature is associated with several vertical jet superposition ID's. The left jet exit region cyclone strengthens, exhibiting a minimum MSLP of $\sim$ 984 hPa. Coincident with this development, the SMH has shifted southward and weakened to a maximum MSLP of $\sim$ 1044 hPa.

One day later (Fig. 4.6c), the core of the West Pacific jet extends eastward. The surface cyclone present within its left exit region continues to strengthen, deepening to $\sim$ 972 hPa. At this time, the jet is not superposed, though contains a mixture of PJ and STJ ID's (not shown). The SMH remains stationary while weakening slightly to a maximum MSLP of $\sim$ 1040 hPa. Finally, on 24 February 1993 (Fig. 4.6d), we observe the robust jet superposition over the West Pacific interest region, as marked by the line of 7 jet superposition ID's within the core of the West Pacific jet (gray shading in Fig. 4.6d). The wind speed maximum associated with the jet remains $>$ 80 m s^{-1}. The jet continues to extend eastward, with the eastern edge of the jet located near the dateline. The surface cyclone associated with the jet strengthens to a MSLP minumum of $\sim$ 964 hPa and continues to move eastward while remaining located in the jet left exit region. The SMH continues to weaken, filling to $\sim$ 1036 hPa southeast of Lake Baikal.

Figures 4.7-4.9 show other meteorological quantities of interest along with the 250 hPa jet stream (red contours) at T-3, T-1 and at the time of superposition, respectively. Alternating positive and negative ϕ anomalies at 250 and 500 hPa are present on 21 February 1993 (Figs. 4.7a and 4.7b), consistent with the wavy nature of the PJ and STJ in the Central and East Pacific. A positive ϕ anomaly resides within the jet core over eastern China, though a negative anomaly is present in this location at 500 hPa (Fig. 4.7b). At 925 hPa (Fig. 4.7c), anomalous warm air associated with the warm sector of the developing surface cyclone is located near Japan ($> 1.5\sigma$), with anomalous cold air $<$ -1.5σ residing over northeastern China. The location of this cold air 3 days prior to robust vertical jet superposition is exactly where cold air anomalies within the composite environments develop. Figure 4.7d shows positive OLR anomalies within the Maritime Continent region, opposite of what is observed 3 days prior to jet superpostion in the composites.

Two days later, as the West Pacific jet extends, anomalous cyclonic flow is now observed at both 250 and 500 hPa poleward of the jet core (Figs. 4.8a and 4.8b). The positive ϕ anomaly at both of these levels remains stationary in northern Russia, though the magnitude of this feature slightly weakens relative to 21 February 1993. At 925 hPa (Fig. 4.8c), the cold air anomaly over the East China Sea moves equatorward towards lower latitudes, with anomalous values $> 1\sigma$ extending as far south as the equator. Anomalous warm air associated with the circulation of the surface cyclone in the West Pacific left jet exit region has grown in area and anomalous magnitude. Figure 4.8d shows anomalous negative OLR beginning to emerge near Indonesia, and anomalous southerly winds in the upper troposphere are present near this region of anomalous convection. It will be shown later that, in concert with the development of this anomalous convection and the southward moving cold air anomaly, a positive pressure depth anomaly increases in magnitude on the equatorward side of the West Pacific jet.

On 24 February 1993 (Fig. 4.9), weak anomalous cyclonic (anticyclonic) flow is observed poleward (equatorward) of the jet core (Fig. 4.9a). The anomalous anticyclonic flow is widespread and not as strong in anomalous magnitude as that of the superposed jet within any of the three composite environments. The center of the anomalous ϕ maximum in Russia has moved southward and weakened. At 500 hPa (Fig. 4.9b), the anomalous cyclonic flow and negative ϕ anomaly remain on the cyclonic shear side of the jet, resembling the 500 hPa composite anomalous trough observed in each composite environment. At 925 hPa (Fig. 4.9c), anomalous cold air is still located over the East and South China Sea and Maritime Continent regions, with the warm anomaly tied to the the jet exit region surface low further eastward. Regions of negative but weak anomalous OLR are found east and west of Indonesia (Fig. 4.9d). Anomalous southerly winds aloft are still present, which (as demonstrated in Fig. 3.14) can play a role in advecting convective outflow towards the equatorward side of the jet.

Figures 4.10 and 4.11 show anomalous values of PV and pressure depth respectively within the STJ isentropic layer (see Chapter 3 for definition of pressure depth). A negative PV anomaly is present within the region where the West Pacific jet resides at time 3 days prior to jet superposition (Fig. 4.10a). This feature is associated with a weak positive pressure depth anomaly (Fig. 4.11a), which, recalling the thermal wind equation in isentropic coordinates from Chapter 3, is associated with an anomalous anticyclonic vertical wind shear that can strengthen (relative to climatology) the westerly flow within the jet core if the pressure depth anomaly maximum is positioned to the south of the jet. Over time, the negative PV and positive pressure depth anomalies propogate eastward along with the West Pacific jet. During this evolution, a longitudinal elongation of both anomalies occurs (Figs. 4.10b-d), while the pressure depth anomaly simultaneously increases in anomalous magnitude (Figs. 4.11b-d). Consistent with Chapter 3, as the positive pressure depth anomaly strengthens, the anomalous westerly wind speeds along the pressure depth gradient north of the anomalous maximum, located within the jet core, increase.

Figure 4.12 shows anomalous PV within the PJ isentropic layer throughout the evolution of the West Pacific vertical jet superposition event. The feature of interest is the positive PV anomaly that develops on the cyclonic shear side of the jet. This development, which coincides with the mid- to upper tropospheric trough observed in Figs. 4.7a-4.9a and 4.7b-4.9b, is associated with geostrophic cold air advection and subsidence within the West Pacific jet entrance region (not shown). As discussed in Chapter 3, geostrophic cold air advection within the jet core entrance region shifts the associated thermally direct circulation equatorward such that subsidence occurs within the core of the jet. This acts to bring high-PV air to lower altitudes within the jet core, which can play a role in strengthening the 1-3 PVU gradient and developing the characteristic vertical PV wall associated with a jet superposition (see conceptual model from Chapter 3). This internal jet dynamical process is consistent with what we find with the 44-case composite environment.

In summary, the large-scale environments associated with the development of the 24 February 1993 1800 UTC West Pacific jet superposition event are generally similar to that of the other composite environments discussed. While anomalous anticyclonic flow and positive ϕ in the upper troposphere is weaker relative to the composites, these features are still present nevertheless. Even though anomalous convection in the Maritime Continent region is nearly non-existent over the 72 hour period, an increase in anomalous pressure depth equatorward of the jet is still observed. Thus, it appears that upper tropospheric anomalous winds (vectors in panel d of Figs. 4.8 and 4.9) over time transport high-θ_e, low-PV air that may be associated with convection that is not anomalous at these times, as locally minimum OLR values are still present in this region (not shown) with anomalous southerlies aloft. Trajectories of this air are similar to those shown in Fig. 3.11a, with air moving anticyclonically from near Indonesia to the equatorward side of the jet (not shown). This, in concert with geostrophic cold air temperature advection and subsidence at an altitude where the PJ is common (i.e., $\sim$ 300 hPa), likely play a role in the development of the anomalous westerly wind and deep, vertical PV wall characteristic of superposed jets, just as observed within the composite scenarios.

4.5.2 *10 January 2007 Case*

Figure 4.13 shows the evolution of 250 hPa wind speed and MSLP with respect to the 10 January 2007 robust West Pacific vertical jet superposition event. On 7 January 2007 (Fig. 4.13a), a jet exhibiting several superposition ID's resides south of Japan. Similar to the February 1993 case, the left jet exit region is associated with a strong surface cyclone (minimum MSLP $\sim$ 968 hPa), with a $\sim$ 1048 hPa SMH centered near Lake Baikal. The cyclone is associated with negative ϕ anomalies at 250 and 500 hPa residing to the southwest of the surface cyclone (Figs. 4.14a and 4.14b). An anomalous ridge is present within the right jet entrance region of the jet $\sim$ 115°E longitude, while a more impressive anomalous ridge is observed east of the surface low associated with anomalous southerly winds and warm air at 925 hPa (Fig. 4.14c). A cold surge type feature resides east of China, with anomalous northerly winds extending as far south as Malaysia, where anomalous convection (diagnosed via negative OLR) associated with upper tropospheric anomalous southerly winds are observed in Fig. 4.14d.

Over the next two days, the West Pacific jet extends eastward, with the core of the jet continuing to maintain approximately the same intensity (Figs. 4.13b,c). The surface cyclone discussed in the previous paragraph continues to remain within the left jet exit region of the West Pacific jet, though it has weakened in intensity. The North-Central Pacific ridge associated with the PJ is now located south-southwest of Alaska, maintaining approximately the same poleward extent (in latitude) as observed one day earlier (Figs. 4.15a and 4.15b). The anomalous anticyclonic flow and positive anomalous ϕ on the anticyclonic shear side of the West Pacific jet at 250 hPa and 500 hPa is still observed (with ϕ increasing between 7-9 January 2007 at 500 hPa), while a negative ϕ anomaly associated with the surface low is also still present (Fig. 4.15b). At 925 hPa (Fig. 4.15c), the thermal structure of the surface cyclone appears occluded, as anomalous warm air wraps towards the cyclone core. The anomalous cold surge over the East China Sea has weakened, with the strongest standardized anomaly over extreme southeastern Asia. Negative anomalous OLR has intensified (Fig. 4.15d), with anomalous southerly winds now extending from the northern edge of this anomalous convection to the West Pacific jet entrance region.

On the day of robust west Pacifc jet superposition (10 January 2007), the jet has extended eastward with the core nearly reaching 180° longitude (Fig. 4.13d). The surface cyclone of interest continues to weaken while the SMH remains relatively stationary and has strengthened slightly. The negative ϕ anomaly at 250 hPa associated with the surface low remains around the same anomalous magnitude (Fig. 4.16a), while the same feature at 500 hPa has weakened (Fig. 4.16b). Similar to the other weak EAWM season case as well as the composite environments, we observe the continued presence of the anomalous anticyclonic flow equatorward of the jet, though this flow has been associated with much more substantial ϕ anomalies than that of the composite and

February 1993 cases (i.e., $> 2\sigma$). Also, the ridge to the east of the jet continues to move eastward and is now located south of Alaska. While a warm air anomaly at 925 hPa occurs with this ridge, the standardized value is less than that of the previous 3 days (Fig. 4.16c). No significant cold surge feature is present anymore at the time of jet superposition within the East and South China Seas, though a localized cold temperature anomaly over Myanmar and Laos still remains. Finally, an area of negative OLR resides east of the Maritime Continent region (Fig. 4.16d), though the northward extension of this feature is not as expansive as that of OLR anomalies observed within the composite environments. This feature is associated with anomalous southeasterlies, which, similar to the previous case and composite cases, can act to advect high-θ_e, low-PV air poleward towards the anticyclonic shear side of the jet core.

Considering PV and pressure depth anomalies within the STJ layer for this case (Figs. 4.17 and 4.18), a negative PV anomaly over northeastern China is observed 3 days prior to superposition (Fig. 4.17a). As this feature propogates eastward over time, the negative PV anomaly becomes elongated as the jet extends eastward and the ridge to the east of the jet over the eastern Pacific extends poleward (Figs. 4.17b-d). Accompanying this negative PV anomaly is a positive pressure depth anomaly stronger than that of the anomaly observed in the 24 February 1993 case as well as that of the 44-case composite environment. Over the 3 day period, this feature, propogates eastward and weakens slightly in magnitude. Despite weakening, its presence on the equatorward side of the jet likely maintains anomalous vertical wind shear and thus westerly winds through the jet core in a similar fashion as observed within the February 1993 case.

A positive PV anomaly within the PJ layer is observed to the northeast of the negative PV anomaly over Japan at time T-3 (Fig. 4.19a). However, as this feature moves eastward, the magnitude of anomalous PV weakens on 8 January 2007. Along with this, although not shown in this section, geostrophic cold air advection in the jet entrance region weakens between times T-3 and T-1, remaining within the jet entrance region as the jet core moves eastward over the 72 hour period. Thus, unlike the February 1993 case, a lack of concentrated, anomalous positive PV on the poleward side of the jet along with subsidence occurring too far west of the jet core is observed. This may imply that the internal jet dynamical forcing is not as significant in this case relative to the influence of the pressure depth anomaly compared to the February 1993 case. Future work requires further quantification of these effects in order to support the above claim.

4.6 Chapter Summary

The goal of this chapter was to expand upon the composite analysis of Chapter 3 and investigate the large-scale environments conducive to PJ/STJ superposition within strong, neutral and weak EAWM seasons. The motivation for this chapter is that the seasonal strength of the EAWM, a phenomena that can lead to northerly cold surge events that influence the strength of the West Pacific jet stream, is statistically-significantly correlated to the frequency of occurrence of jet superposition ID's within our West Pacific interest region such that more (less) ID's occur during strong (weak) EAWM winters.

The results in this chapter reveal that, out of the 44 cases considered from Chapter 3, more (less) robust vertical jet superposition events occur during strong (weak) EAWM seasons (i.e., 18 vs. 2 cases), while 24 of the 44 cases occur during "neutral" EAWM seasons. Despite differences in frequency of occurrence of these events within each seasonal type, the large-scale environments tied to superposition events within strong, neutral and weak EAWM seasons do not appear to differ significantly from each other. In the strong and neutral composites as well as two weak EAWM season events, the following large-scale features appear to be within the vicinity of a developing vertical jet superposition event in the West Pacific between times T-3 and T=0: 1) anomalous anticyclonic flow on the anticyclonic shear side of the jet in the middle to uppper troposphere, though the magnitude of anomalous ϕ and wind may vary on a case-by-case basis, 2) an anomalous mid-tropospheric trough feature (identified by anomalous cyclonic flow and a negative ϕ anomaly at 500 hPa) on the cyclonic shear side of the West Pacific jet that is likely generated in mid-latitude eastern Asia prior to interacting with the jet, 3) a cold surge feature associated with anomalous negative temperature and northerly winds in the lower troposphere off the coast of China, though the timing of such a feature may vary depending on each case, and 4) anomalous convection (i.e., negative OLR anomalies) within the Malaysia-Indonesia region, with the magnitude of anomalous OLR again varying depending on the case. Note that the anomalous anticyclonic flow equatorward of the jet manifests itself as a positive pressure depth anomaly in the STJ layer, which plays an integral role in the development of anomalous westerly winds and the strengthening of the gradient of the 1-3 PVU channel within the jet core. Subsidence within the jet entrance region, similar to that described in Chapter 3, is present and may also play a role in the development of the PV wall characteristic of superposed jets through transport of high-PV air in the stratosphere into the upper troposphere.

The large-scale environments observed in these composites and cases are generally consistent with those present within the 44-case composite environment in Chapter 3. Therefore, it appears that the conceptual model revealed there serves as a general conceptual model for all composite environments considered in this chapter (Fig. 3.14). Despite the lack of widespread anomalous negative OLR in the weak EAWM cases relative to the composites, it may be possible that the presence of any convection in the Maritime Continent region (regardless of its anomalous magnitude) can play a role in transporting high-θ_e, low-PV air towards the equatorward side of the jet and produce/maintain positive anomalous pressure depth. This is a topic that will be considered in future work. Thus it appears that the development of jet superpositions in the West Pacific depends upon a particular set of large-scale environmental conditions. Though such conditions are apparently available in any cold season, by virtue of their strong assocaition with the cold surge phase of the EAWM, they appear to be preferentially available during strong EAWM seasons.

One topic that has not been considered up to this point is how robust West Pacific superposed jets and their associated large-scale environments evolve after the time of superposition. Given the impacts such structures may have both on downstream weather as well as the broader large-scale circulation, this question will be explored in detail in the next chapter.

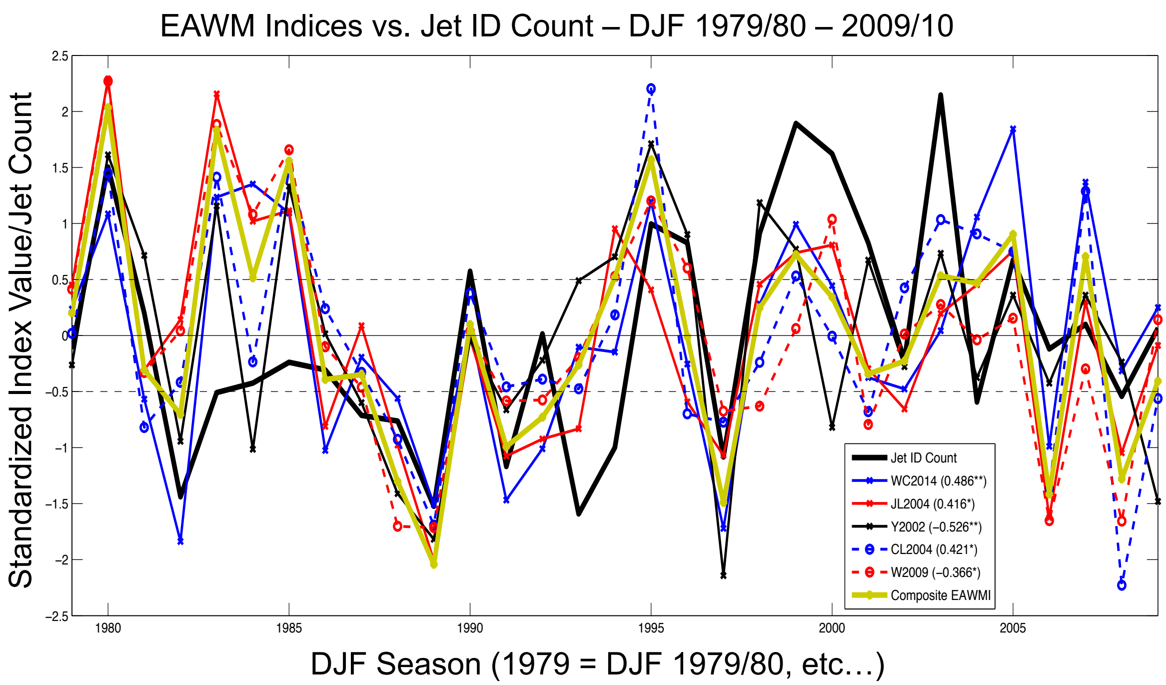

Figure 4.1 Time Series of cold season standardized jet superposition ID frequency in the West Pacific interest region (thick black solid line) along with 6 standardized EAWM indices for winters 1979/80 - 2009/10, including the composite EAWMI (thick olive-colored line). Note that for the Yang et al. (2002) and Wang et al. (2009) time series plots, the time series were multiplied by -1 so that for all indices shown, positive (negative) values imply strong (weak) EAWM winters. Also included are the correlation coefficients between each EAWMI and superposition ID frequency, where values with a single (double) asterisk are significant at the 95% (99%) level (note that it is assumed that each winter season is independent of the others such that the number of degrees of freedom = N-2, with N = 31).

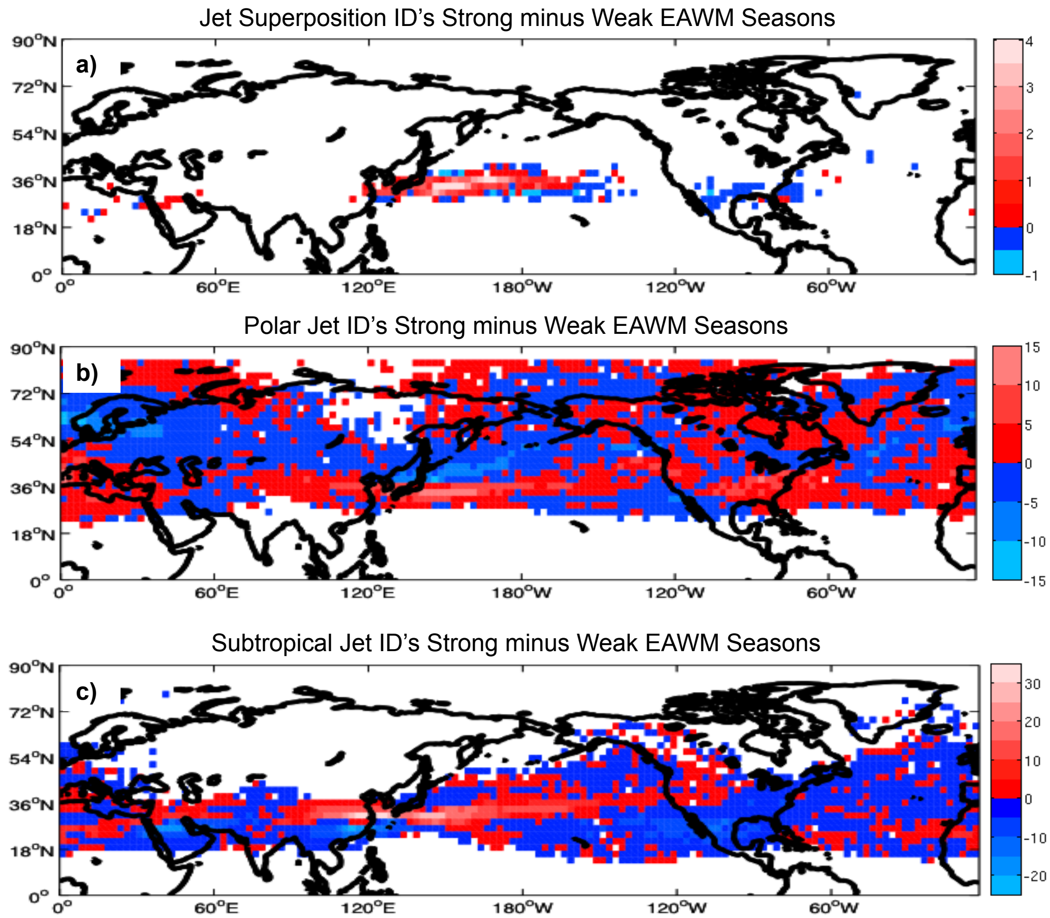

Figure 4.2 Difference between the number of a) jet superposition ID's, b) PJ ID's, and c) STJ ID's that occur in each grid point over the Northern Hemisphere per winter season during strong versus weak EAWM seasons. Grid points shaded red (blue) indicate more ID's occurring during strong (weak) EAWM seasons.

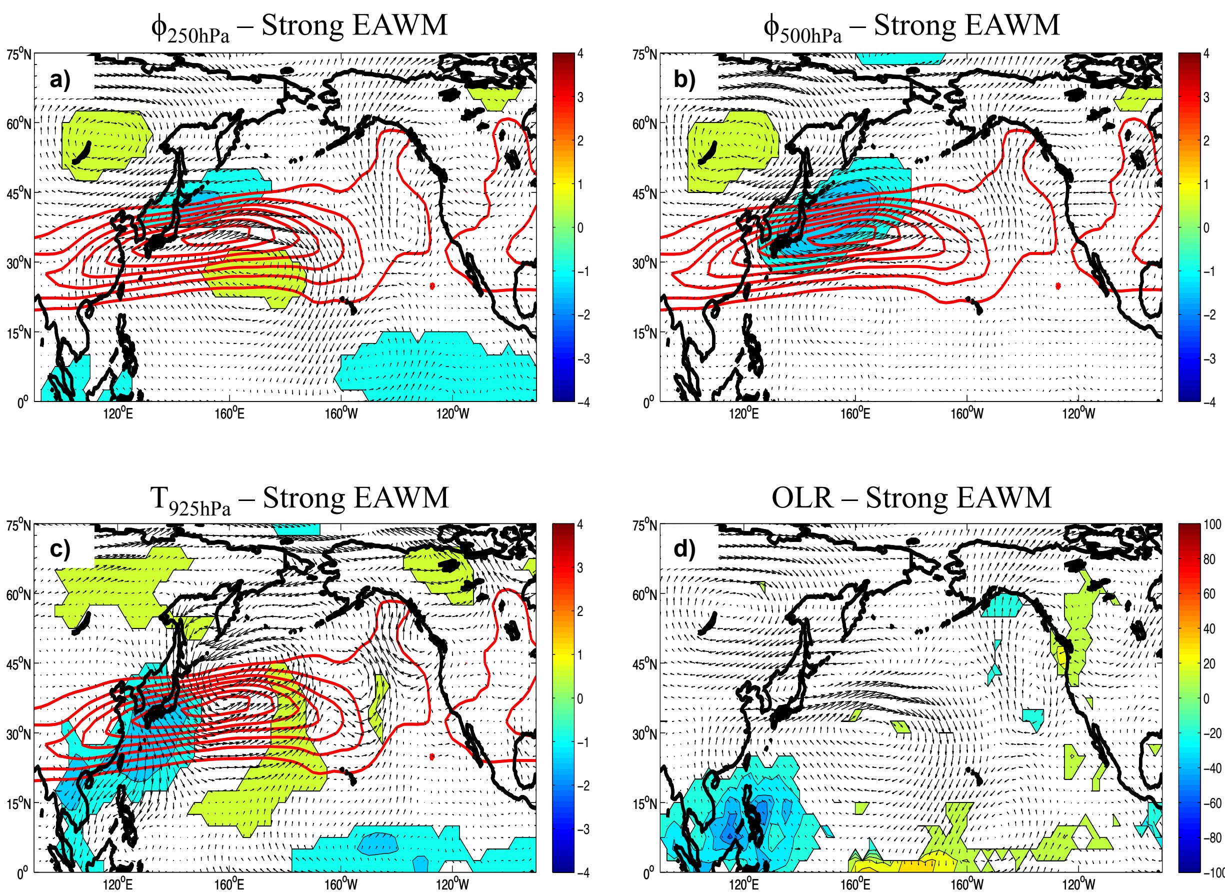

Figure 4.3 Composite large-scale features at time of composite vertical jet superposition in our West Pacific interest region. Shaded regions show positive (negative) standardized anomalous a) ϕ_{250}, b) ϕ_{500}, c) T_{925} and d) Daily-Averaged anomalous (non-standardized) OLR. Anomalous (non-standardized) winds are shown as black vectors with 250 hPa anomalous winds shown in panel d. The red contour represents 250 hPa composite isotachs every 10 m s^{-1} starting at 30 m s^{-1}.

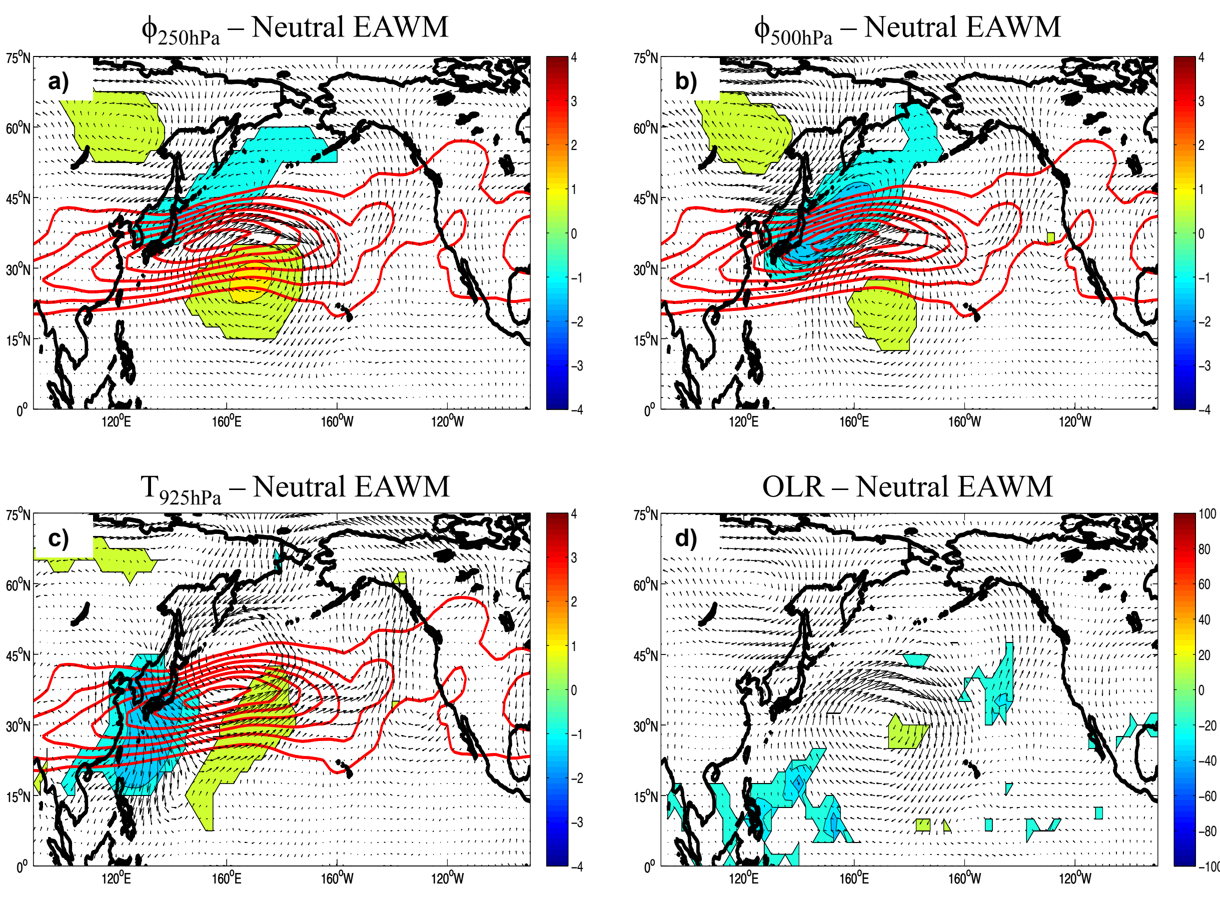

Figure 4.4 Same as Fig. 4.3 except for neutral EAWM season vertical jet superposition events.

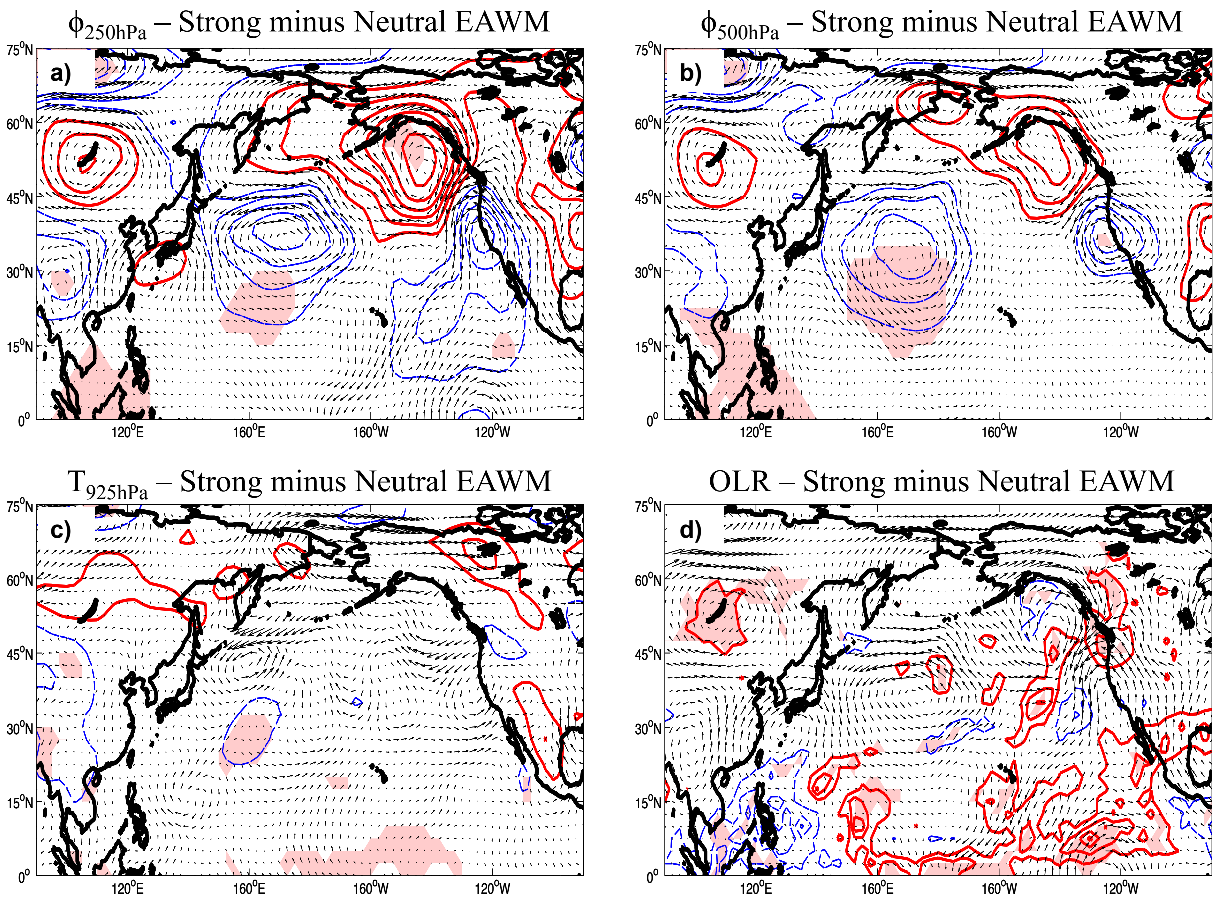

Figure 4.5 Difference between strong and neutral EAWM season West Pacific vertical jet superposition composite environments. The variables plotted in each panel are consistent with Figs. 4.3 and 4.4. Red solid (blue dashed) contours are contoured every a) 20 m for ϕ_{250} starting at + (-) 20 m, b) 20 m for ϕ_{500} starting at + (-) 20 m, c) 2 K for T_{925} starting at + (-) 2 K, and d) 10 W m^{-2} for OLR starting at + (-) 10 W m^2. Shaded pink regions represent areas where the difference between the two environments exceeds 95% statistical significance. Note that all vectors represent differences in wind speed between the two environments.

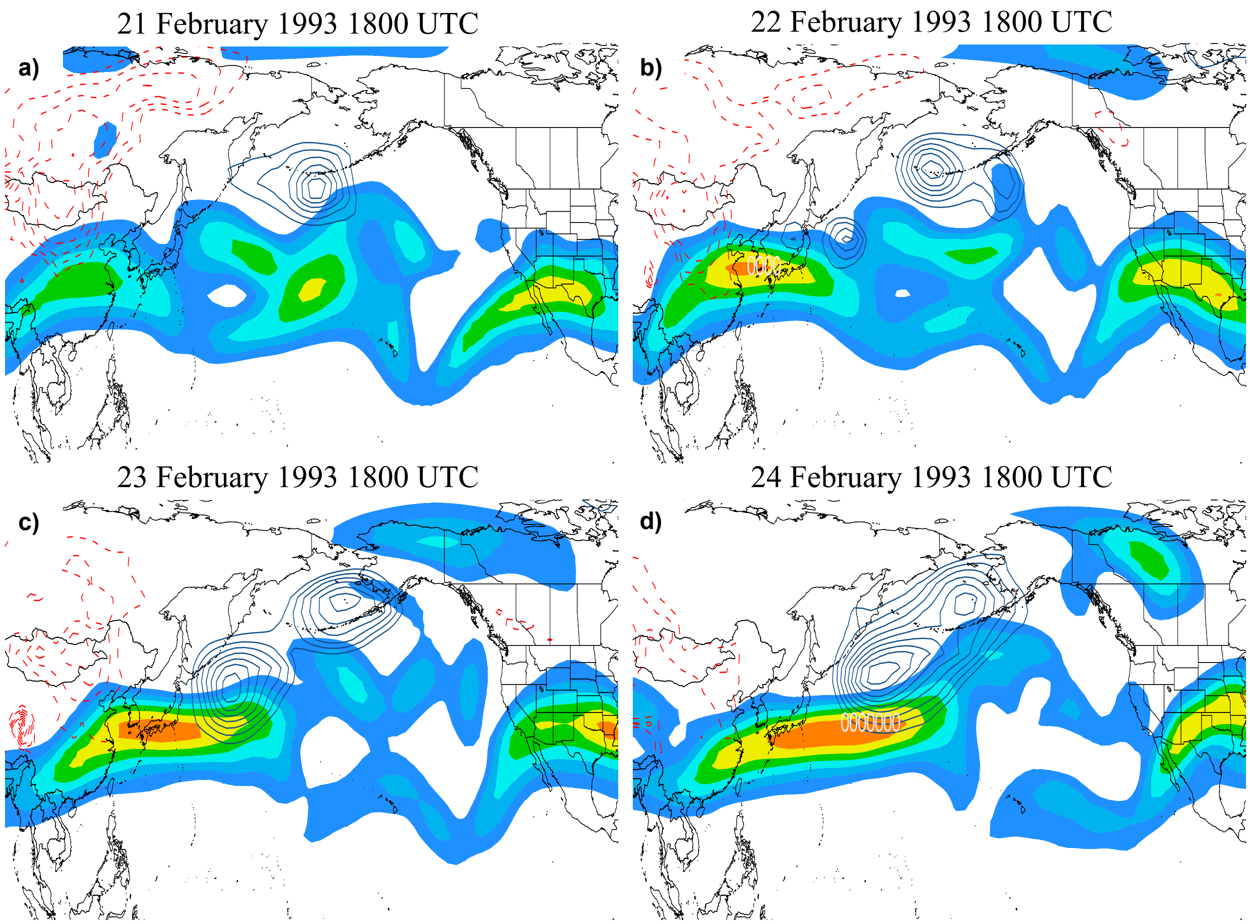

Figure 4.6 250 hPa wind speed (fill every 10 m s^{-1} starting at 30 m s^{-1}) and mean sea level pressure (dark blue solid contours decreasing every 4 hPa starting at 996 hPa; red dashed contours increasing every 4 hPa starting at 1032 hPa) at 1800 UTC on a) 21 February 1993, b) 22 February 1993, c) 23 February 1993 and d) 24 February 1993. White "0" symbols represent grid points where jet superposition ID's were observed using the jet ID scheme described in Chapter 2.

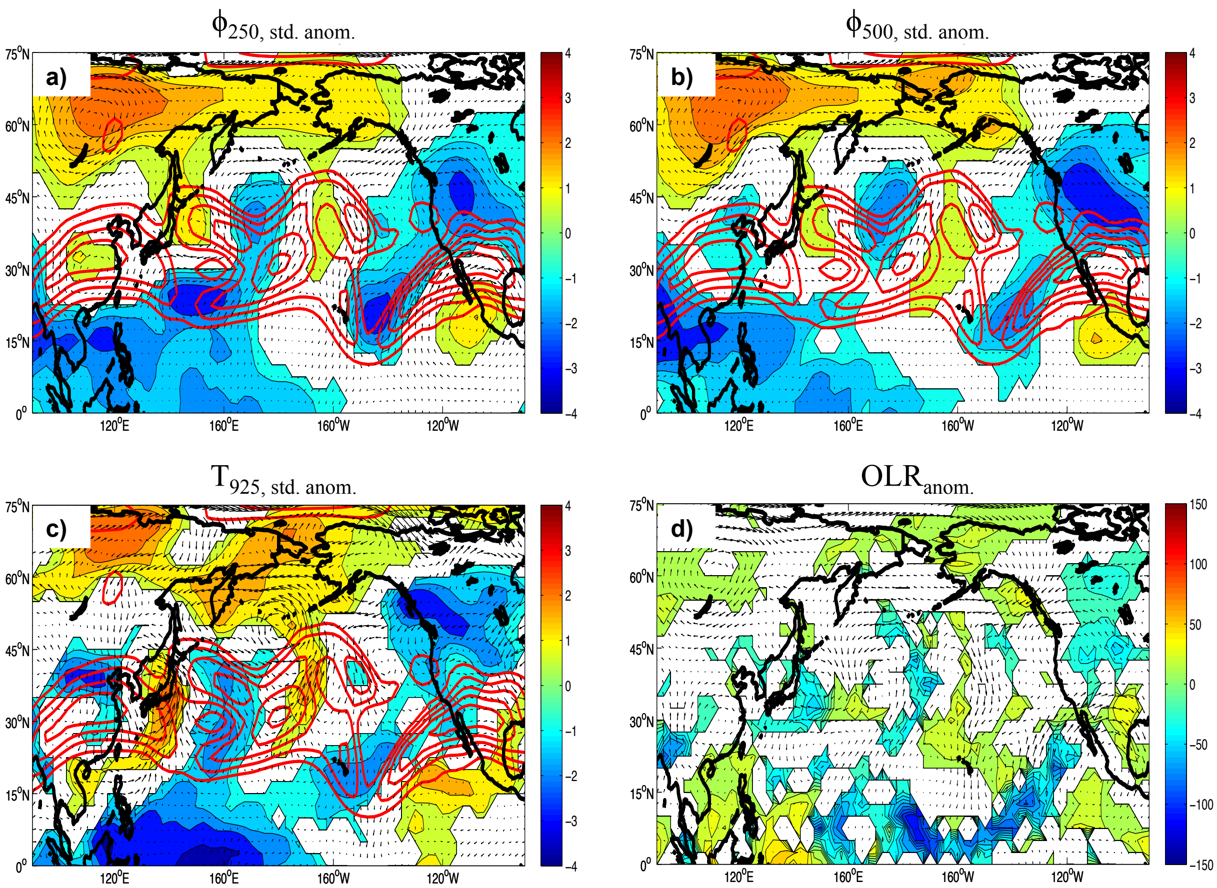

Figure 4.7 Same as Figs. 4.3 and 4.4 but for 21 February 1993.

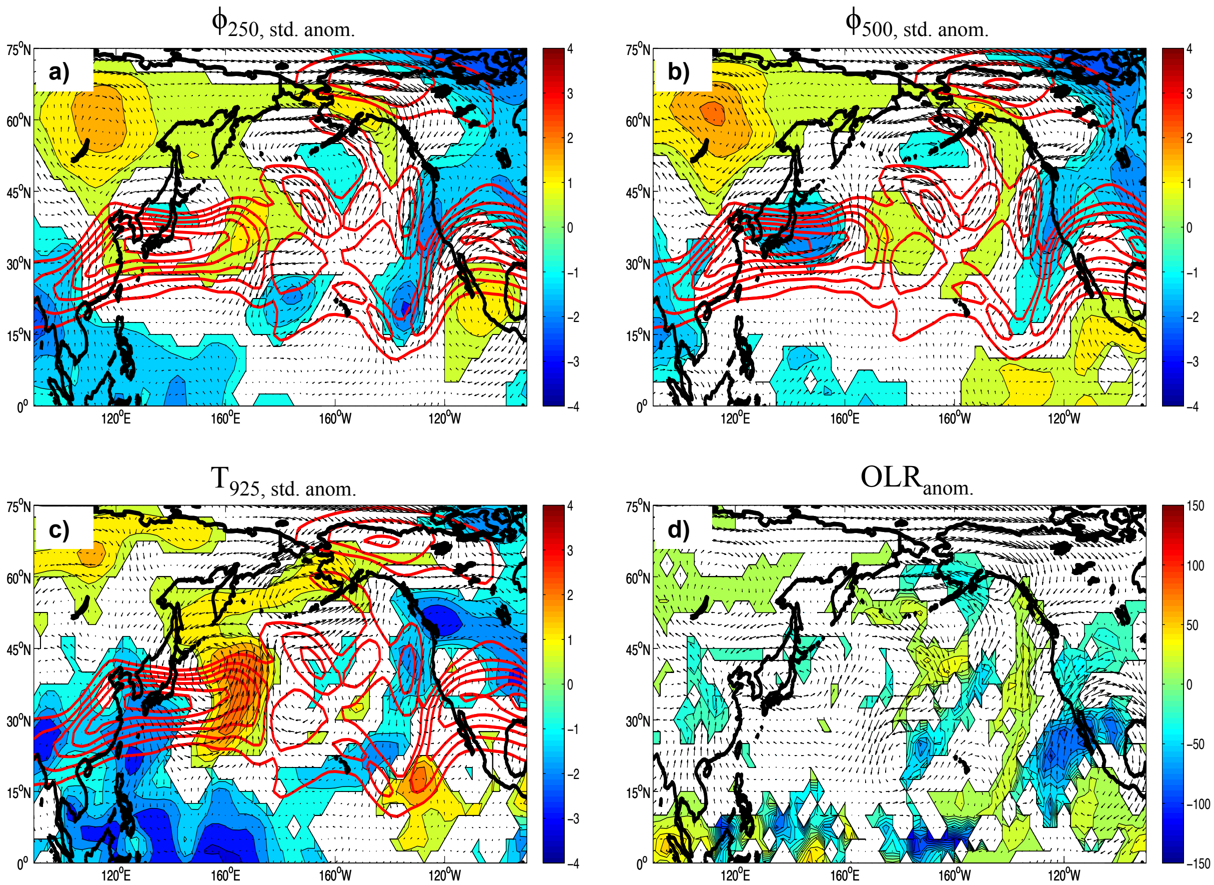

Figure 4.8 Same as Figs. 4.3 and 4.4 but for 23 February 1993.

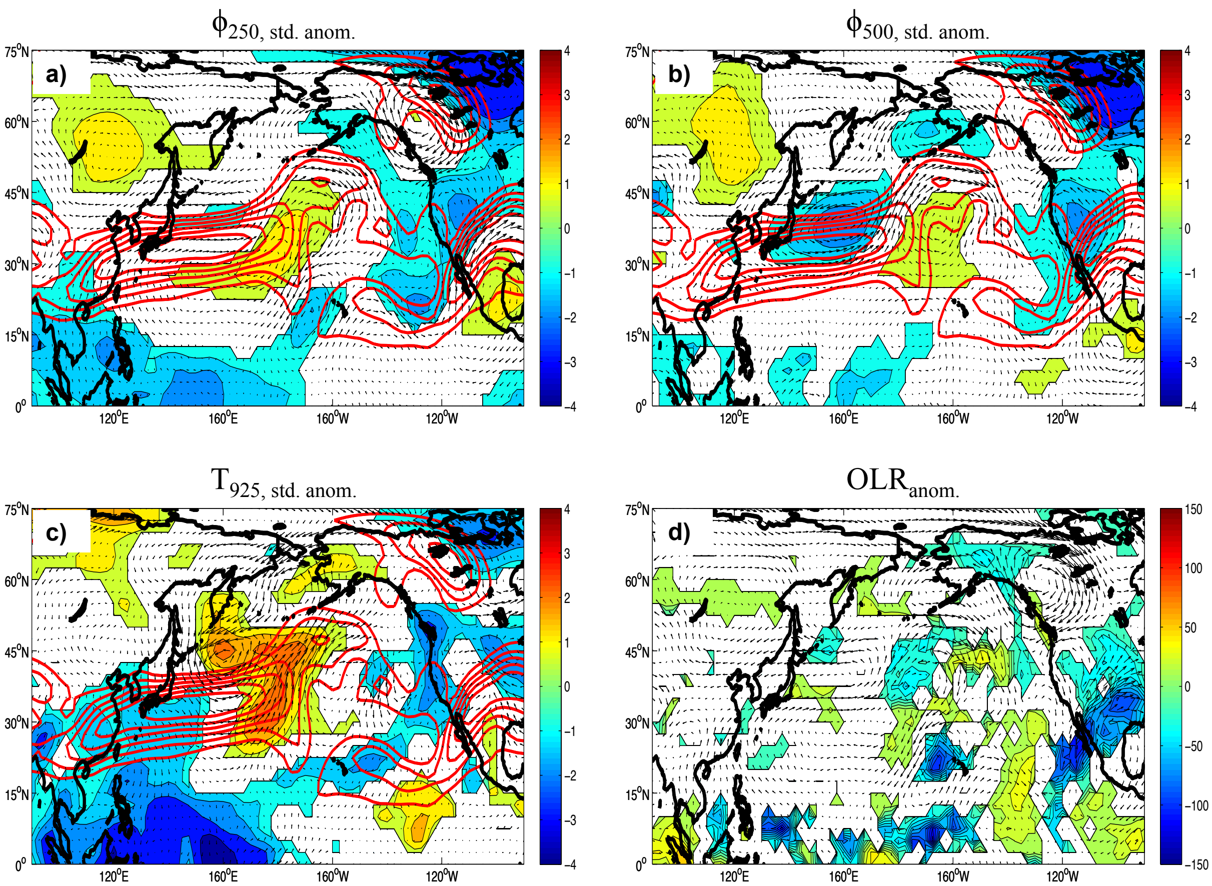

Figure 4.9 Same as Figs. 4.3 and 4.4 but for 24 February 1993.

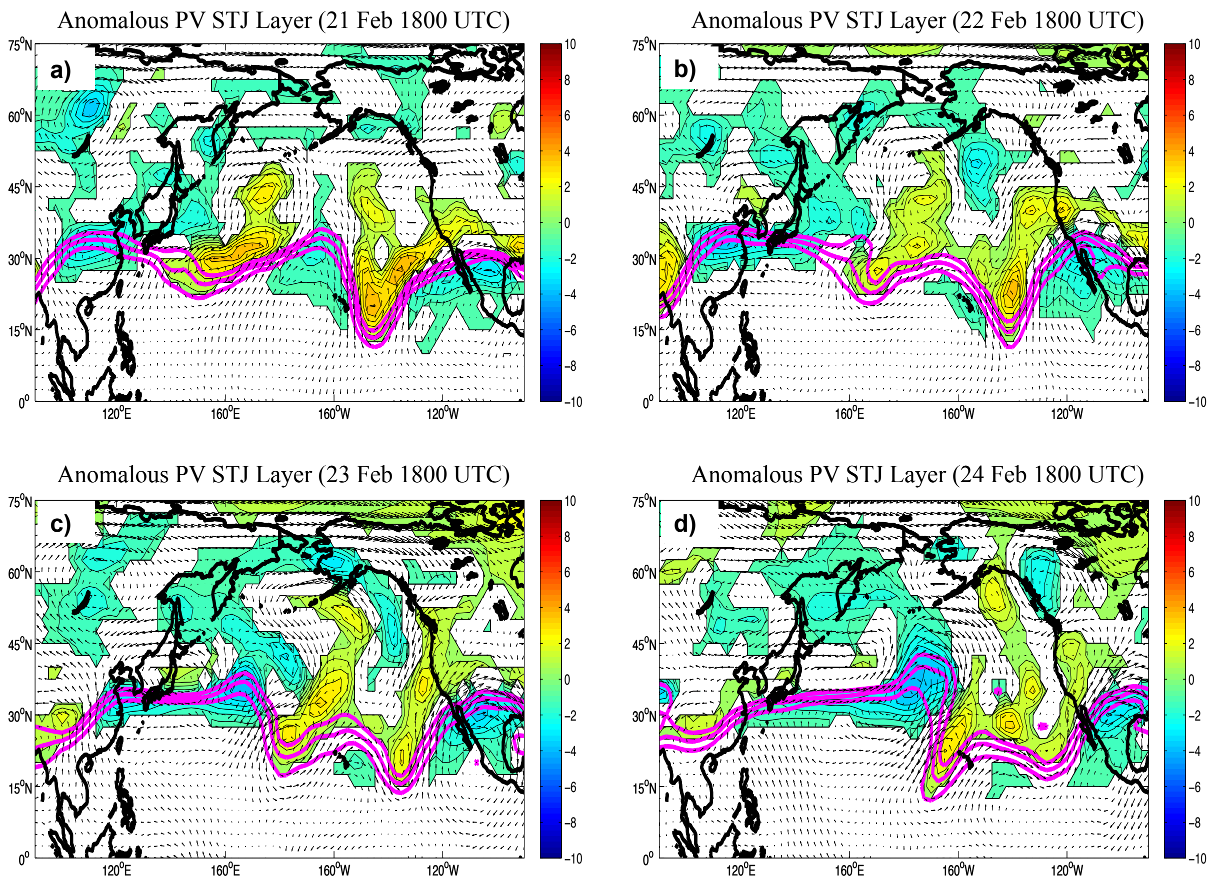

Figure 4.10 STJ (340-355K) isentropic layer-averaged anomalous PV (fill; units PVU), 1-3 PVU surfaces (solid purple contours) and anomalous wind (vectors) at 1800 UTC on a) 21 February 1993, b) 22 February 1993, c) 23 February 1993 and d) 24 February 1993.

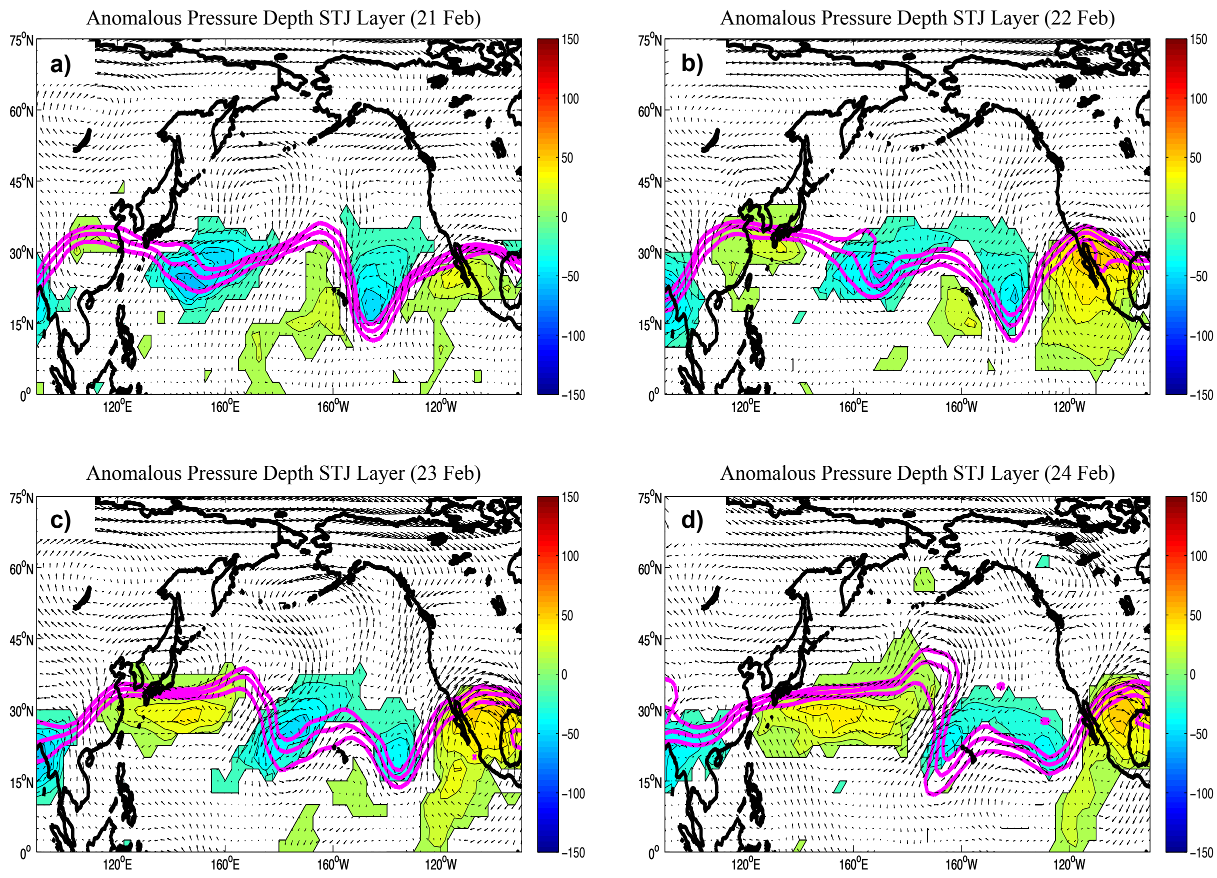

Figure 4.11 STJ (340-355K) isentropic layer-averaged anomalous pressure depth (fill; units hPa), 1-3 PVU surfaces (solid magenta contours) and anomalous wind (vectors) at 1800 UTC on a) 21 February 1993, b) 22 February 1993, c) 23 February 1993 and d) 24 February 1993.

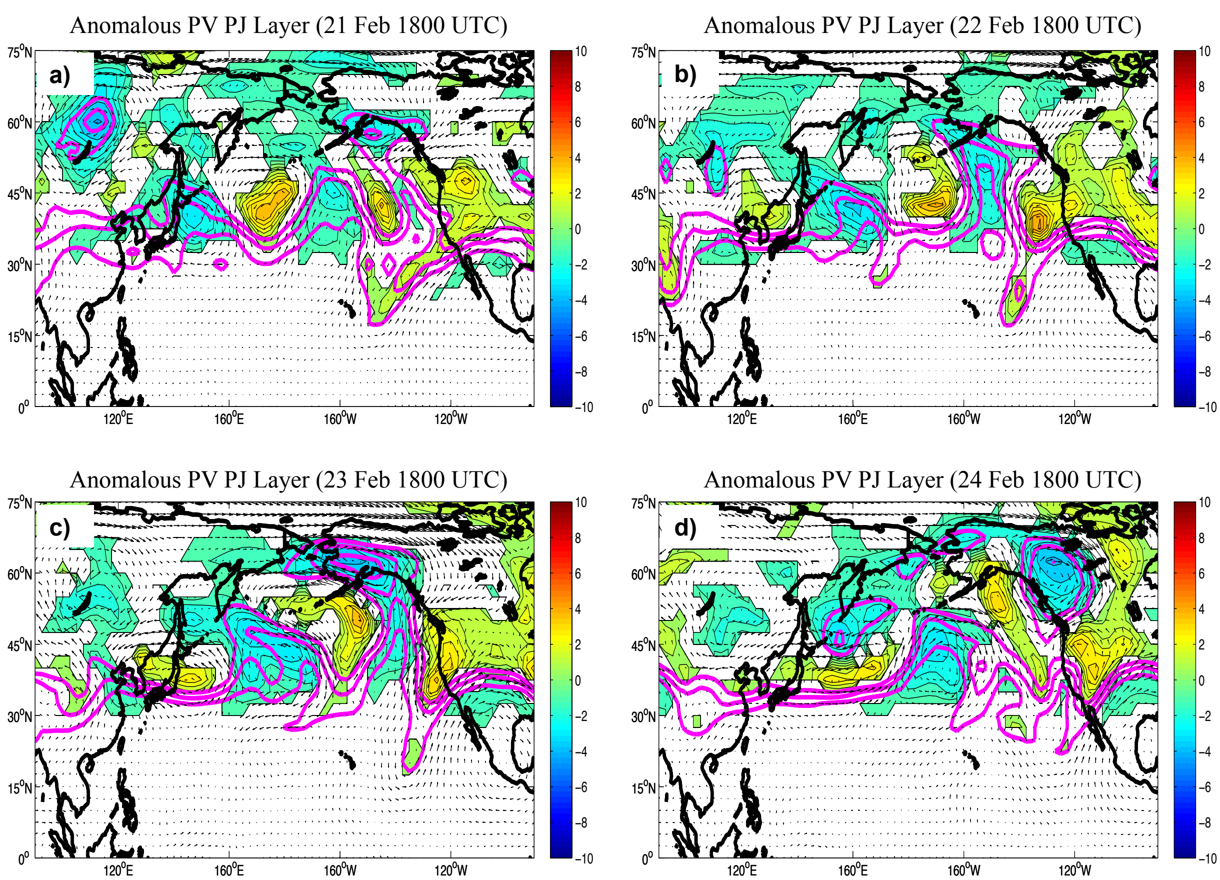

Figure 4.12 Same as Fig. 4.10 but within the PJ (315-330K) isentropic layer.

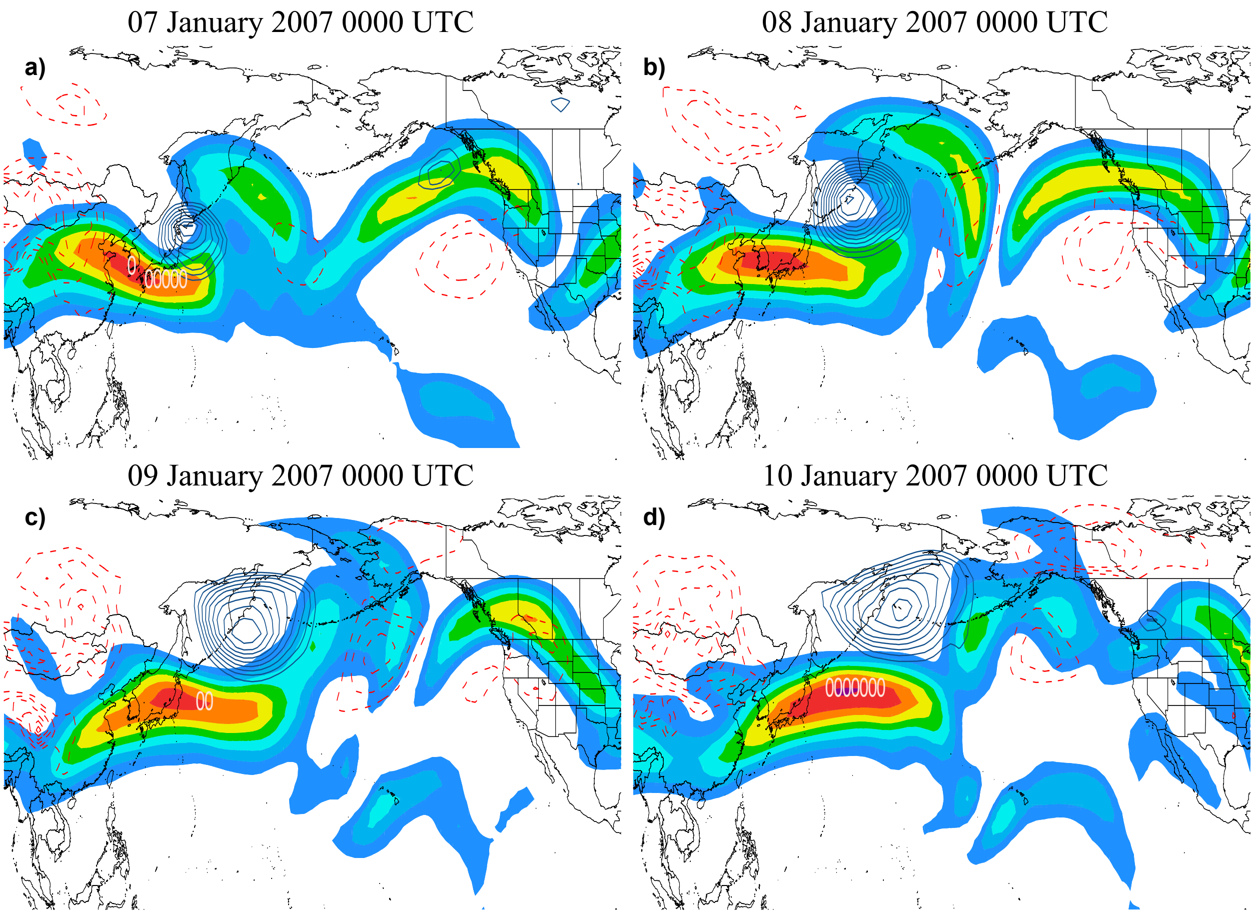

Figure 4.13 Same as Fig. 4.6 but at 0000 UTC on a) 7 January 2007, b) 8 January 2007, c) 9 January 2007 and d) 10 January 2007.

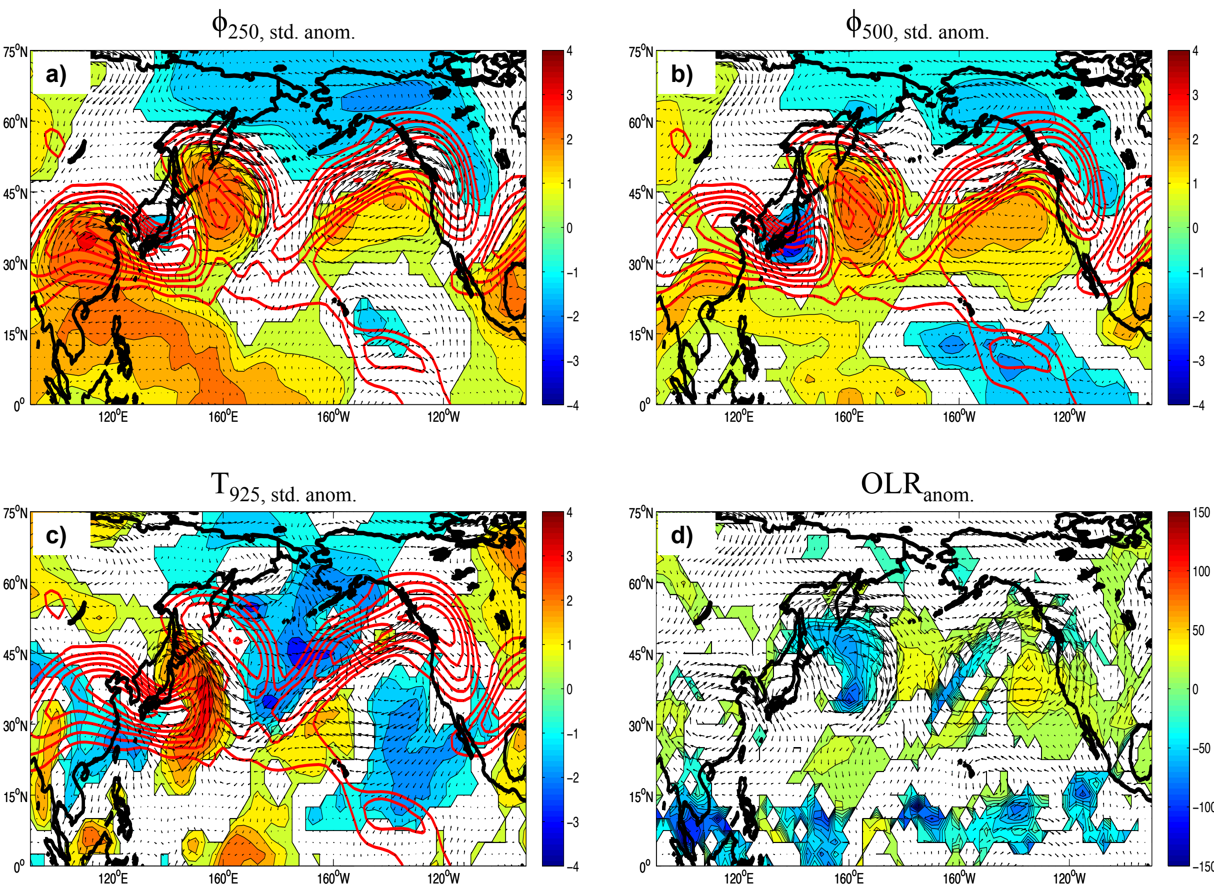

Figure 4.14 Same as Figs. 4.3 and 4.4 but for 7 January 2007.

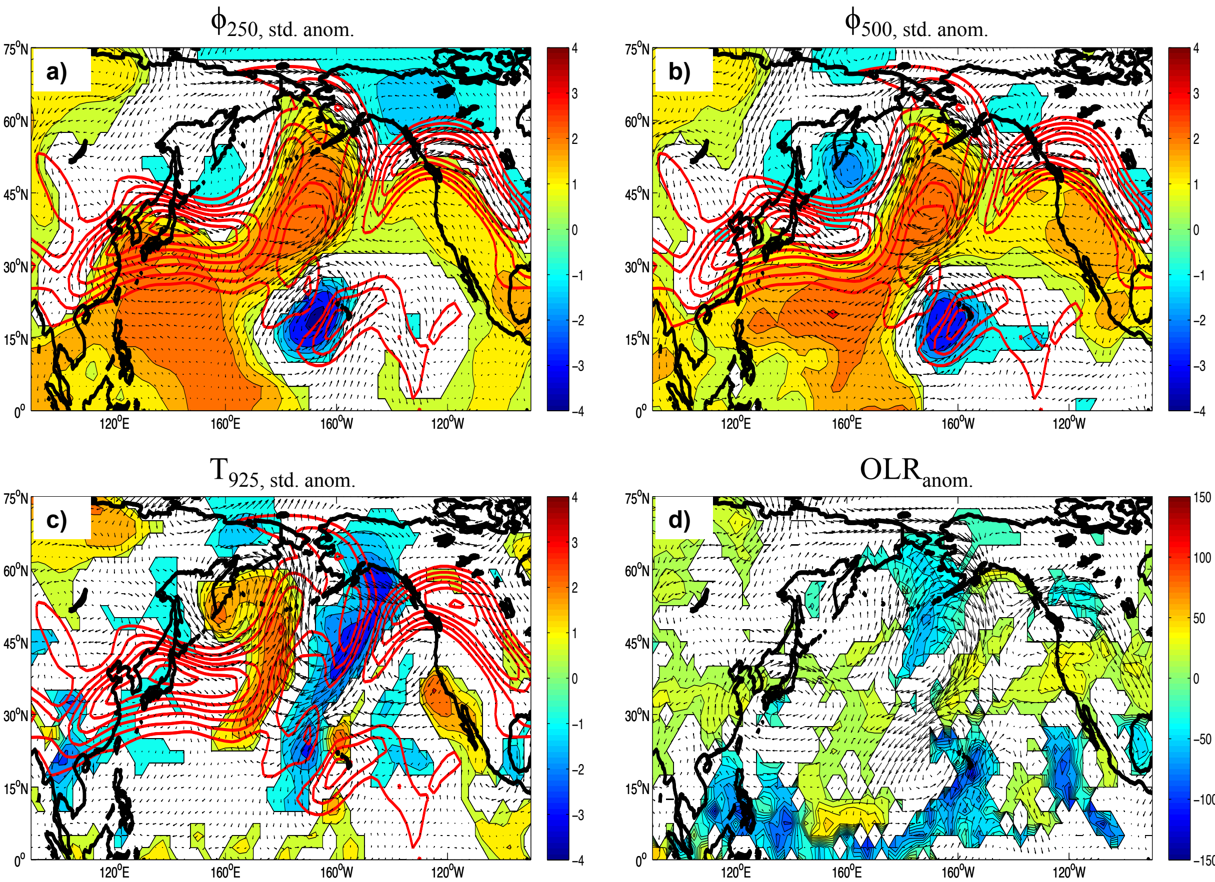

Figure 4.15 Same as Figs. 4.3 and 4.4 but for 9 January 2007.

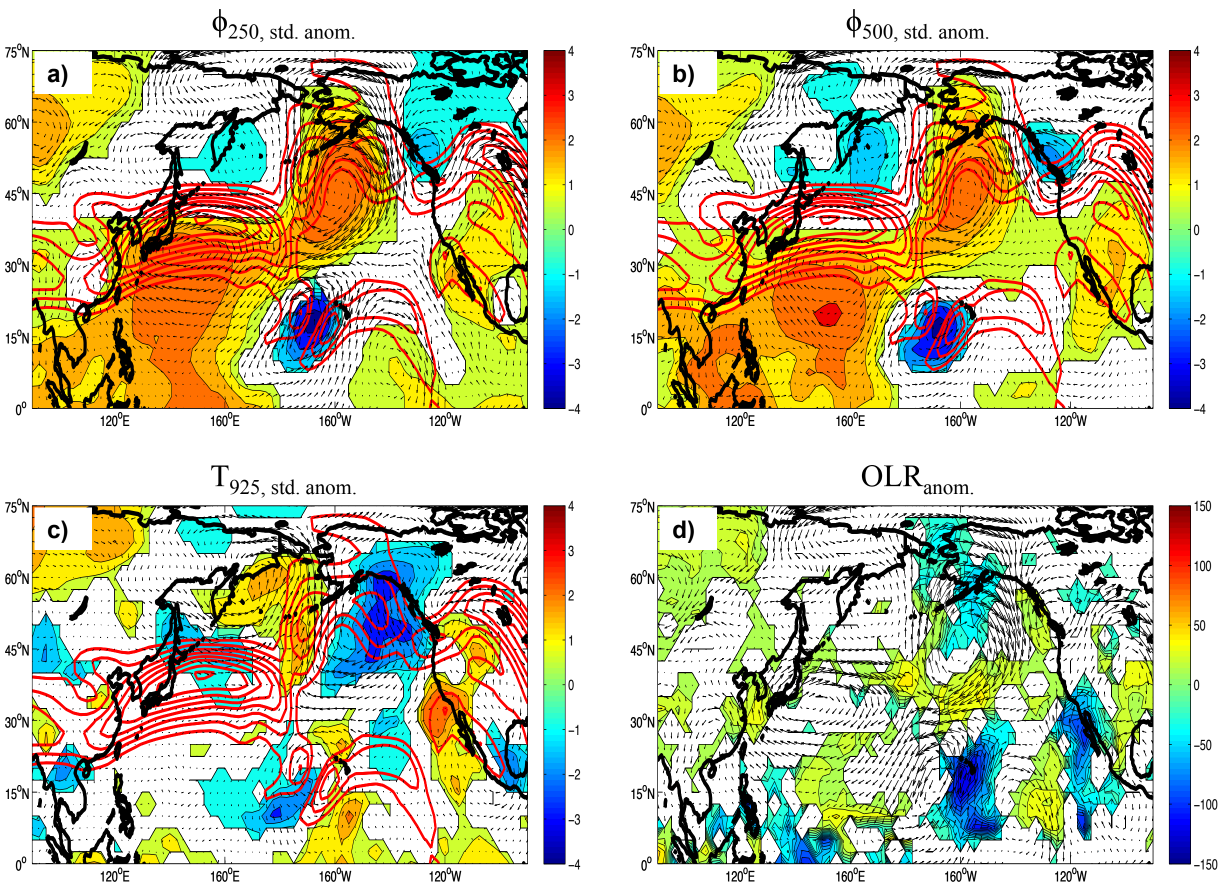

Figure 4.16 Same as Figs. 4.3 and 4.4 but for 10 January 2007.

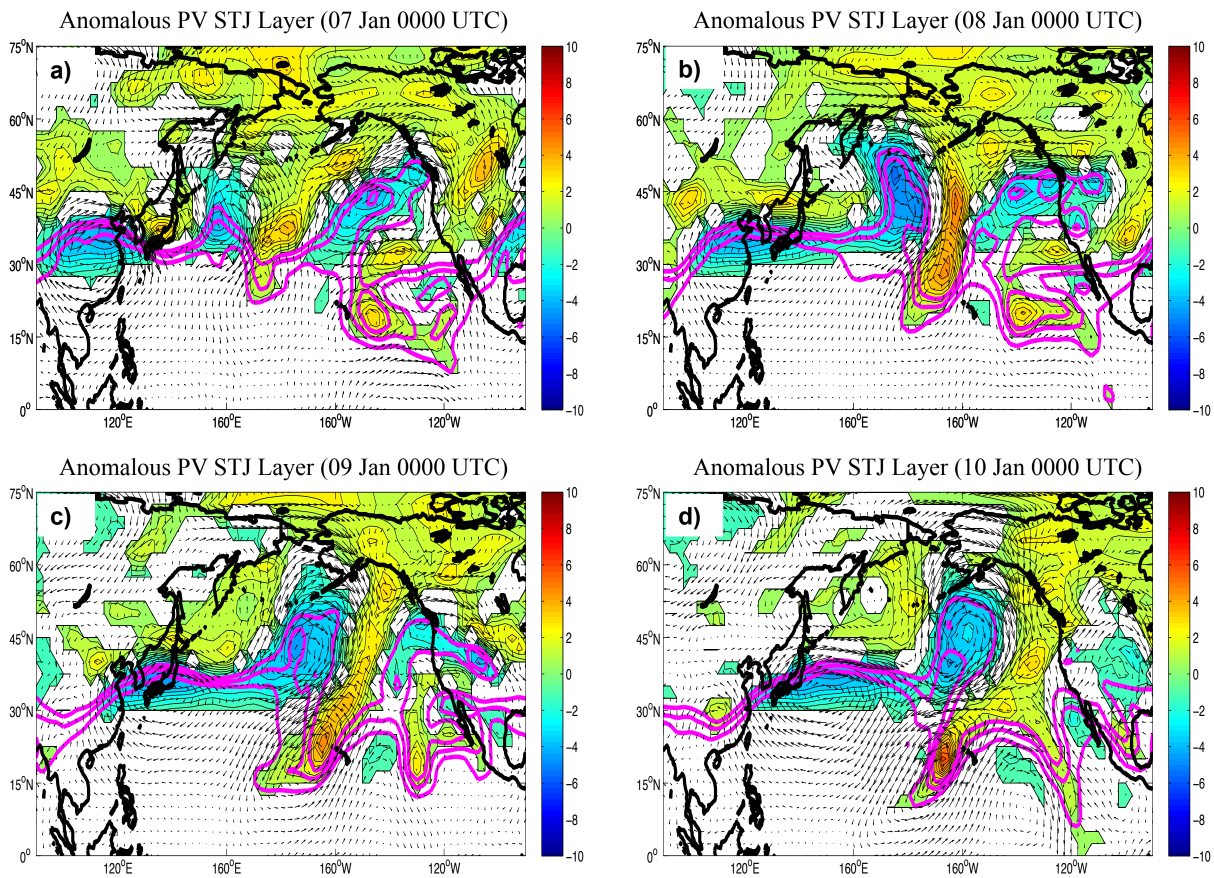

Figure 4.17 Same as Fig. 4.10 but at 0000 UTC on a) 7 January 2007, b) 8 January 2007, c) 9 January 2007 and d) 10 January 2007.

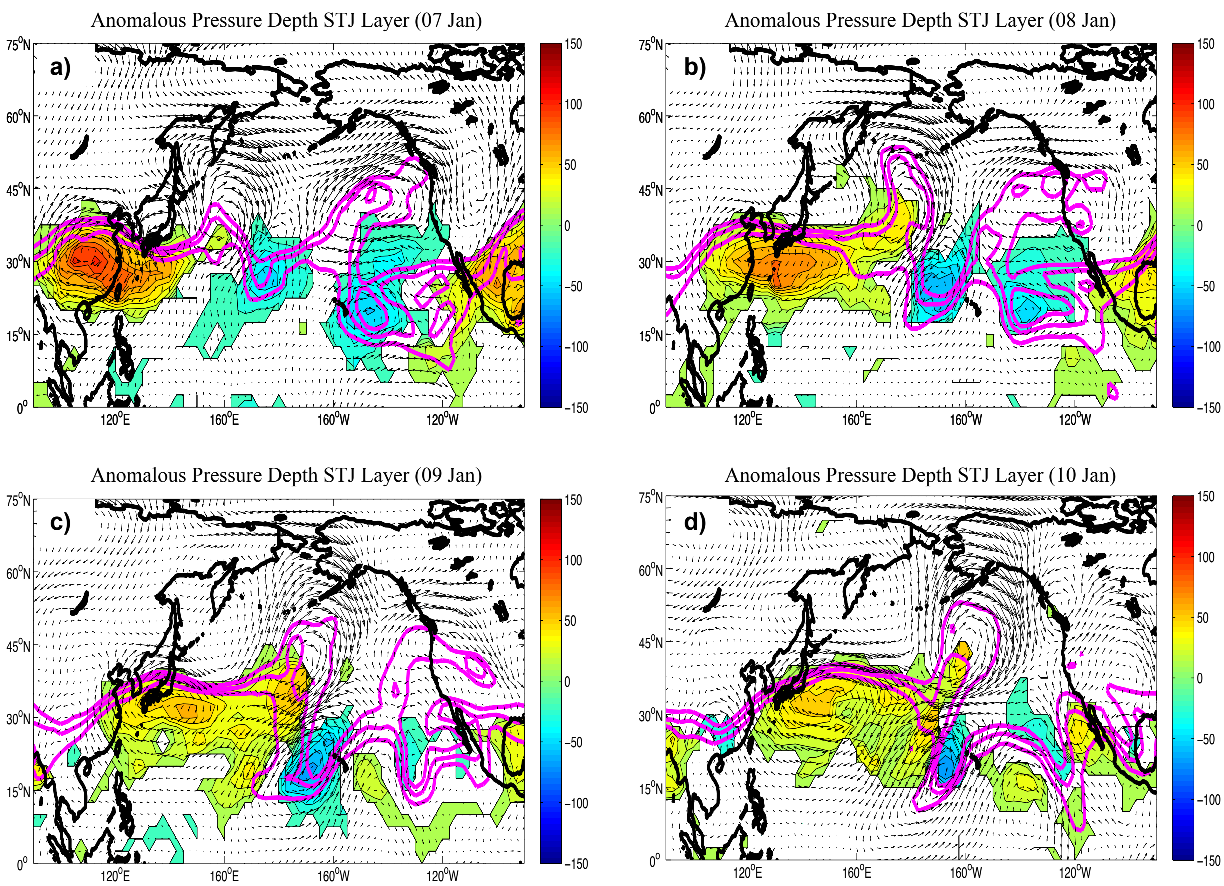

Figure 4.18 Same as Fig. 4.11 but at 0000 UTC on a) 7 January 2007, b) 8 January 2007, c) 9 January 2007 and d) 10 January 2007.

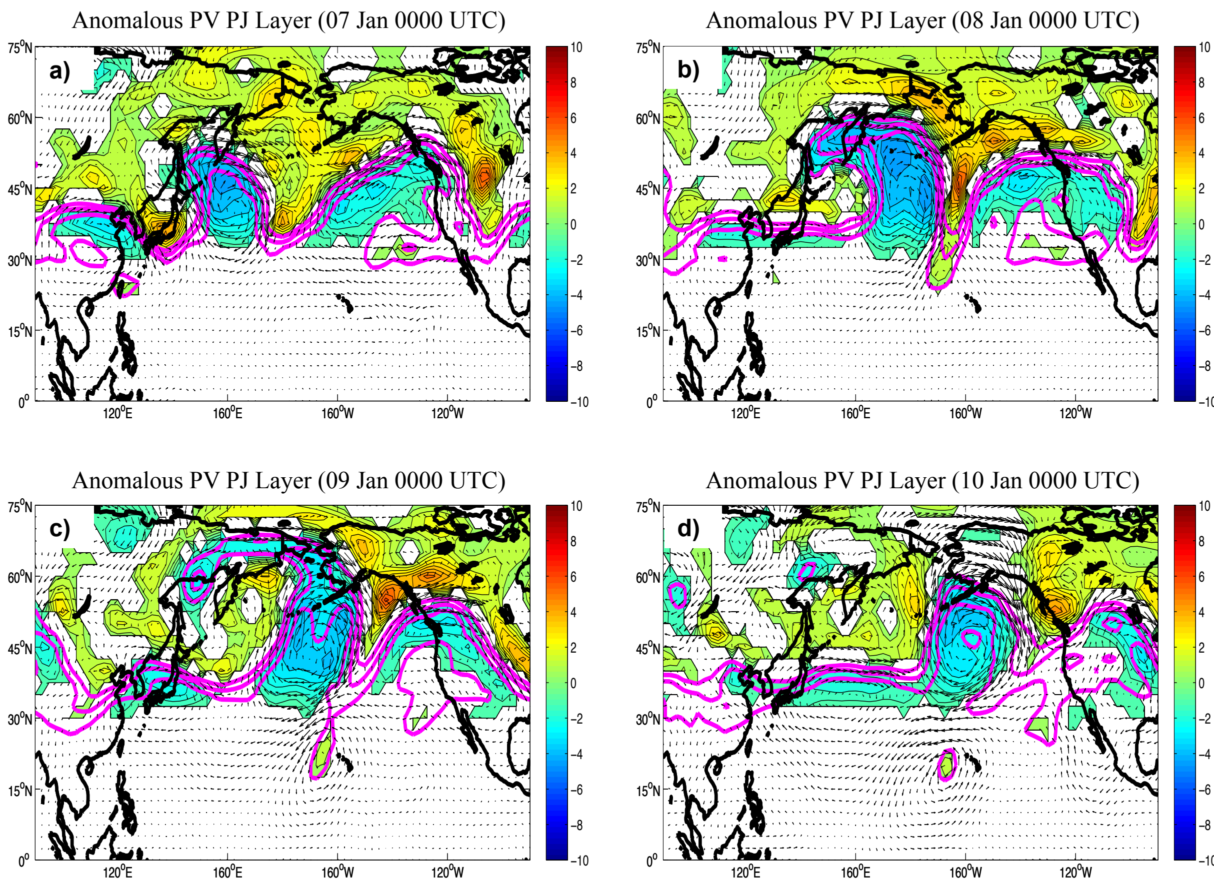

Figure 4.19 Same as Fig. 4.12 but at 0000 UTC on a) 7 January 2007, b) 8 January 2007, c) 9 January 2007 and d) 10 January 2007.

Table 4.1 Strong, Neutral and Weak EAWM seasons identified using the composite EAWMI index from Fig. 4.1. The year listed corresponds to the month of December for that particular DJF boreal winter (i.e., 1979 = DJF 1979-80). Numbers within parenthesis next to a year represent the number of robust vertical jet superposition cases that occurred during that particular winter season. The number of total seasons listed under each category is written in parenthesis next to each column heading.

Strong EAWM Seasons (10)	Neutral EAWM Seasons (13)	Weak EAWM Seasons (8)
1980 (3), 1983, 1984, 1985, 1994, 1995 (4), 1999 (4), 2003 (3), 2005 (1), 2007 (3)	1979 (1), 1981 (2), 1986 (1), 1987 (1), 1990 (3), 1993, 1996 (3), 1998 (4), 2000 (6), 2001 (1), 2002, 2004, 2009 (2)	1982, 1988, 1989, 1991, 1992 (1), 1997, 2006 (1), 2008

Chapter 5

The Evolution of West Pacific Jet Superposition Events and associated Large-Scale Environments after Time of Jet Superposition

5.1 Introduction

In Chapters 3 and 4, the physical processes and large-scale environments conducive to the superposition of the PJ and STJ in the West Pacific were considered. Robust West Pacific vertical jet superposition events are a result of a combination of internal jet dynamics as well as the advection of high-θ_e, low-PV tropical convective outflow into the STJ isentropic layer on the anticyclonic shear side of the West Pacific jet. Regardless of EAWM seasonal strength, it appears that West Pacific superposition events occur preferentially within an environment that contains anomalous ridging on the anticyclonic shear side of the West Pacific jet, an anomalous middle-tropospheric trough poleward of the jet, an anomalous cold surge feature that is a function of the location of the SMH, and convection within the lower latitudes of the Maritime Continent region influenced by a cold surge event in many cases. However, the strength of the EAWM is associated with the frequency of occurrence of vertical jet superposition ID's in the West Pacific (Figs. 3.3 and 4.1).

One research topic that has not been considered up to this point is how West Pacific jet superposition events and associated large-scale features evolve after the time of robust vertical jet superposition (i.e., RQ3 from Chapter 1). Improving understanding of this topic is beneficial for two reasons. First, by understanding how all of these phenomena evolve after superposition occurs, a full understanding of the entire life cycle of robust vertical jet superposition events can be developed. Second, exploring RQ3 can provide insight regarding the influence that large-scale features associated with jet superposition can have on the general circulation of the Northern Hemisphere.

Motivated by the above, the spatial and temporal evolutions of West Pacific jet superposition events and their environments after the time of superposition are investigated in detail in this chapter. Section 5.2 briefly outlines the methodology used in this chapter. Sections 5.3 and 5.4 discuss results pertaining to RQ3 with respect to the 44-case composite as well as the strong/neutral/weak EAWM environments, respectively. A summary of the results from this chapter are presented in Section 5.5.

5.2 Methodology

The same dataset and methodologies employed in Chapters 2-4 are used in this chapter. With respect to addressing RQ3, an analysis of the time evolution of these cases in a composite and/or case-study sense at times T+n (where $n \geq 0$ is the number of days after time of composite jet superpostion) is conducted. Standardized anomalous variables of interest (except for PV, pressure depth, and daily-averaged OLR) and their frequency of occurrence, similar to that of previous chapters, will be investigated.

5.3 Composite Environments Associated with West Pacific Jet Superposition Events after Time of Superposition

Figures 5.1-5.4 show standardized anomalous quantities of interest with respect to composite robust West Pacific vertical jet superposition 1-4 days after time of composite jet superposition, respectively. At time T+1 (Fig. 5.1), the composite jet has extended eastward and weakened to a maximum wind speed in the range of 80-90 m s^{-1}. Figure 5.1a shows a strengthening of the magnitude of $\phi_{250,std.anom.}$ relative to the previous composite day (i.e., Fig. 3.1b), and this feature remains associated with strong anomalous anticyclonic flow. The anomalous negative ϕ on the cyclonic shear side of the composite jet remains about the same magnitude at 250 and 500 hPa (Figs. 5.1a and 5.1b). Figure 5.1c shows that the anomalous cold air associated with anomalous northerly winds over the East and South China Seas still persists, though by this time the feature has started to shift eastward as the jet extends eastward. Anomalous negative OLR values continue to persist near Indonesia (Fig. 5.1d). However, with the eastward movement of the positive $\phi_{250,std.anom.}$ feature equatorward of the jet, the anomalous southwesterlies in the upper troposphere that were in a position to advect anomalous convective outflow away from the Maritime Continent region at time T=0 are now shifting away from the anomalous convection. Thus, the primary mechanism for advecting convective outflow over Indonesia towards the jet is no longer present.

Throughout the rest of the Northern Hemisphere, there are few locations where any of the variables plotted exceed $\pm$ 0.5σ (or $\pm$ 10 W m^{-2} for anomalous OLR) except for northern Russia and Azerbaijan, where significant ϕ anomalies in the mid- to upper troposphere are observed, as well as a warm anomaly in the lower troposphere over the Northwest Territories. A $\sim$ 50 m s^{-1} composite jet resides over the east coast of the U.S., though the wind anomalies associated with this jet do not exceed 0.5σ. Thus, at time T+1, the majority of standardized anomalous large-scale environments exceeding the 0.5σ threshold are located near the West Pacific superposed jet.

At time T+2 (Fig. 5.2), the composite jet continues to extend eastward, maintaining about the same magntiude within its core. While the positive and negative $\phi_{250,std.anom.}$ and $\phi_{500,std.anom.}$ features remain relatively unchanged at this time (with a slight weakening of the negative ϕ anomaly at 500 hPa), these features reside within the right (left) jet exit region as the jet extends (Figs. 5.2a,b). The composite cold surge feature has now weakened substantially, with remnant anomalous northerly winds and cold air present northeast of Indonesia. Anomalous warm air associated with anomalous southerly winds south and east of the center of anomalous cyclonic circulation is observed south of Alaska. In British Columbia, anomalous positive ϕ and anticyclonic flow in the middle to upper troposphere indicate the presence of a composite anomalous ridge. Finally, the areal extent of anomalous convection in the Maritime Continent region, as well as the magnitude of these negative OLR anomalies, decreases. With the anomalous convection and its outflow dissociated from the upper tropospheric anomalous anticyclonic flow on the anticyclonic shear side of the jet, the convective flux of high θ_e, low-PV air is unable to influence the core of the West Pacific jet.

Revisting other notable large-scale environments throughout the Northern Hemisphere, anomalous anticyclonic flow is still present over northern Russia, however the magnitude of $\phi_{250,std.anom.}$

has fallen below the 0.5σ threshold over the majority of the region. The ϕ anomaly at 250 and 500 hPa over the Caspian Sea still remains, shifting slightly northeastward relative to the previous day (Figs. 5.2a and 5.2b). There is a small area where $T_{925,std.anom.} \geq 0.5\sigma$ in this region as well, and this threshold is also exceeded in extreme northern Russia and again within the Northwest Territories (Figs. 5.2c). Lastly, the jet over the western Atlantic has remained relatively stationary, weakening slightly.

At time T+3 (Fig. 5.3), the core of the composite jet continues to extend eastward. The anomalous ϕ features in the jet exit regions are still present in the 250 hPa and 500 hPa composites. The region of $\phi_{250,std.anom.} > 0.5\sigma$ over the Northwestern Territories (i.e., anomalous ridge) expands in areal extent (Figs. 5.3a and 5.3b). Figure 5.3c shows the remnants of the anomalous cold surge propogating eastward, with the area of cold air $\leq$ -0.5σ shrinking. A warm air anomaly associated with the ridge over Alaska still persists, while the warm air anomaly region southeast of the West Pacific jet core shrinks in size. The region of negative OLR values near Indonesia continues to shrink as well (Fig. 5.3d). Outside of the continued presence of a ϕ anomaly just east of the Caspian Sea, the majority of the Northern Hemisphere does not exhibit any features of interest in a composite sense at this time outside of observations discussed within the Pacific basin and near Alaska.

Finally, 4 days after composite West Pacific vertical jet superposition (Fig. 5.4), the majority of large-scale environments referenced earlier begin to dissipate. For example, the maximum wind speed associated with the composite jet decreases, though the jet does extend slightly eastward. The ϕ anomalies at 250 and 500 hPa remain around the same magnitude, again shifting slightly eastward with the extension of the jet (Figs. 5.4a and 5.4b). The cold surge anomaly at 925 hPa has nearly dissappeared. A lower tropospheric warm air anomaly is still present over eastern Alaska and northwestern Canada, though the warm air feature in the jet exit region has weakened such that only a slight signature of this feature remains (Fig. 5.4c). Along with the dissipation of the cold and warm air anomalies observed in the jet exit region, both the areal extent and magnitude of negative OLR near Indonesia continues to decrease. The Caspian sea ϕ anomaly in the mid- to upper troposphere has also weakened by this time.

Figures 5.1-5.4 show that the following elements characterize the large-scale environment thoughout this 4-day period: 1) an eastward extension of the West Pacific jet, 2) the continued presense of the mid- to upper tropospheric positive and negative ϕ anomalies, particularly within the right and left jet exit regions, respectively, 3) the dissipation of the anomalous cold surge event as it propogates eastward across the Pacific ocean, 4) a disconnect between the anomalous convection and West Pacific jet, and 5) the lack of any significant features of interest outside of the Pacific basin besides the anomalous positive ϕ features in northern Russia and near the Caspian Sea. The next subsection explores the percentage of cases within the composite exhibiting these 5 features.

5.3.1 *Frequency of Occurrence of Key Large-Scale Environmental Features and their Coherence Post-Jet Superposition Occurrence*

Recall that, in Chapter 3, the percent occurrence of cases for each grid point in which the $\pm$ 0.5σ threshold was exceeded for all standarized variables of interest was considered. This was done in order to determine whether the observed features in the 44-case composite occurred within the majority of cases considered. The same analysis is repeated in this subsection for times T+1 through T+4 in order to determine if the large-scale evolutions shown in this section occur consistently throughout the majority of the 44 cases. Also, this provides insight as to the times at which the large-scale environments within each case "diverge" from each other. Such an occurrence can lead to the smoothing of composite results, weakening the magnitude of anomalous variables that appear within the composites.

Figures 5.5-5.8 show plots of the frequency of occurrence of grid points $\geq \pm$ 0.5σ out of the 44 total vertical jet superposition events used in our composite analysis at times shown in Figs. 5.1-5.4. In the interest of comparison with Fig. 3.3, $\vec{u}_{250,std.anom.}$ is considered. With respect to $\vec{u}_{250,std.anom.}$, as many as $> 90\%$ of cases fulfill this requirement within the West Pacific jet core at time T+1 (Fig. 5.5a). $\geq$ 70-80$\%$ of cases exhibit grid points $\leq$ -0.5σ in regions flanking the jet core meridionally. Throughout the evolution of the extension of the composite jet (Figs. 5.6a, 5.7a and 5.8a), the frequency of occurrence of all wind magnitude anomalies associated with the extended, narrow jet remains $\geq$ 60-70$\%$. Within the western portion of the jet, the percent occurrence decreases throghout the extension. Thus, while the eastward extension of the jet occurs within the majority of cases included in the composite, significant jet variablity exists upstream.

Panel b in Figs. 5.5-5.8 show that the $\phi_{250,std.anom.}$ feature on the anticyclonic shear side of the composite jet occurs in as many as 90% of cases or more in some grid points as this anomaly moves eastward over time. Interestingly, the number of events where the negative standardized anomalous threshold is met at 250 hPa with respect to the anomalous negative ϕ feature in the composite left jet exit region increases between days 1 and 2 after superposition (Figs. 5.5b and 5.6b), remaining relatively constant even up to time T+4 (Figs. 5.7b and 5.8b). Thus, the persistence of the anomalous ϕ features within the jet exit region is consistent amongst the majority of cases comprising the composite.

The findings above are also observed at 500 hPa (Figs. 5.5-5.8 panel c). The number of cases where $\phi_{500,std.anom.} \leq$ -0.5σ on the cyclonic shear side of the jet (associated with the anomalous trough-like feature) is as high as $\geq$ 90% of cases at time T+1 (Fig. 5.5c), with the maximum percent of cases in the core of this anomaly remaining somewhere between $\geq$ 70-80% through time T+4. The anomalous positive ϕ feature equatorward of the jet at 500 hPa exceeds the 0.5σ threshold in more cases at time T+4 than time T+1 (Figs. 5.5c vs. 5.8c).

Finally, with respect to the eastward propogation and dissipation of the anomalous cold surge feature, we observe a decrease in the number of cases exhibiting anomalous cold air exceeding the 0.5σ threshold (panel d of Figs. 5.5-5.8). Over 50-70% of cases are associated with the development of the warm air anomaly near Alaska throughout the 4-day period. This coincides with a weak signature (based on this metric) of consistent anomalous positive ϕ in the mid- to upper troposphere, where the highest percent occurrence over the Northwest Territories exceeds 60% of cases at times T+2 and T+3 (Figs. 5.6b,c and 5.7b,c). Therefore, many of the robust superposition cases exhibit anomalous ridging and warming in this region within a few days after superposition.

Recall that regions of anomalous positive ϕ at 250 hPa and 500 hPa were identfied over the Caspian Sea and northern Russia. These features occur within > 50% of cases at times T+1, T+2 and T+3 (panels b and c of Figs. 5.5-5.7). At time T+4, the percent occurrence of ϕ over northern Russia disspiates, and the percent occurrence maximum over the Caspian Sea shifts northeastward.

While there are some other regions of the hemisphere that exhibit grid points exceeding 50% for $\vec{u}_{250,std.anom.}$, $\phi_{250,std.anom.}$, $\phi_{500,std.anom.}$ and $T_{925,std.anom.}$, these regions are not associated with any features of interest from the composites of Figs. 5.1-5.4.

To summarize, Figs. 5.5-5.8 show that the the occurrence of an extended jet, anomalous ϕ maximum and minimum at 250 hPa and 500 hPa, dissipation of the northerly cold surge anomaly and anomalous warm air in Alaska at 925 hPa occur within the majority of the cases included in the composite. The evolution of these features is consistent up to 4 days after superposition occurrence. These results suggest that the large-scale environments associated with the composite jet after the occurrence of robust jet superposition may play a role in the extension of the jet as well as phenomena that develop as a result of this jet extension, including the formation of significant surface cyclones in the left jet exit region of the composite jet.

5.4 Evolution of Strong, Neutral and Weak EAWM Season Jet Superposition Events

In Chapter 4, it was concluded that although jet superposition events occur more (less) frequently during strong (weak) EAWM seasons, the large-scale environments conducive to the superposition of the PJ and STJ are similar in both types of seasons. This analysis holds true not only at the time of robust superposition occurrence, but also at times prior to superposition. In this section, analysis of the evolution of the large-scale environments after the time of superposition will be considered for cases that occur within strong, neutral and weak EAWM environments.

Figures 5.9 and 5.10 show the same variables as Figs. 5.1-5.4, except only strong EAWM cases are composited and only at times T+2 and T+4 relative to composite superposition. Many similarities exist at time T+2 between the strong EAWM composite and 44-case composite environments (Figs. 5.2 vs. 5.9), including the extension of the West Pacific jet, eastward propogation of the anomalous positive (negative) ϕ feature on the anticyclonic (cyclonic) shear side of the composite jet, the demise of the cold surge event near eastern China and the movement of upper tropospheric anomalous anticyclonic flow eastward and away from the anomalous negative OLR over Indonesia. A greater areal extent of $\phi_{250,std.anom.} \geq 0.5\sigma$ is observed over the Northwest Territories in the strong composite relative to the 44-case composite (Figs. 5.9a,b), suggesting that the downstream ridge in the composite strong environment near eastern Alaska is stronger relative to the 44-case composite. Also, anomalous warm air at 925 hPa is more widespread and greater in magnitude compared to Fig. 5.2c (Fig. 5.9c).

At time T+4 days, the large-scale environments discussed above within the strong EAWM composite environment are again similar to those observed within the 44-case composite (Figs. 5.10 vs. 5.4). One difference between the two environments is that the composite jet core is stronger in magnitude over the Pacific within the strong EAWM environment. This is also true for the anomalous ridge over northwestern North America. Anomalous convection appears to persist longer near Indonesia in the strong composite, whereas in the 44-case composite, anomalous convection decreases by this time.

Considering the rest of the Northern Hemisphere, note the negative ϕ anomaly at 250 hPa associated with a lower tropospheric cold air anomaly near the equator from the dateline eastward to $\sim$ 90°W longitude at times T+2 and T+4 (Figs. 5.9a,c - 5.10a,c). This feature is not as strong within the 44-case composite, though a slight hint of negative anomalous ϕ appears at these times. As for the region of positive $\phi_{250,std.anom}$ near the Caspian Sea in the 44-case composite, an analogous feature is present further equatorward near Oman, decreasing in magnitude over the 4 day period (Figs. 5.9a,b - 5.10a,b). Such a decrease in magnitude is also observed for the ϕ anomaly in northeastern Russia, consistent with what is observed in this region within the 44-case composite.

Figures 5.11 and 5.12 show the percent occurrence of the features shown in Figs. 5.9-5.10. With respect to the evolution of the composite jet, wind speeds exceeding the 0.5σ threshold within the jet core occur for as many as $\geq$ 80$\%$ of cases at times T+2 and T+4 as the jet extends (Figs. 5.11a - 5.12a). As for the reduction in wind speed north (south) of the jet, this occurs in as many as $>$ 70-80$\%$ of strong EAWM cases both at T+2 and T+4. As the negative wind anomalies at 250 hPa move eastward over time, the areal extent of grid points exceeding 50$\%$ of cases decreases for the poleward negative anomaly feature, but the equatorward feature maintains a similar geometry.

The anomalous cyclonic (anticyclonic) feature positioned in the left (right) jet exit region occurs within the majority of strong EAWM cases (panels b and c of Figs. 5.11 and 5.12). The mid- to upper tropospheric anomalous ridge over southeastern Alaska and northwestern Canada appears within 50-70% of cases at these times, with many of the cases meeting the 0.5σ threshold for standardized anomalous ϕ further east over North-Central Canada at time T+4 relative to T+2. While the cold surge feature east of Japan at time T+1 is present in nearly all of the strong EAWM cases (not shown), the frequency of occurrence of this feature as it weakens and continues to move eastward decreases to 50-60% of cases by time T+4 (Fig. 5.12d). As for the warm air anomaly associated with the ridge, the majority of cases exhibit $T_{925,std.anom.} > 0.5\sigma$ in the eastern Pacific, Alaska and northwest Canada (Figs. 5.11d and 5.12d).

The presence of negative $\phi_{250,std.anom.}$ and cold air at 925 hPa within the equatorial eastern Pacific occurs within as many as 70-80% of strong EAWM cases at all times shown. The ϕ anomaly near the Caspian Sea exhibits a frequency of occurrence of 50-60% (Figs. 5.11b,c - 5.12b,c) at time T+2. By time T+4 (Figs. 5.12b,c), the 0.5σ threshold is still met for over half of the cases for several grid points over Saudi Arabia, though Fig. 5.10a and 5.10b show no composite ϕ anomaly exceeding this threshold at this time. This may be due to the fact that this feature may only barely exceed the threshold in many cases, but is well below in others such that, in the compositing, no feature appears in Fig. 5.10. Other features, such as the negative $\phi_{250,std.anom.}$ and $\phi_{500,std.anom.}$ features over Indonesia, appear within 50-70% of strong EAWM cases, though this is not observed within the 44-case composite.

5.4.1 *Strong vs. Neutral EAWM Post-Jet Superposition Evolution*

It was shown in the previous chapter that the large-scale envirnoments conducive to jet superposition in the West Pacific within strong EAWM seasons were very similar to those present within neutral EAWM seasons. To determine whether or not such an observation holds true after time of jet superposition occurrence, Figs. 5.13 and 5.14 consider differences between strong and neutral EAWM superposition environments at times T+2 and T+4. Fig. 5.13 overall shows similar differences observed between the two composite environments as that of Fig. 4.5.

A few of the large-scale environments discussed throughout this chapter exhibit statistically significant differences in magnitude between the two composite environments. For example, as the 500 hPa anomalous trough north of the jet core propogates eastward, the strong EAWM environment exhibits a significantly stronger trough relative to the neutral environment (panel b of Figs. 5.13 and 5.14). While the anomalous ridge over Alaska and northwest Canada is consistently stronger in magnitude in the strong EAWM composite at both times, significant differences are only observed at time T+4. The same observation holds true for anomalous negative ϕ at 250 and 500 hPa over the northeastern U.S., where this anomalous trough may be the result of the anomalous ridge upstream.

Convection over Indonesia consistently remains significantly stronger at its core in the strong EAWM composite (Figs. 5.13d and 5.14d). OLR values are significantly greater in the strong environment east of the anomalous Indonesian convection where anomalous negative $\phi_{250,std.anom.}$ and $T_{925,std.anom.}$ were observed in Figs 5.9 and 5.10. This is tied to significant differences in temperature, though the temperature differences at 925 hPa are less than 2 K (Figs. 5.13c and 5.14c).

Over northern Europe, ϕ remains significantly lower in the strong EAWM environment over the timeframe at 250 and 500 hPa (Figs. 5.13a,b and 5.14a,b). This is associated with significantly colder lower tropospheric temperatures extending equatorward towards northeastern Africa at time T+2 (Fig. 5.14b), though the areal extent of this significance is reduced at time T+4 (Fig. 5.14c). Larger ϕ is observed south of the Caspian Sea as well as southwest of Lake Baikal. While a "wavetrain" of ϕ differences resides in the northern Atlantic and western Europe, only the regions of maximum differences west of Africa and the UK possess statistical significance.

Although the differences shown in Figs. 5.13 and 5.14 have a similar spatial distribution and magnitude to that of Fig. 4.5, regions of statistical significance are greater in extent at times after superposition relative to at time T=0. Despite this, the strong and neutral seasons produce similar large-scale environments associated with the extension of the West Pacific jet post-superposition. Thus, the West Pacific jet and associated large-scale environments evolve in a similar fashion within the strong and neutral environments.

5.4.2 *Weak EAWM Environment Jet Superposition Evolution*

Although only 2 of 44 West Pacific vertical jet superposition events occur during weak EAWM seasons, the analysis of these events in Chapter 4 revealed the same large-scale evolutions as observed in the strong and neutral composite environments. The case study analysis methods in the previous chapter are used to provide preliminary insight towards determining similarities and differences in large-scale evolutions for the two weak EAWM cases in this subsection.

5.4.2.1 *24 February 1993 Case*

Figure 5.15 shows the same variables as that of Figs. 5.1 and 5.9, but for the 24 February 1993 case at time T+2 (i.e., 26 February 1993). Similar to the composite environments, the West Pacific jet is extended and associated with a ridge over the eastern Pacific (Figs. 5.15a,b). Anomalous negative ϕ is present west of the continental U.S. with a downstream anomalous ridge over the Atlantic. Anomalous cold air is still present in the South China Sea and near the equator. Anomalous warm air resides at 925 hPa just west of the positive ϕ associated with the Alaskan ridge (Fig. 5.15c). Anomalous convection is confined to a small area east of Indonesia. However, southwest of Mexico over the East Pacific, anomalous convection appears to be developing.

Two days later (Fig. 5.16), the jet remains extended but is less purely zonal across the Pacific. The eastern Pacific ridge now resides over western North America, and the ridge over the north Atlantic now extends as far poleward as $\sim$ 75°N latitude. A cyclonic mid- to upper tropospheric disturbance that appeared to be impacting the southwestern U.S. in Fig. 5.15 has weakened in anomalous negative ϕ intensity. This feature is associated with anomalous negative OLR extending from northern Mexico southwestward to $\sim$ 10°N, 140°W highlighted in the previous paragraph. Given the position and orientation of this linear negative OLR feature, this may be an "atmospheric river" type of feature, a region in which high precipitable water air is transported towards the southwestern U.S. This air can aid in the development or enhancement of any convection within this region.

5.4.2.2 *10 January 2007 Case*

Figure 5.17 shows the large-scale environments associated with the 10 January 2007 superposed jet case at time T+2 (i.e., 12 January 2007 0000 UTC). Figure 5.17a shows the eastern edge of the West Pacific jet extended past the dateline similar to that of the February 1993 case. Anomalous ridging is present near Alaska as well as within the eastern U.S. (Figs. 5.17a,b). Furthermore, anomalous negative OLR is minimal in magnitude and area near Indonesia, just as was observed 2 days prior (Fig. 4.16d). Anomalous cyclonic flow associated with anomalous convection is present southwest of Hawaii, appearing similar to that of the "Kona Low" like feature observed in the February 1993 case.

Two days later (T+4), the West Pacific jet extends slightly eastward and weakens to a wind speed maximum < 90 m s^{-1} (Fig. 5.18). The majority of features observed at T+2 are still present at this time, including the Kona Low anomaly (Figs. 5.18a,b) and ridge-trough-ridge pattern in the upper troposphere over North America. Also, similar to the February 1993 case, a negative OLR anomaly at this time extends from anomalous convection near the Kona Low northeastward to the southwestern continental U.S. (Fig. 5.18d). This again may be associated with an atmospheric river transporting higher precipitable water values towards the southwestern U.S. This may play a role in enhancing precipitation development associated with the Kona Low-type feature, though a more in-depth analysis is required.

5.5 Chapter Summary

The goal of this chapter was to explore the evolution of West Pacific vertical jet superposition events and their associated large-scale environments in the days following superposition. The same composite and case-study analysis techniques used in Chapters 3 and 4 were applied but at times T+n relative to superposition (n $>$ 0 days). These evolutions were investigated within the context of the 44-case, strong and neutral EAWM season composites as well as the two weak EAWM season jet superposition cases.

Figures 5.19 and 5.20 highlight the key large-scale phenomena observed at the time of jet superposition (Fig. 5.19a; adopted from Fig. 3.14c), after time of jet superposition within the 44-case composite (Fig. 5.19b), and after superposition within the strong/neutral (Fig. 5.20a) and weak (Fig. 5.20b) EAWM seasonal environments. Recall from Chapters 3 and 4 that West Pacific jet superposition events are commonly associated with an EAWM northerly cold surge event that propogates equatorward and enhances convection via enhanced surface convergence (dark blue oval with purple arrows interacting with cloud symbols in Fig. 5.19a). Convective outlow (green stippled arrow) is then advected toward the anticyclonic shear side of the West Pacific jet, increasing the anomalous vertical wind shear such that the magnitude of the jet core increases. This convection, in concert with internal jet dynamics, also acts to develop the deep, vertical PV wall characteristic of West Pacific jet superposition (Fig. 3.14d).

Over the next few days, an extension of the West Pacific jet stream eastward is observed within the 44-case composite (extension of solid black oval with black vector in Fig. 5.19b; jet at previous time shown in light gray). The magnitude of the peak winds within the West Pacific jet weaken over this timeframe. Anomalous positive (negative) ϕ features in the mid- to upper troposphere also propogate eastward over time, residing within the right (left) West Pacific jet exit region as it extends (blue and gold circulation symbols, respectively). The resulting anomalous cyclonic flow appears to be associated with the development of a ridge over northwestern North America (thick red arrow). Also, the cold surge observed over the West Pacific moves eastward and weakens over time (faded dark blue circle). With the cold surge no longer within the vicinity of the anomalous Indonesian convection, the magnitude of anomalous convection weakens (faded cloud symbols). The influence of convective outflow on the jet weakens as well due to the lack of southwesterly flow in the upper troposphere over this convection (faded green stippled arrow). While the majority of features exceeding the 0.5σ threshold occur within the Pacific or over North America, anomalous anticyclonic features over the Caspian Sea and northern Russia are observed, with the Russian feature weakening over time.

Similar results are observed with respect to the strong and neutral composite environments relative to the 44-case composite. For example, the extension of the West Pacific jet and associated cyclonic and anticyclonic anomalies within the jet exit regions are observed in both the strong and neutral cases. Also, the dissipation of the cold surge is also similar. However, some differences do exist and are highlighted in Fig. 5.20a. For example, a more wavy trough-ridge-trough pattern is observed over North America in the composite strong environment relative to the neutral environment (red and blue circulation arrows), though both environments exhibit wavy flow in this region. Stronger anomalous negative ϕ and associated cyclonic flow are observed over North-Central Eurasia (blue circulation arrows), though it is not immediately clear how such a feature ties to other changes in the large-scale circulation of the Northern Hemisphere. Finally, the magnitude of anomalous convection in the Maritime Continent region is consistently stronger over the timeframe in the strong EAWM composite relative to the neutral composite.

Figure 5.20b shows common features associated with the evolution of the West Pacific jet post-jet superposition for the two weak EAWM cases. Again, many of the features observed in these cases are similar to that of the composites. One feature of interest that does not appear in the composite environments is that of a “Kona Low” like feature near Hawaii. This feature, which appears strongest in the mid- to upper troposphere, propogates northeastward over the timeframe (blue dashed arrow flanked by blue circulation arrows), and becomes associated with a line of anomalous negative OLR extending from the East Pacific towards northwestern Mexico (green stippled arrow with cloud symbols). Given the proximity of this feature within the “Pineapple Express” region, the negative OLR may be a result of enhanced advection of high precipitable water air from the tropics towards the southwestern U.S. Further investigation of such a feature is saved for future research.

Overall, the evolution of the composite and case-study environments are all associated with the following: 1) the extension of the West Pacific jet stream, 2) the maintenance of anomalous cyclonic (anticyclonic) flow in the left (right) jet exit region that reside within these exit regions as the jet extends, 3) ridging downstream of the extended jet, which can lead to trough/ridge development downstream over eastern North America and the North Atlantic, 4) weakening of the EAWM northerly cold surge feature, and 5) the detachment of upper tropospheric anomalous southwesterly flow from anomalous convection over the Maritime Continent region. These environments evolve in a manner that appears to displace the West Pacific jet from the environment that originally induces jet superposition and perturbs the large-scale flow downstream, impacting North America and western Europe. Ideas for future work that include further investigation of the downstream effects of the resulting large-scale environments after superposition occurrence are discussed in Chapter 6.

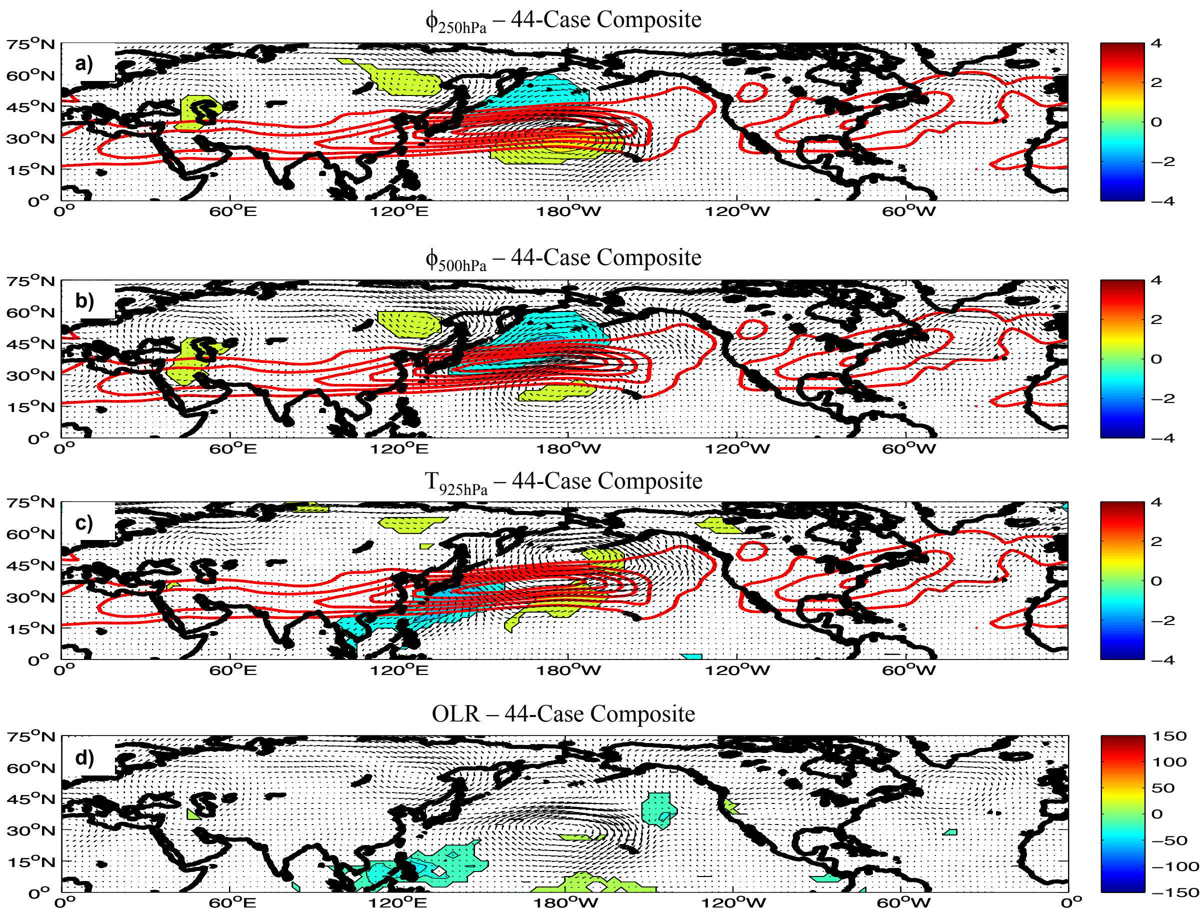

Figure 5.1 Composite large-scale features 1 day after composite West Pacific vertical jet superposition (i.e., time T+1). Shaded regions show positive (negative) standardized anomalous a) ϕ_{250}, b) ϕ_{500}, c) T_{925} and d) daily-averaged anomalous (non-standardized) OLR. Anomalous (non-standardized) winds are shown as black vectors. The red contour represents 250 hPa composite isotachs every 10 m s^{-1} starting at 30 m s^{-1}.

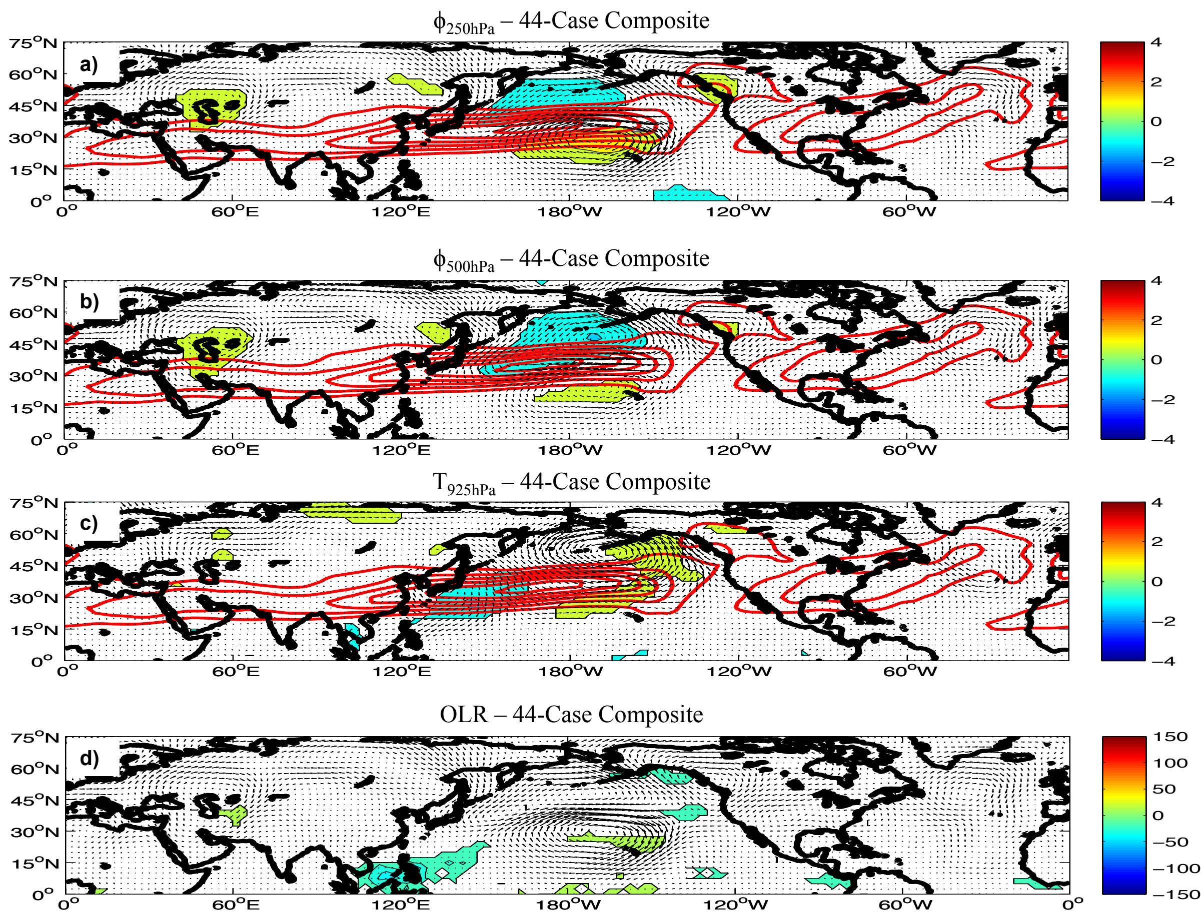

Figure 5.2 Same as Fig. 5.1 but 2 days after composite West Pacific jet superposition (i.e., time T+2).

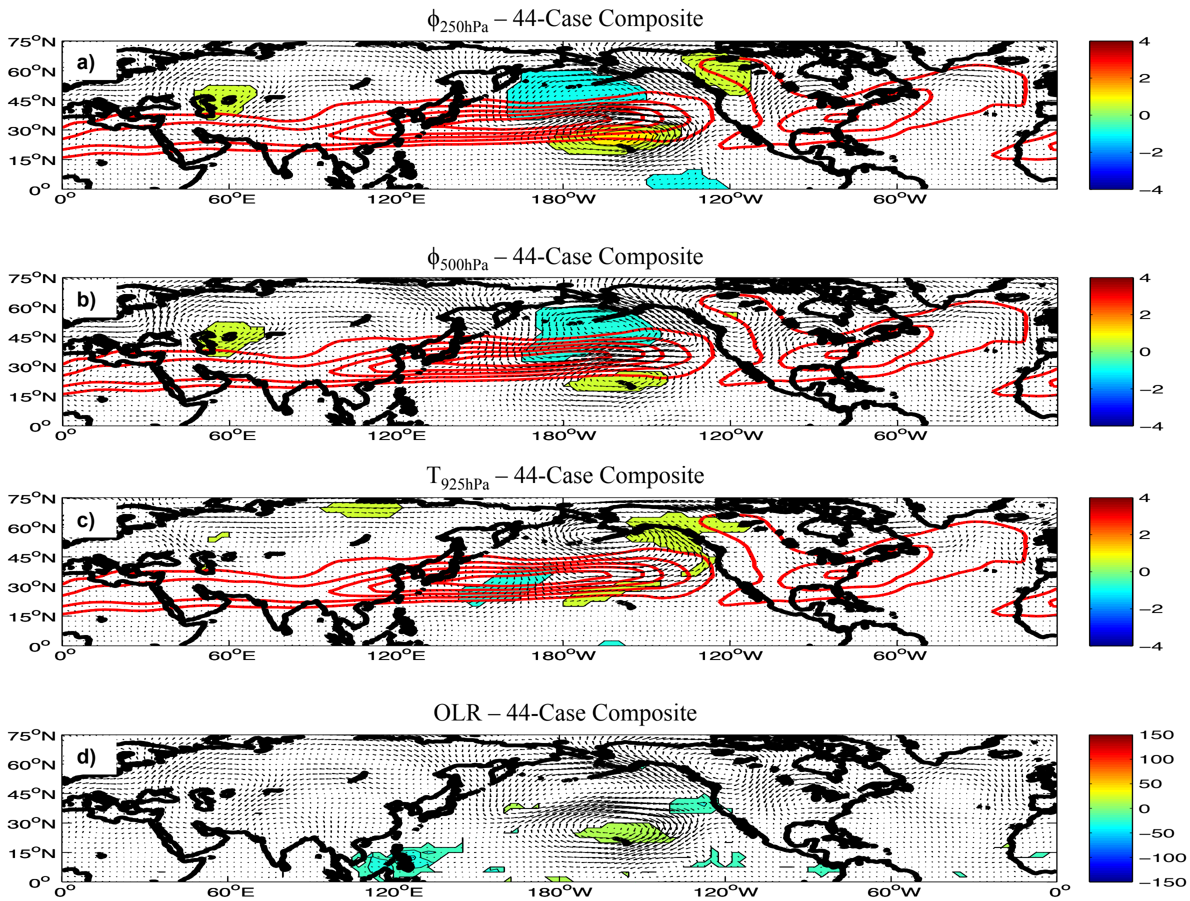

Figure 5.3 Same as Fig. 5.1 but 3 days after composite West Pacific jet superposition (i.e., time T+3).

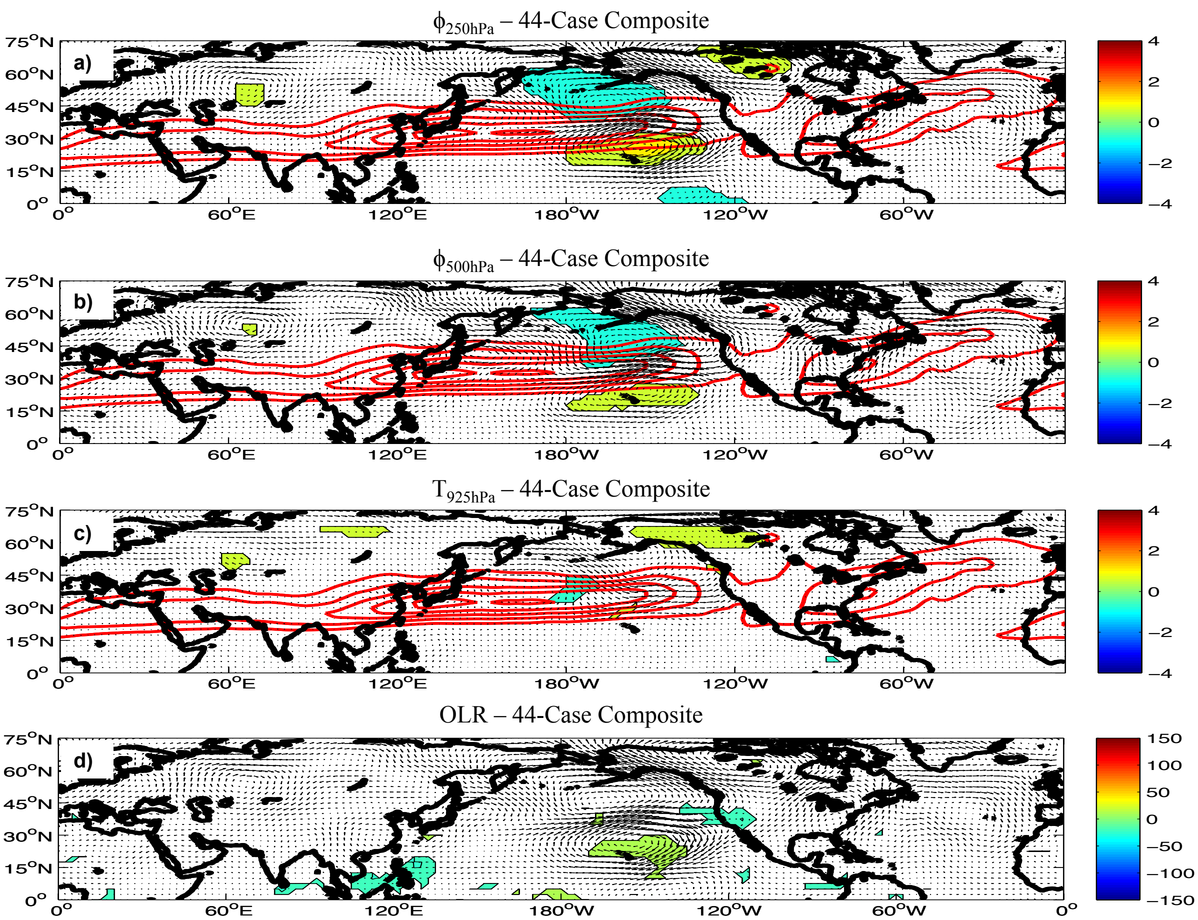

Figure 5.4 Same as Fig. 5.1 but 4 days after composite West Pacific jet superposition (i.e., time T+4).

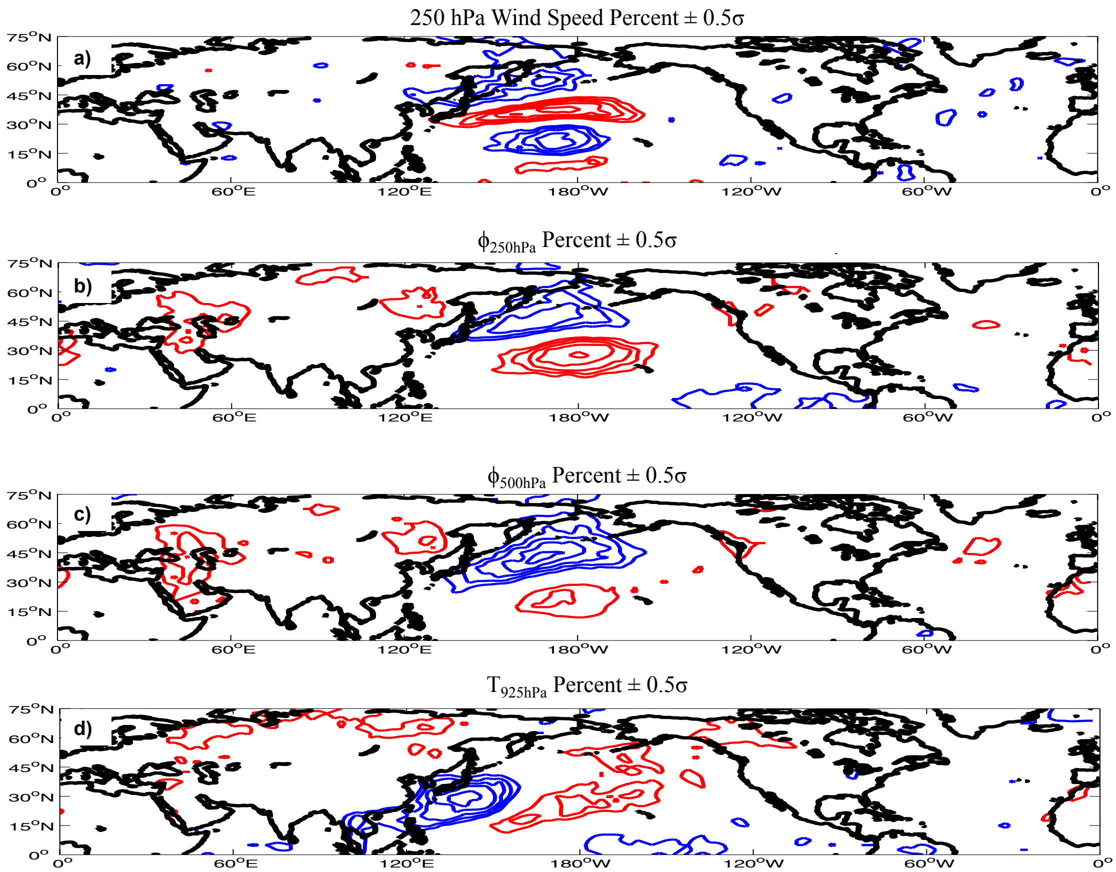

Figure 5.5 Percent occurrence of each of the standardized variables in Fig. 5.1 for all 44 cases used in the composite 1 day after composite West Pacific vertical jet superposition (time T+1). Red (blue) contours indicate regions where the variable of interest with standardized value $\geq 0.5\sigma$ ($\leq$ -0.5σ) occurs in at least 50% of cases contoured every 10%.

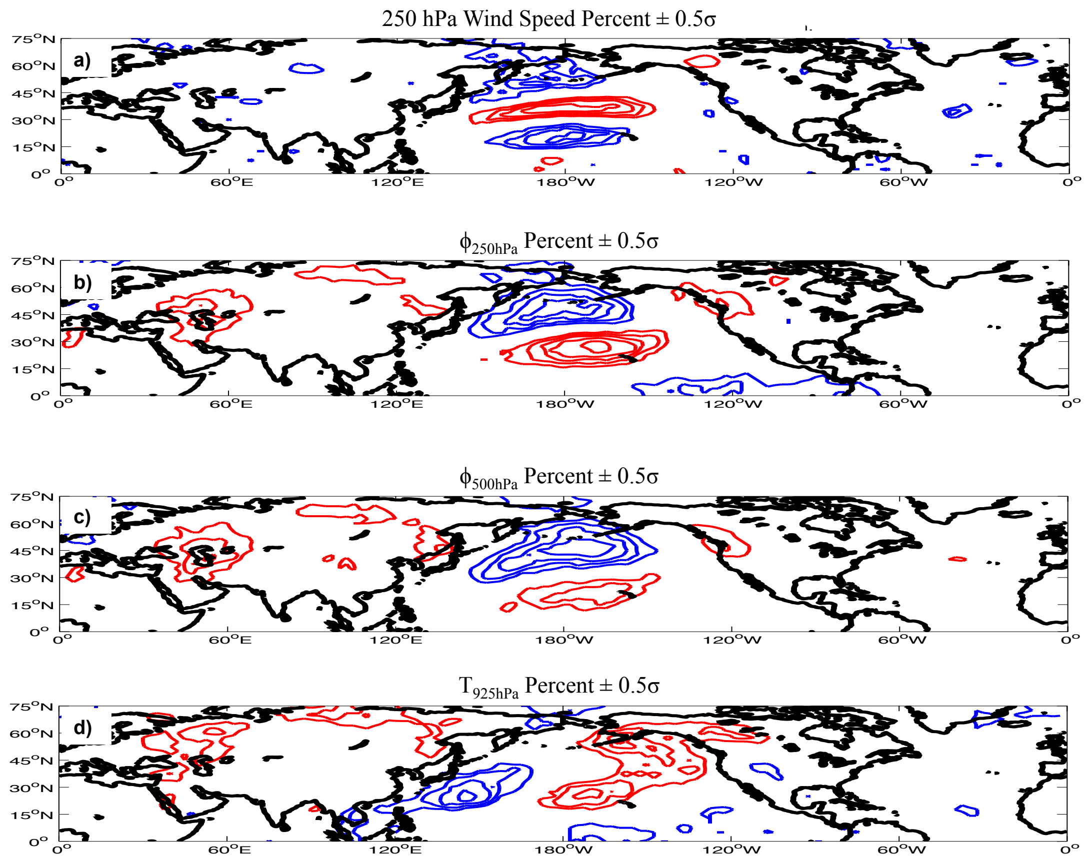

Figure 5.6 Same as Fig. 5.5 but 2 days after composite West Pacific jet superposition (i.e., time T+2).

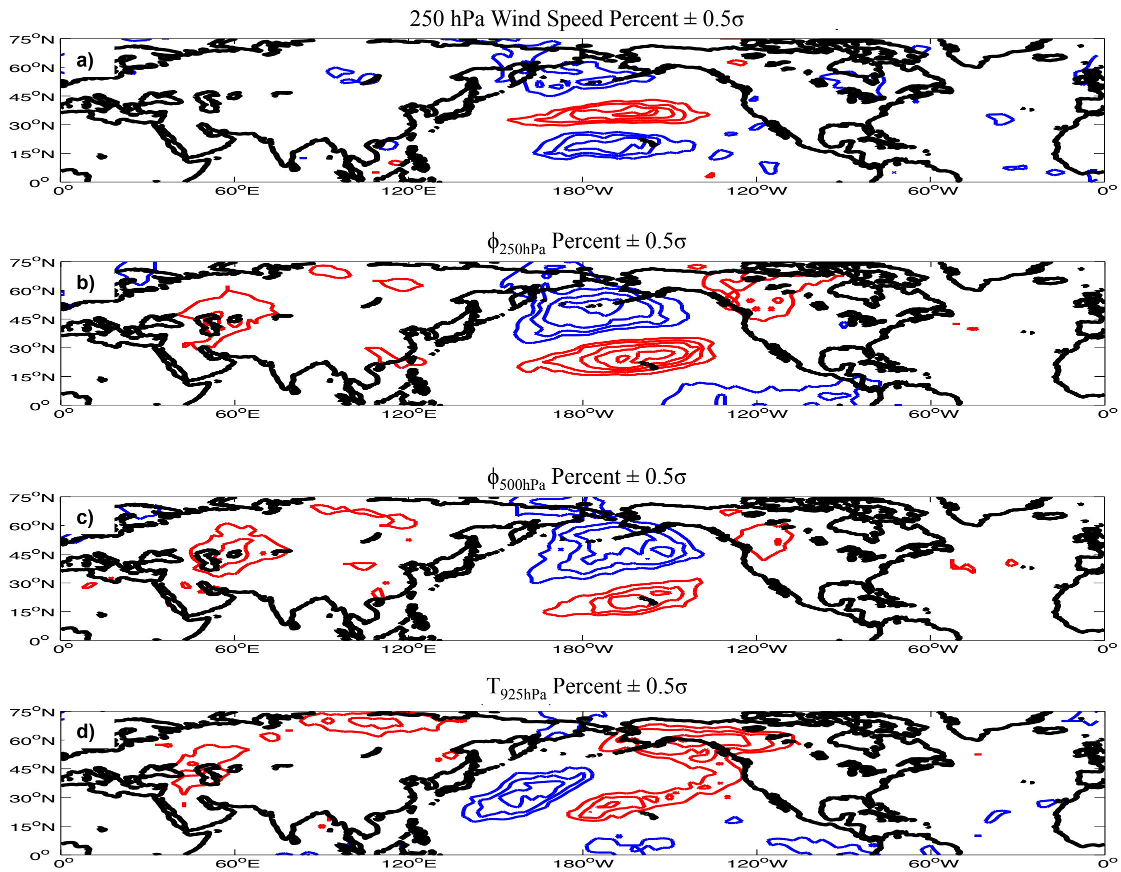

Figure 5.7 Same as Fig. 5.5 but 3 days after composite West Pacific jet superposition (i.e., time T+3).

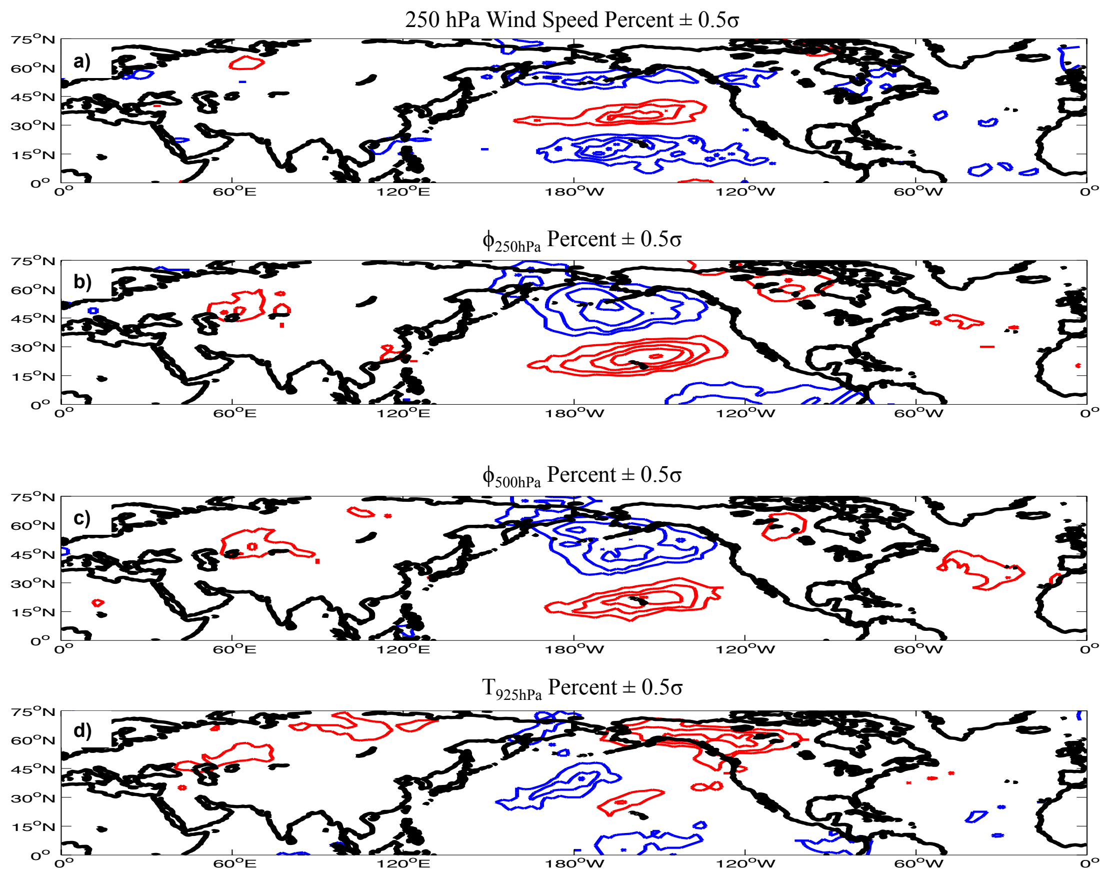

Figure 5.8 Same as Fig. 5.5 but 4 days after composite West Pacific jet superposition (i.e., time T+4).

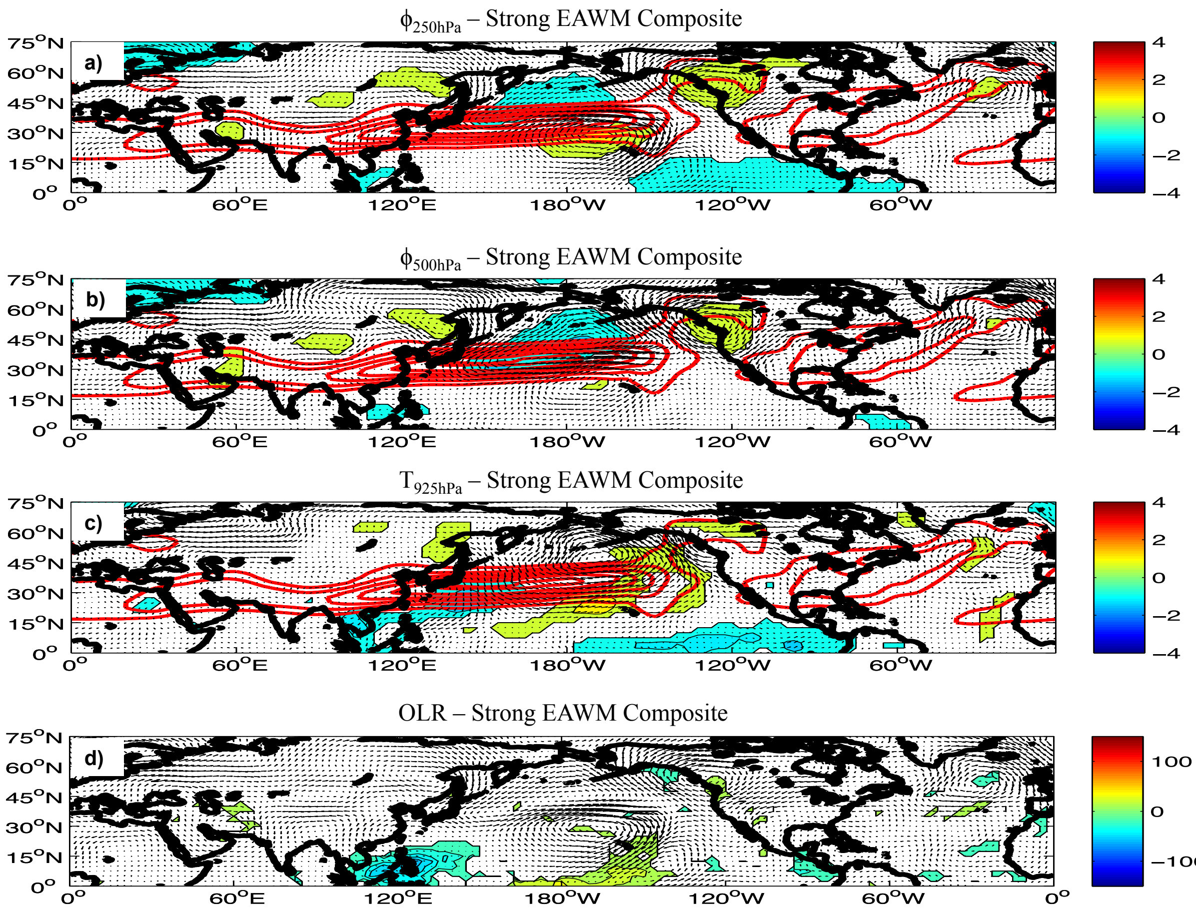

Figure 5.9 Same as Fig. 5.1 but with respect to the strong EAWM season composite environment 2 days after composite West Pacific jet superposition (i.e., time T+2).

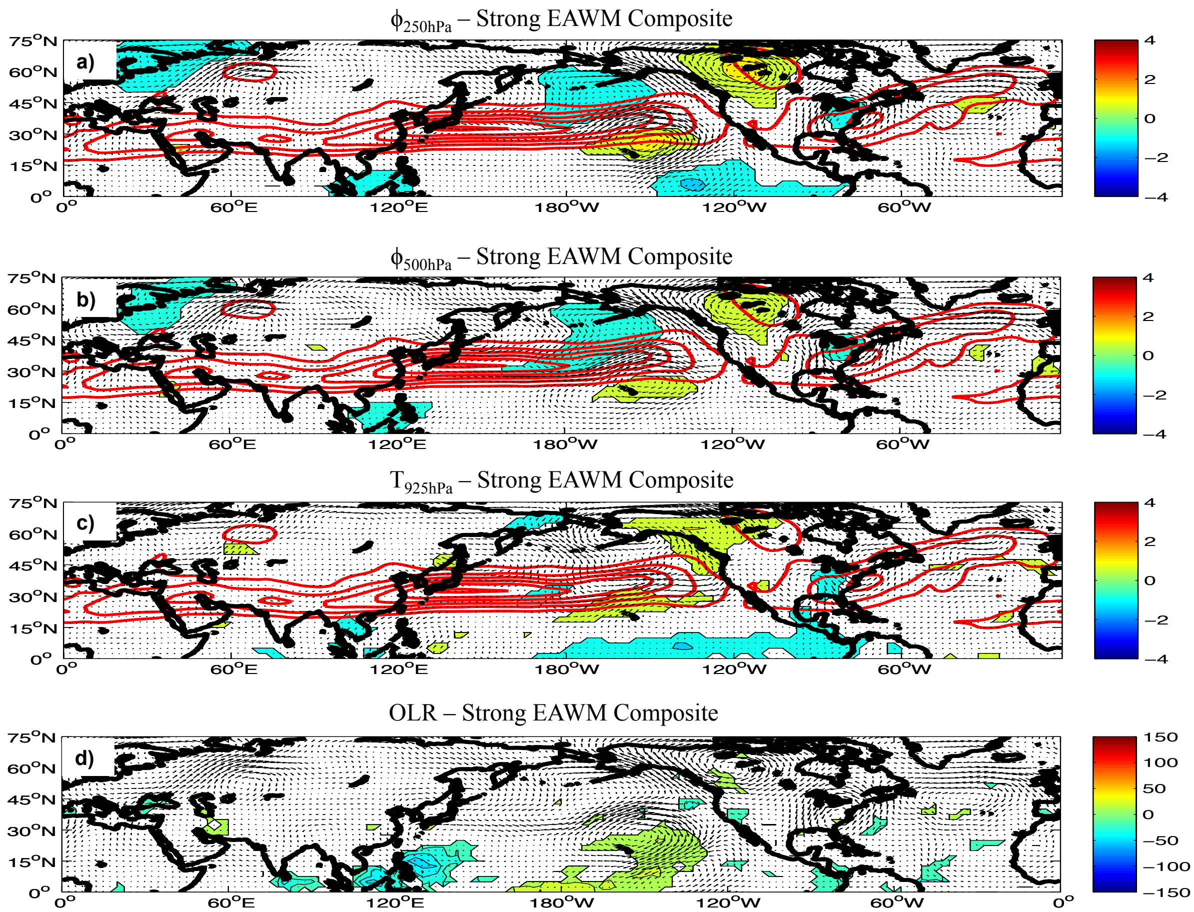

Figure 5.10 Same as Fig. 5.1 but with respect to the strong EAWM season composite environment 4 days after composite West Pacific jet superposition (i.e., time T+4).

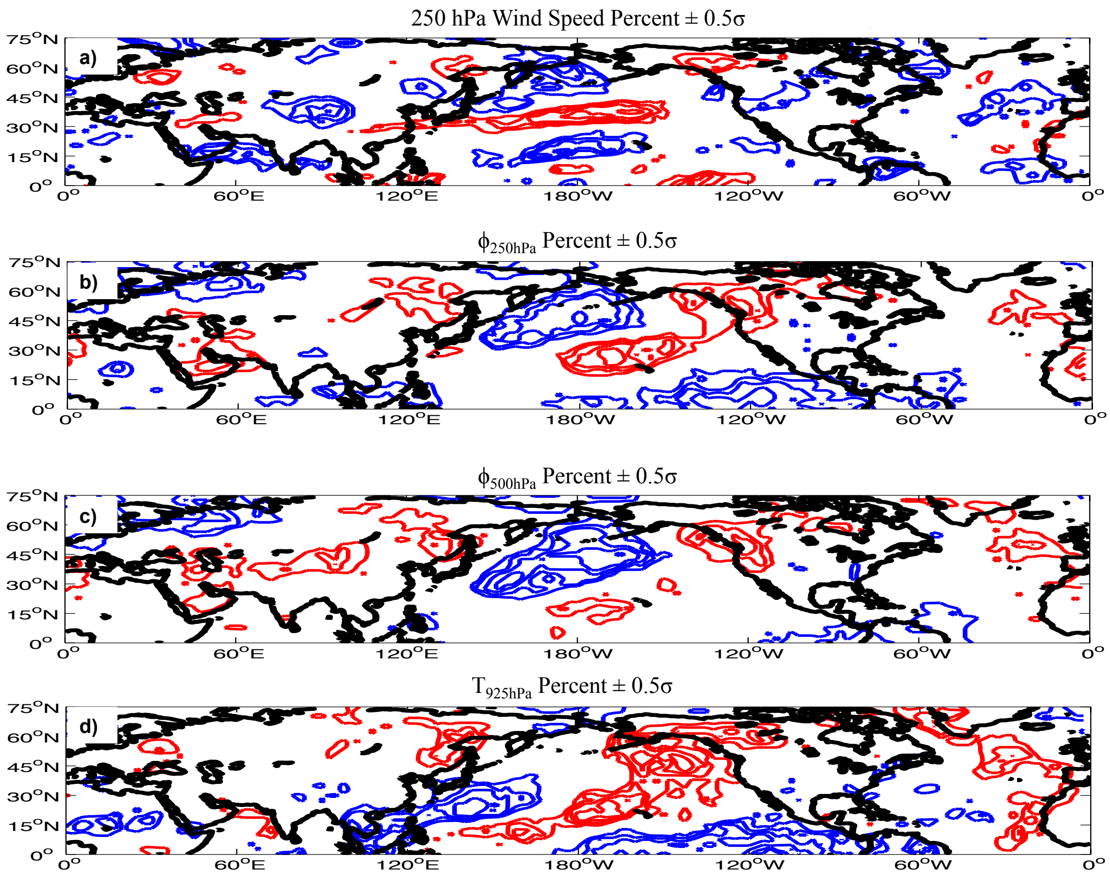

Figure 5.11 Same as Fig. 5.5 but with respect to the strong EAWM season composite environment 2 days after composite West Pacific jet superposition (i.e., time T+2).

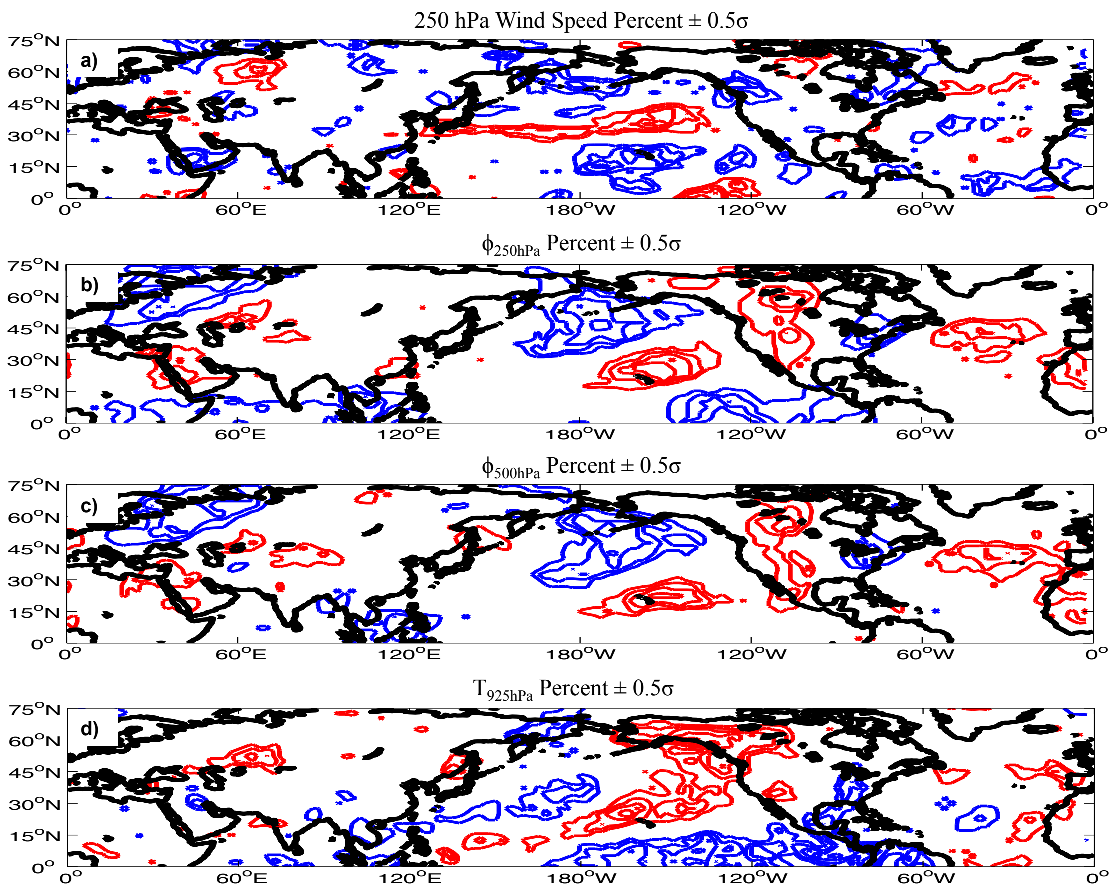

Figure 5.12 Same as Fig. 5.5 but with respect to the strong EAWM season composite environment 4 days after composite West Pacific jet superposition (i.e., time T+4).

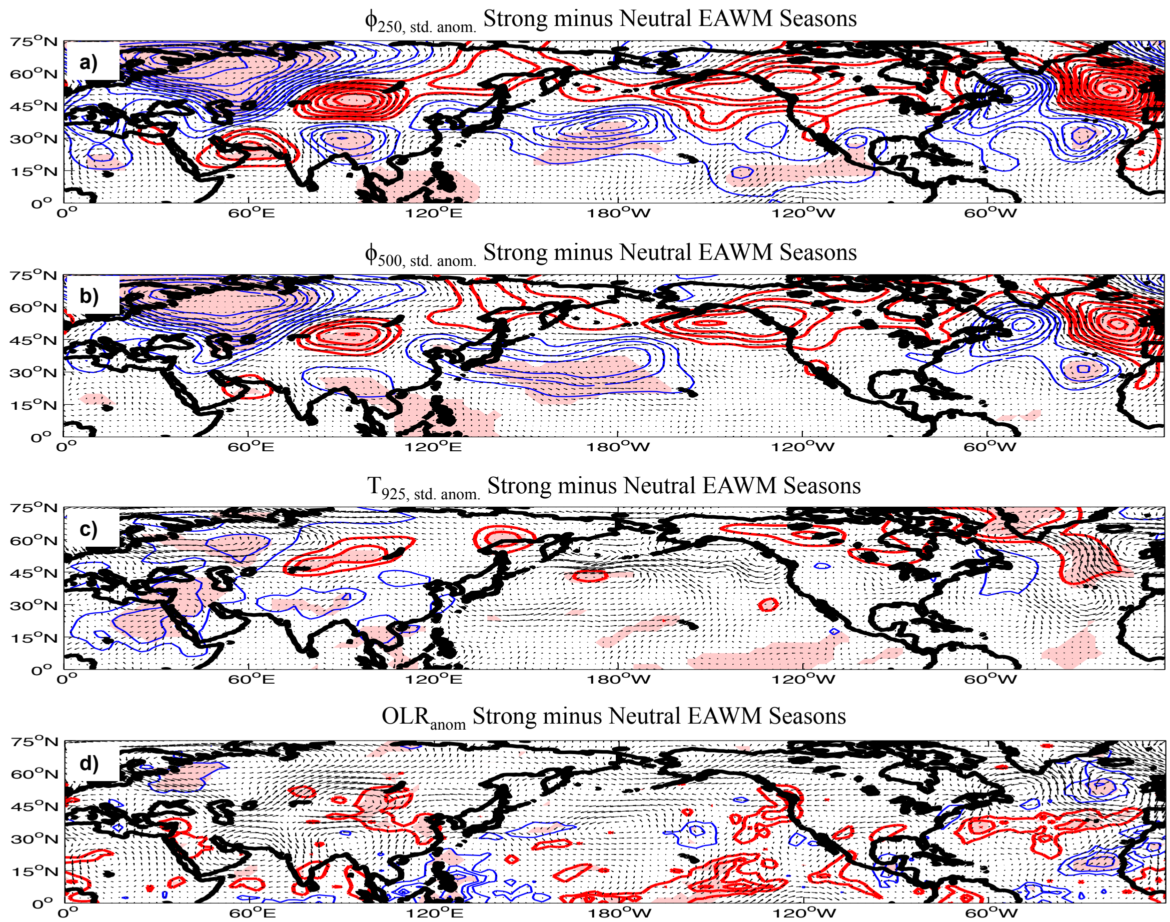

Figure 5.13 Difference between strong and neutral EAWM season West Pacific vertical jet superposition composite environments at time T+2. The variables plotted in each panel are consistent with Fig. 5.1. Red solid (blue dashed) contours are contoured every a) 20 m for ϕ_{250} starting at + (-) 20 m, b) 20 m for ϕ_{500} starting at + (-) 20 m, c) 2 K for T_{925} starting at + (-) 2 K, and d) 10 W m^{-2} for OLR starting at + (-) 10 W m^{2}. Shaded pink regions represent areas where the difference between the two environments exceeds 95% statistical significance. Note that all vectors represent differences in wind speed between the two environments.

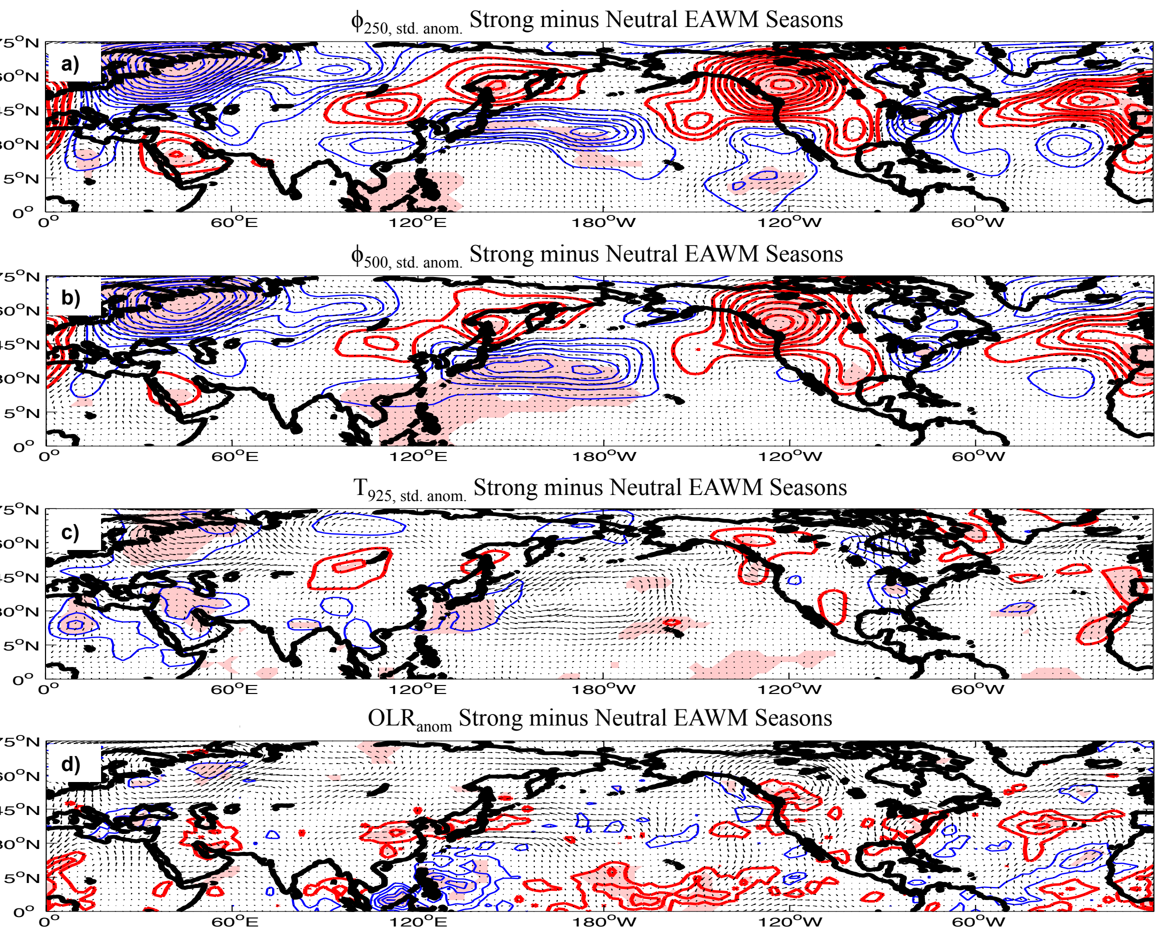

Figure 5.14 Same as Fig. 5.13 but at time T+4.

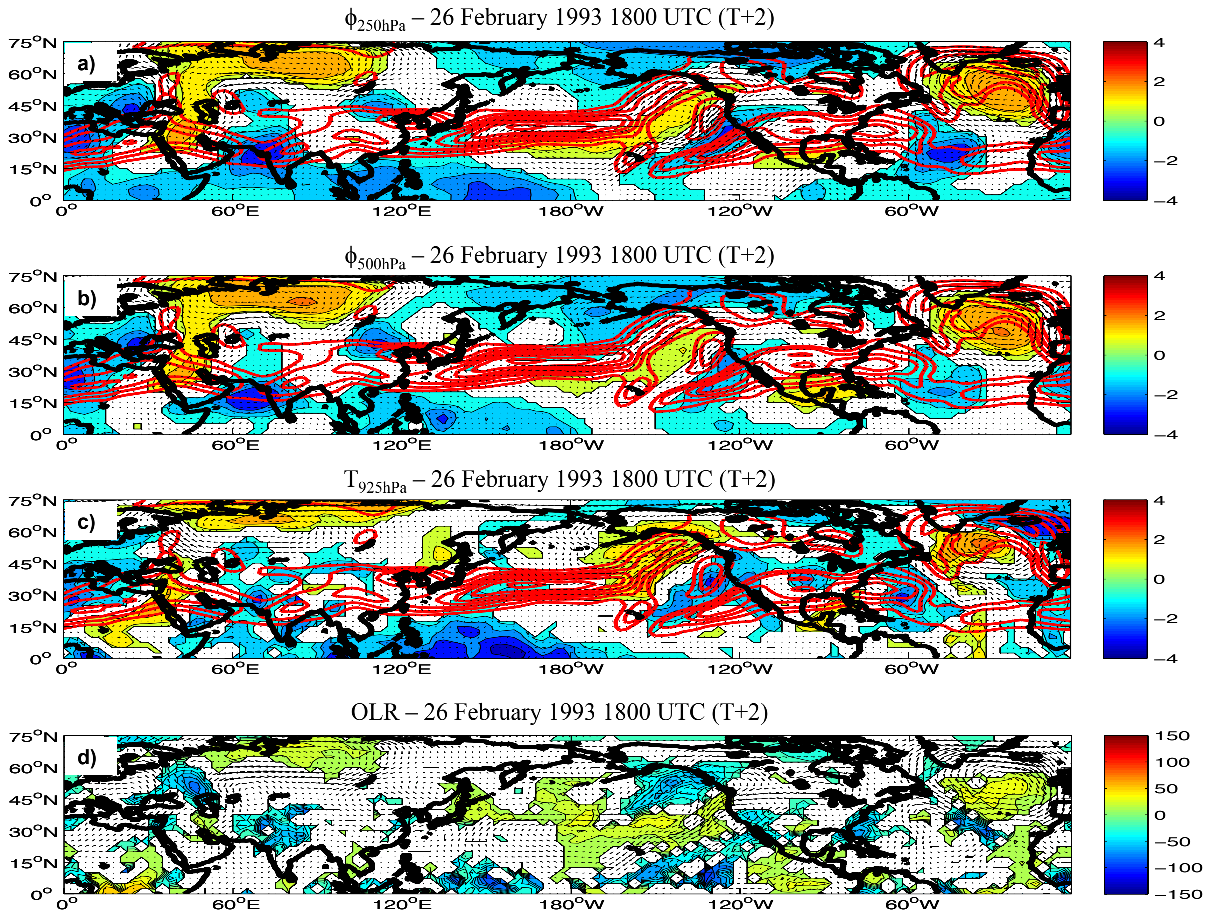

Figure 5.15 Large-scale environments associated with the February 1993 West Pacific jet superposition case at time T+2 (i.e., 1800 UTC 26 February 1993). Variables plotted here are consistent with those plotted in Fig. 5.1 for each panel with the same conventions and units.

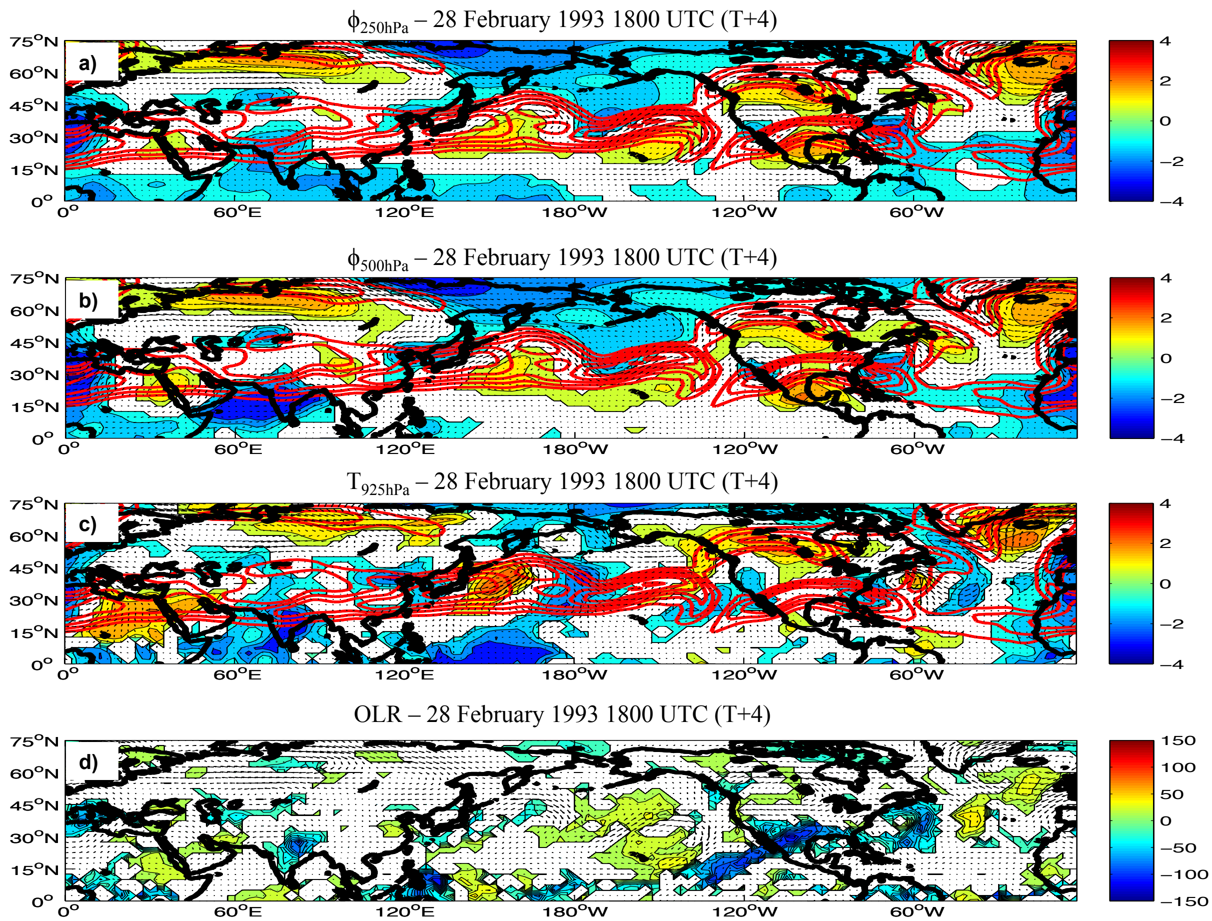

Figure 5.16 Same as Fig. 5.15 but at time T+4 (i.e., 1800 UTC 27 February 1993).

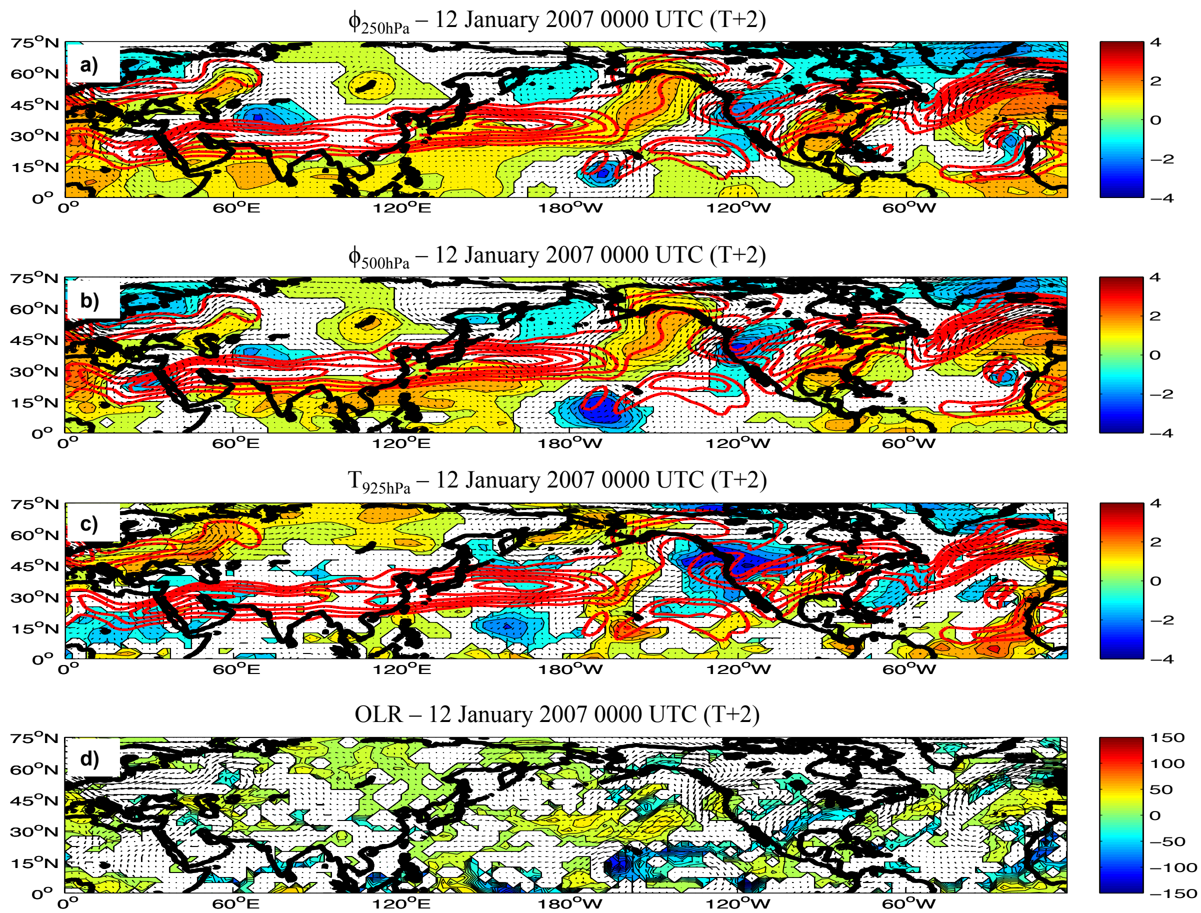

Figure 5.17 Large-scale environments associated with the January 2007 West Pacific jet superposition case at time T+2 (i.e., 0000 UTC 12 January 2007). Variables plotted here are consistent with those plotted in Fig. 5.1 for each panel with the same conventions and units.

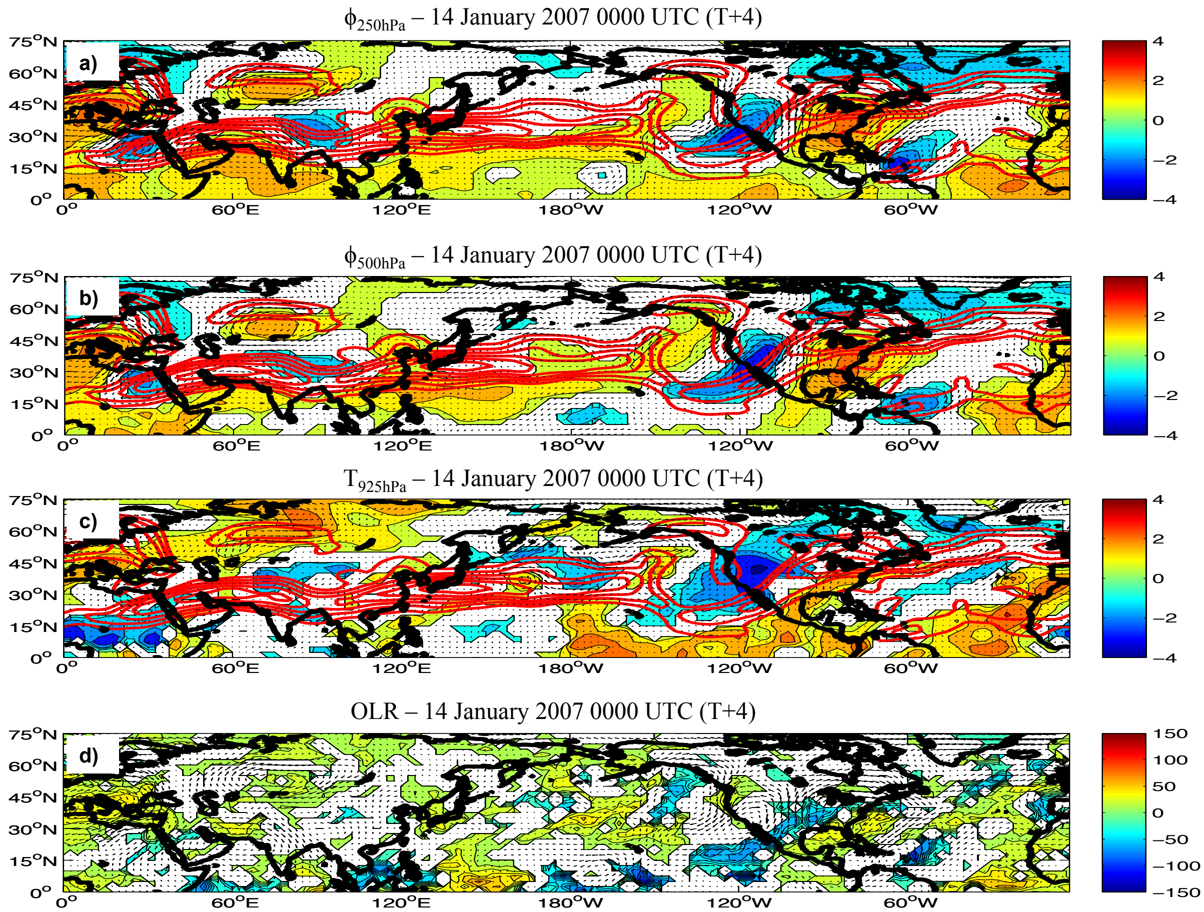

Figure 5.18 Same as Fig. 5.17 but at time T+4 (i.e., 0000 UTC 14 January 2007).

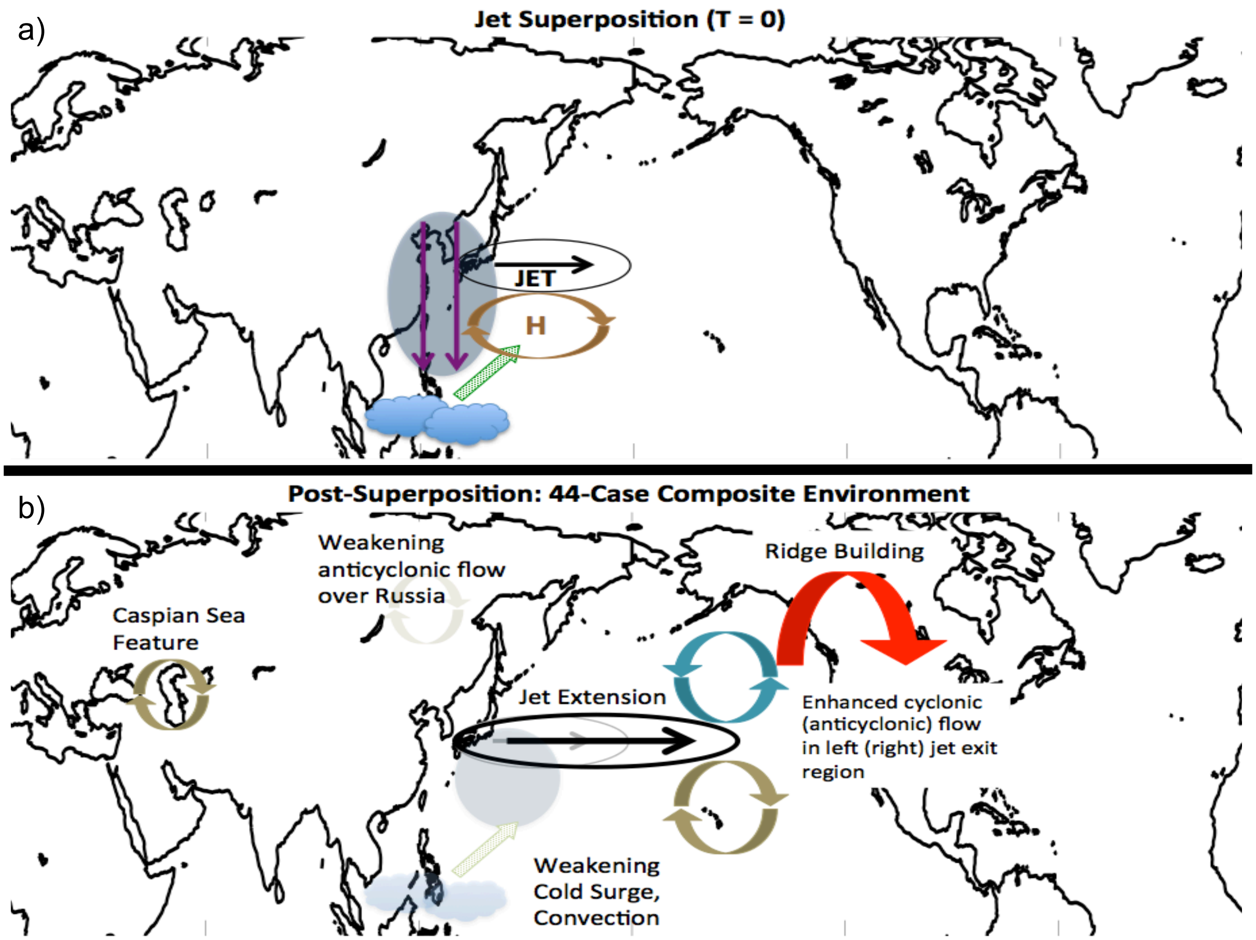

Figure 5.19 Conceptual model highlighting evolution of the West Pacific jet and associated large-scale environments after time of West Pacific vertical jet superposition occurrence. a) Key large-scale components associated with West Pacific jet superposition (same conventions as that of Fig. 3.14c) at time T=0. b) Same as panel a) but 1-4 days after superposition occurrence. The features shown in this panel are those that occur within the majority of cases within the 44-case composite. The jet extension that occurs during this timeframe is shown as a black solid contour with a black vector; the jet at time T=0 (from Fig. 5.19a) is shown in light gray contour with a gray vector. The cyclonic (anticyclonic) circulation in teal (gold) represents the anomalous negative (positive) ϕ within the left (right) jet exit region that propogates eastward as the West Pacific jet extends. The red arrow over northwestern Canada represents the ridge that develops associated with anomalous positive ϕ at 250 and 500 hPa. This ridge develops as the jet extends eastward along with the anomalous cyclonic (anticyclonic) feature in the left (right) jet exit region. Finally, features that were significant in the 44-case composite environment at time T=0 but have weakened at times T+1 through T+4 are faded, including the weakening of the northerly cold surge event, anomalous convection over Indonesia and anticyclonic flow over northern Russia.

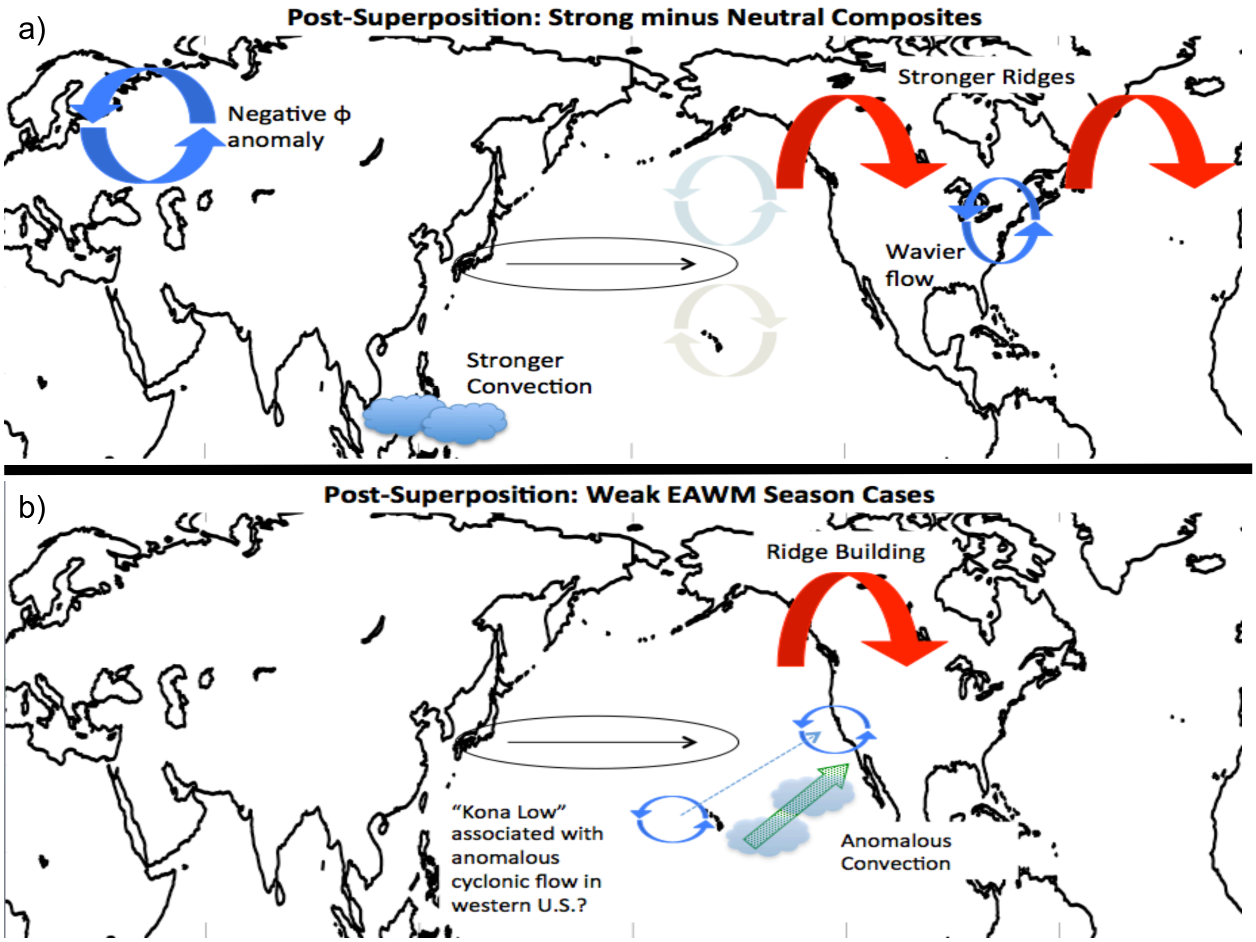

Figure 5.20 Conceptual model highlighting relevant large-scale features associated with West Pacific jet superposition events during strong, neutral and weak EAWM seasons. a) Large-scale features (labeled on diagram) associated with strong EAWM season superposition events relative to events during neutral EAWM seasons. Environments highlighted include a more wavy "trough-ridge-trough" pattern over North America, stronger convection near Indonesia and stronger anomalous cyclonic flow over northern Europe. Note that while these features are also present in the composite neutral environment, the highlighted features are amplified during strong EAWM seasons post-superposition. b) Large-scale features (labeled on diagram) associated with the two weak EAWM season jet superposition cases. The key large-scale features observed include the development of a ridge over northwestern Canada, the northeastward propogation of a "Kona-Low" type feature and anomalous convection that develops southeast of the Kona Low over the 4-day period.

Chapter 6

Conclusions and Future Work

The vertical superposition of the polar and subtropical jets, while rare, leads to the formation of a single strong and narrow jet structure that is at times associated with extreme weather events and can have an impact on large-scale envrionments throughout the Northern Hemisphere. Outside of a few studies investigating superposition events in the mid 20^{th} century as well as within the past decade (e.g., Mohri, 1953; Reiter, 1963; Reiter and Whitney, 1969; Christenson, 2013; Winters and Martin, 2014, 2016), only one study has investigated the life-cycle of a superposed jet over the West Pacific (Mohri, 1953). Christenson (2013) showed that jet superposition events occur most often within the West Pacific near Japan during boreal winter. Given this, the impact the West Pacific jet has on the Northern Hemisphere circulation and the connection between the EAWM and this jet, motivated the research questions explored throughout this dissertation.

The goals of this study were to: 1) understand the large-scale environments conducive to West Pacific PJ/STJ superposition and their relation to the EAWM (RQ1), 2) reconsider RQ1 in the context of superposition events occuring during strong, neutral and weak EAWM seasons (RQ2) and 3) investigate the structural evolution of the West Pacific jet and associated large-scale environments post-superposition (RQ3). These topics were explored using the NCEP/NCAR Reanalysis 1 dataset, where an innovative jet superposition ID scheme was used to identify and subsequently analyze 44 robust West Pacific vertical jet superposition events during DJF winters 1979/80-2009/10. Section 6.1 summarizes the main findings with respect to each RQ, and Section 6.2 discusses future research topics of interest.

6.1 Summary of Conclusions from Chapters 3-5

To determine the large-scale environments conducive to West Pacific PJ/STJ superposition (RQ1), a composite analysis of robust superposition events was performed in Chapter 3. 44 events were considered and analyzed as composite data at times 3 days prior to jet superposition occurrence (T-3) up to time of superposition (T=0).

Equatorward directed anomalous lower tropospheric cold air on the eastern edge of the SMH over northeastern China is present within nearly all of the cases considered at time T-3 (Fig. 3.14a) as is anomalous convection near Indonesia. Over the next few days, the anomalous cold air is advected equatorward towards the anomalous convection. The northerly winds associated with this "cold surge" act to strengthen the convection by enhancing surface convergence, which induces enhanced upward vertical motion (Fig. 3.14b). The West Pacific jet is observed to increase in magnitude in concert with the enhancement of anomalous convection.

The increase in the speed of the jet responds to two forcings. First, the enhanced rising motion within the lower latitude convection increases the magnitude of the West Pacific jet entrance region circulation. This is a manifestation of the enhanced local Hadley Cell circulation observed in earlier studies of the impact of northerly cold surge events on the West Pacific jet (e.g., Chang et al., 1979; Chang and Lau, 1980; Chan and Li, 2004). Poleward flow aloft within this circulation can turn eastward due to the Coriolis force, which increases the magnitude of the West Pacific jet. Second, the convective outflow of high-θ_e, low-PV air (originating from the tropical boundary layer) is advected northeastward towards the anticyclonic shear side of the jet (Fig. 3.14c). This acts to increase the pressure depth within the STJ isentropic layer. Via the thermal wind equation (Eqn. 3.2), anomalous anticyclonic wind shear increases such that westerly flow within the West Pacific jet increases in magnitude. Furthermore, the insertion of low-PV air within this isentropic layer aids in the construction of the deep, vertical PV wall characteristic of a superposed jet (Fig. 2.1d) through the increase in the vertical distance between the 340 K and 355 K surfaces on the equatorward side of the jet (Fig. 3.14d).

In concert with the convective outflow, internal jet dynamics also contribute to the construction of the characteristic PV wall. Geostrophic cold air advection in cyclonic shear is observed within the West Pacific jet entrance region. This cold air advection acts to shift the enhanced jet entrance region circulation equatorward such that subsidence occurs through the jet core (orange arrow in Fig. 3.14d). High-PV values within the lower stratosphere are thus transported downward, forcing the tropopause into a more vertical orientation and increasing the steepness of the PV wall.

The superposed jet at time T=0 is associated with the following large-scale environments: 1) anomalous anticyclonic flow and positive ϕ in the upper troposphere equatorward of the jet, 2) the anomalous mid- to upper tropospheric trough discussed in the previous paragraph, 3) the continuation of the cold surge event over eastern China and the South China Sea, and 4) anomalous convection over Indonesia (Fig. 3.1). Such environments are present within the majority of cases included within the 44-case composite throughout the development and occurrence of jet superposition (e.g., Fig. 3.2). Interestingly, strong EAWM winters have been shown to be associated with anomalous lower-tropospheric cold air and northerly winds, an enhancement of the sea level pressure gradient between the SMH and Aleutian Low, anomalous negative ϕ at 500 hPa, and enhanced westerly flow within the West Pacific jet. Since many of these large-scale environments are also observed during West Pacific superposition, the relationship between West Pacific jet superposition occurrence and the EAWM was explored.

It was shown that the frequency of occurrence of jet superpositions in the West Pacific interest region is statistically significantly correlated to EAWM seasonal strength such that more (less) superposition events occurred during strong (weak) EAWM seasons (Figs. 3.3 and 4.1). However, as shown in Chapter 4, differences in superposition frequency of occurrence do not imply differences in the large-scale environments conducive to robust West Pacific jet superpositions. All composite and case-study environments contain, in some form, the features listed in the previous paragraph throughout the superposition life-cycle. Based on these findings, it is concluded that robust superposition events, regardless of EAWM seasonal strength, form within a preferred large-scale environment.

Lastly, in considering the evolution of superposed jets and associated large-scale environments after time T=0 (RQ3), the following evolutions were observed: 1) the eastward extension and weakening of the West Pacific jet, 2) the formation of an anomalous ridge downstream of the extended jet over northwestern North America, 3) the weakening of the East Asian cold surge as it propogates eastward, and 4) the eastward propogation of anomalous anticyclonic flow on the equatorward side of the jet core. Regarding the last point, this appears to inhibit the continued advection of convective outflow into the STJ isentropic layer towards the jet, as the southwesterly winds associated with this anticyclone move away from the Indonesian convection (Fig. 5.19b). While these evolutions occur within the majority of superposition cases considered regardless of EAWM seasonal strength, some differences do exist with respect to large-scale features throughout the rest of the Northern Hemisphere between strong, neutral and weak EAWM seasonal cases. For example, a wavier "ridge-trough-ridge" pattern resides over North America in the strong EAWM environment relative to the neutral environment (Figs. 5.13, 5.14 and 5.20a). Also, a stronger anomalous cyclonic circulation resides over northeastern Europe, and convection is stronger near Indonesia after superposition occurrence during strong EAWM superpositions. Many of these differences are statistically significant.

Within the 2 weak EAWM cases, anomalous convection appears within the eastern Pacific (Fig. 5.20b). This feature, associated with anomalous precipitable water values (not shown), appears to the east of a northeastward propogating "Kona Low" like feature. The enhanced convection is in a position to enhance precipitation within the southwestern U.S. as it extends northeastward. This convection is not observed within the composite environments. However, since only 2 weak EAWM cases are identified, it is difficult to determine whether the occurrence of this convection in both cases is associated with the weak EAWM seasonal stength or if these features are purely coincidental.

This dissertation research is the first to investigate West Pacific jet superposition events and their associated large-scale environments in a composite sense as well as with respect to the partition of all cases based on EAWM seasonal strength. While past research has shown that environments containing northerly cold surge events and other EAWM-like features act to strengthen the

West Pacific jet (Chang et al., 1979; Chang and Lau, 1980), this research arrives at this conclusion in the context of a superposed West Pacific jet. This perspective in the context of EAWM cold surge events has not been considered in the literature. Furthermore, the use of the composite and case-study analyses helped to reveal the role that convective outflow and internal jet dynamics play in the development of a robust West Pacific superpositon. Such an occurrence in this region in the context of superposition has also not been considered in prior research.

6.2 Future Work

While this study provides a starting point for understanding the life cycle of West Pacific jet superpositions and their effects on the Northern Hemisphere large-scale circulation, extensive future work is required in order to develop a deeper and more comprehensive understanding of these events. A few future research avenues are presented in the subsections below.

6.2.1 *Detailed Case-Study Analysis of West Pacific Superposition*

An investigation of 44 events in a composite sense does not provide specific insight into the physical processes that drive individual cases. While there is general agreement regarding the large-scale evolutions conducive to West Pacific jet superposition among the 44 cases (e.g., Fig. 3.2), differences in the magnitude and position of these evolutions exist depending on the case. This is demonstrated by considering differences between environments within the two weak EAWM cases discussed in Chapters 4 and 5. Also, there may be other physical processes unique to some of the cases that are integral towards PJ/STJ superposition, though such features may be "smoothed" out in a composite sense. A simple remedy to this issue is to conduct a rigorous case-study analysis of a few of the cases comprising the 44-case composite. This includes investigating strong, neutral and weak EAWM cases in more detail.

Along with this, it was mentioned in Chapter 1 that superposition events are at times associated with extreme weather events. Research studies that have investigated this relationship (Christenson, 2013; Winters and Martin, 2014, 2016) have primarily focused on the U.S./Atlantic region. There are no published studies that have investigated in detail extreme weather events specifically associated with West Pacific jet superposition. Since it is difficult to investigate extreme weather events in a composite sense given the variability in location, spatial scale and magnitude of extreme weather, the case-study analysis framework is preferred.

6.2.2 *Investigation of West Pacific Superposed Jet Secondary Circulations*

The vertical structure of West Pacific superposition events was considered briefly in order to get a sense of the PV anomalies associated with the composite jet core as well as the jet entrance region circulation (Figs. 3.4 and 3.5). However, these cross-sections were only performed at time T=0. It would be beneficial to consider cross sections at other times throughout the evolution of the composite superposed jet. This would provide more insight regarding the evolution of the jet entrance region circulation.

Furthermore, a more detailed investigation of the jet entrance (and exit) region circulation can be considered by quantifying the magnitude of the ageostrophic transverse circulations in these regions via the solution of the Sawyer-Eliasion equation (Sawyer, 1956; Eliassen, 1962) as in Winters and Martin (2014, 2016). Such an analysis may produce greater insight into the role of internal jet dynamics in inducing jet superposition.

6.2.3 *West Pacific Jet Extension Post-Superposition*

One of the primary post-superposition evolutions within the composite and case-study environments was the extension of the West Pacific jet across the dateline (Figs. 5.19 and 5.20). This extension was associated with the development of a downstream ridge over Alaska and the Northwest Territories, which may have downstream impacts over North America via inducing a wavier flow. Jet extension can also have an impact on the development of Kona Low systems near Hawaii, as the large-scale environment is less (more) favorable for the formation of these systems when the jet is zonally extended (retracted) across the dateline (e.g., Chu et al., 1993; Otkin and Martin, 2004; Jaffe et al., 2011). Thus, understanding the relationship between superposition onset, the extension of the West Pacific jet and its downstream effects would help improve understanding of the effects of these superpositions on the Northern Hemisphere large-scale circulation.

Recent studies by Jaffe et al. (2011) and Griffin and Martin (2016) perform an Empirical Orthogonal Function (EOF) analysis on 300 hPa zonal wind speed to extract the two most dominant modes of West Pacific jet variability. The first (second) mode of variability explains the extension/retraction (north/south shift) of the jet. The principal components (PC's) associated with each mode, which represent a time series of each EOF, can be compared with other large scale indices to determine first order relationships with other large-scale phenomena as well as predict the extension/retraction (north/south) shift of the jet. Similar to Figs. 3.3 and 4.1, each PC could be correlated with the time series of jet superposition ID frequency in order to explore differences in the onset of robust jet superposition relative to extension/retraction or north/south shift occurrence. This analysis would also include determining the lead/lag time between the time series. It is hypothesized that PC1 is positive within a few days after jet superposition occurrence given the observed post-superposition extension of the West Pacific jet. However, the relationship between PC2 and superposition onset is unclear, though such an analysis in future work would help to determine if any relationship exists.

6.2.4 *Sensitivity of Robust Jet Superposition Results to Jet ID Threshold and West Pacific Interest Region Definition*

For all cases considered throughout this dissertation, it was required that at least 7 superposition ID's occurred within the West Pacific interest region outlined in Chapter 2. This criterion was chosen based on Table 2.2, which shows that less than 1% of 6-hourly times exhibit 7 or more ID's within this region. The sensitivity of the results in this dissertation to the choice of 7 ID's, as well as to the location of the boxed region chosen, was not discussed. It is worthwhile to consider such sensitivities. For example, if the use of a 6 or 8 ID threshold and/or shift of the interest region box a few degrees latitude or longitude leads to similar results, then the results of this dissertation could be applied towards describing other superposition cases that may have not met the original definiton of a robust superposition event. However, if the results of such slight changes to the methodology differ significantly from that of those presented in the dissertation, then this might suggest that other large-scale environments not present within the 7+ ID composite can also play a role in inducing superposition.

6.2.5 *Jet Superpositions and Climate Change*

One topic that was not addressed within this dissertation is the effect of global climate change on the frequency, distribution and magnitude of West Pacific jet superpositions. With a warming climate projected over the next century throughout the majority of the Northern Hemisphere, water vapor content in the atmosphere is expected to increase, which may induce more intense precipitation events globally (Trenberth, 1998, 1999). An increase in precipitation associated with extratropical cyclones is also anticipated (e.g., Watterson, 2006; Bengtsson et al., 2009; Champion et al., 2011). This could lead to more diabatic outflow produced as a result of more extreme precipitation events. Given the impact that diabatic outflow has with respect to the development of a deep, vertical PV wall associated with the poleward movement of the STJ towards the PJ in the Northern Hemisphere (see Chapter 3 and Winters and Martin, 2014), vertical jet superposition events may increase in frequency as a result of climate change.

A warmer climate is also projected to increase tropopause height more in the tropics relative to the poles (Yin, 2005; Lorenz and DeWeaver, 2007). This would increase the gradient in tropopause height as well as shift middle latitude jet streams upward and poleward. The greater increase in tropopause height in the tropics relative to higher latitudes may play a role in strengthening the magnitude of the PJ, STJ and superposed jets given that the gradient in tropopause height may increase as a result of this.

In order to explore changes in the frequency of occurrence of West Pacific superposition events, a time series of the number of superposition ID's per season analogous to that of Figs. 3.2 and 4.1 could be constructed for such events at the end of the 21^{st} century and compared to that of the time series showed in these figures. For example, superposition events could be identified using output from an ensemble of Coupled Model Intercomparison Project Phase 5 (CMIP5) General Circulation Model (GCM) simulations. After verifying that these simulations accurately reproduce the climatology of jet superposition events within the 31-year timeframe considered in this dissertation (e.g., verify with NCEP/NCAR Reanalysis 1 ID's), the comparison described in the previous sentence could then be conducted. Two "future" climates could be considered: 1) the Representative Concentration Pathway 4.5 (RCP4.5) scenario, which assumes that the increase in radiative forcing due to climate change stabilizes at (exceeds) 4.5 W m^{-2}, and 2) the RCP8.5 scenario, which assumes that radiative forcing exceeds 8.5 W m^{-2} by the year 2100 (IPCC, 2013).

As for investigating changes in the spatial distribution of superpositions with climate, a superposition climatology similar to that of Christenson (2013) and Fig. 2.2 could be constructed for all years simulated at the end of the 21^{st} century using CMIP5 GCM output data. This climatology could be compared/contrasted with that of the years considered in this dissertation to learn how this distribution may be altered within the two climate change scenarios defined above. Finally, to investigate changes in the magnitude of West Pacific superpositions, the composite and case-study analysis methods used throughout Chapters 3-5 could be repeated for identified robust superposition cases within the future climate change environments. In this manner, changes in the large-scale environments conducive to superposition events could also be compared and contrasted with the environments associated with superpositions identified in this dissertation.

Bibliography

Bengtsson, L., K. I. Hodges, and N. Keenlyside, 2009: Will Extratropical Storms Intensify in a Warmer Climate? *J. Climate*, **22**, 2276–2301.

Boyle, J. S. and T.-J. Chen, 1987: Synoptic Aspects of the Wintertime East Asian Monsoon. *Monsoon Meteorology*, C.-P. Chang and T. N. Krishnamurti, Eds., Oxford University Press, 125–160.

Champion, A. J., K. I. Hodges, L. O. Bengtsson, N. S. Keenlyside, and M. Esch, 2011: Impact of Increasing Resolution and a Warmer Climate on Extreme Weather from Northern Hemisphere Extratropical Cyclones. *Tellus*, **63A**, 893–906.

Chan, J. C. L. and C. Y. Li, 2004: The East Asian Winter Monsoon. *The Asian Monsoon*, C. Chang, Ed., World Scientific, 54–106.

Chang, C.-P., J. Erickson, and K.-M. Lau, 1979: Northeasterly Cold Surges and Near-Equatorial Disturbances over the Winter-MONEX Area during 1974. Part 1: Synoptic Aspects. *Mon. Wea. Rev.*, **107**, 812–829.

Chang, C.-P. and K.-M. Lau, 1980: Northeasterly Cold surges and Near-Equatorial Disturbances over the Winter-MONEX Area during 1974. Part 2: Planetary-Scale Aspects. *Mon. Wea. Rev.*, **108**, 298–312.

Cheng, C. S., 1955: On the Occurrences of Cold Spell in the Lower Yangtze. *Acta Met. Sinica*, **26**, 125–134.

Chin, P., 1969: Cold surges over South China. Tech. rep., Tech. Note No. 28, Royal Observatory Hong Kong, 40 pp.

Christenson, C. E., 2013: A Synoptic-Climatology of Northern Hemisphere Polar and Subtropical Jet Superposition Events. M.S. thesis, Department of Atmospheric and Oceanic Sciences, University of Wisconsin - Madison, 62 pp.

Chu, P. S., A. J. Nash, and F. Y. Porter, 1993: Diagnostic Studies of Two Contrasting Rainfall Episodes in Hawaii: Dry 1981 and Wet 1982. *J. Climate*, **6**, 1457–1462.

Chyou, Y. Y., 1957: Examples of Development of Cold Fronts in Cold Outburst. Tech. rep., Monthly Weather (Peking), 1–7 pp.

Cunningham, P. and D. Keyser, 2004: Dynamics of Jet Streaks in a Stratified Quasi-Geostrophic Atmosphere: Steady-State Representations. *Quart. J. Roy. Meteor. Soc.*, **130**, 1579–1609.

Dao, S. Y., 1957: A Synoptic and Aerological Study of Cold Wave in the Far East showing the Period of the Break-down of the Blocking Situation over Eurasia and Atlantic. *Acta Met. Sinica*, **28**, 63–73.

Defant, F. and H. Taba, 1957: The Threefold Structure of the Atmosphere and the Characteristics of the Tropopause. *Tellus*, **9**, 259–275.

Draxler, R. R., 1999: HYSPLIT4 User's Guide. NOAA Tech. Memo. Tech. rep., ERL ARL-230, NOAA Air Resources Laboratory, Silver Spring, MD.

Draxler, R. R. and G. D. Hess, 1997: Description of the HYSPLIT_4 Modeling System. NOAA Tech. Memo. Tech. rep., ERL ARL-224, NOAA Air Resources Laboratory, 24 pp., Silver Spring, MD.

Draxler, R. R. and G. D. Hess, 1998: An Overview of the HYSPLIT_4 Modeling System of Trajectories, Dispersion, and Deposition. *Aust. Meteor. Mag.*, **47**, 295–308.

Draxler, R. R. and G. D. Rolph, 2015: HYSPLIT (HYbrid Single-Particle Lagrangian Integrated Trajectory) Model Access via NOAA ARL READY Website (http://ready.arl.noaa.gov/HYSPLIT.php). NOAA Air Resources Laboratory, Silver Spring, MD.

Eliassen, A., 1962: On the Vertical Circulation in Frontal Zones. *Geophys. Publ.*, **24**, 147–160.

Gherzi, E., 1951: The Meteorology of China, Servico Meteorologico 1951. Tech. rep., 28 pp.

Griffin, K. S. and J. E. Martin, 2016: Synoptic Features Associated with Temporally Coherent Modes of Variability of the North Pacific Jet Stream. *J. Climate*, **29**, (submitted).

Halley, E., 1686: An Historical Account of the Trade Winds, and Monsoons, Observable in the Seas between and Near the Tropicks, with an Attempt to Assign the Phisical Cause of the Said Winds. *Philosophical Transactions*, **16**, 153–168.

Haude, W., 1930: Die Ausbreitung and Auswirkung von Kaltewellen in den zentralen Wuslengebieten Asiens im Winterhalbjahr, Bericht uber die Tatigkeit des Preuss. Tech. rep., Meteor Institutes, Berlin.

Heywood, G. S. P., 1957: Surface Pressure-Patterns and Weather Around the Year in Hong Kong. Tech. rep., R.O.T.M., 29 pp.

Hoskins, B. J. and P. Berrisford, 1988: A Potential Vorticity Perspective of the Storm of 15-16 October 1987. *Weather*, **43**, 122–129.

Hsu, Y. C. and S. D. Wang, 1958: A Discussion of Forecasting a Polar Outbreak, Meteorological Bulletin. Tech. rep., Weather Forecasting and Research Centre, Taiwan, 6–14 pp.

IPCC, 2013: Climate Change 2013: The Physical Science Basis. *Contribution of Working Group I to the Fifth Assessment Report of the Intergovernmental Panel on Climate Change*, T. Stocker, D. Qin, G.-K. Plattner, M. Tignor, S. Allen, J. Boschung, A. Nauels, Y. Xia, V. Bex, and P. Midgley, Eds., Cambridge University Press, Cambridge, United Kingdom and New York, NY, USA, 1535 pp.

Jaffe, S. C., J. E. Martin, D. J. Vimont, and D. J. Lorenz, 2011: A Synoptic-Climatology of Episodic, Sub-Seasonal Retractions of the Pacific Jet. *J. Climate*, **24**, 2846–2860.

Jhun, J. G. and E. J. Lee, 2004: A New East Asian Winter Monsoon Index and associated Characteristics of the Winter Monsoon. *J. Climate*, **17**, 711–726.

Kalnay, E., et al., 1996: The NCEP/NCAR 40-Year Reanalysis Project. *Bull. Amer. Meteor. Soc.*, **77**, 437–471.

Keyser, D. and M. J. Pecnick, 1985: A Two-Dimensional Primitive Equation Model of Frontogenesis forced by Confluence and Horizontal Shear. *J. Atmos. Sci.*, **42**, 1259–1282.

Keyser, D. and M. A. Shapiro, 1986: A Review of the Structure and Dynamics of Upper-Level Frontal Zones. *Mon. Wea. Rev.*, **114**, 452–499.

Koetswaram, P., 1953: An Analysis of the High Tropospheric Wind Circulation over India in Winter. *Indian J. Meteor. Geophys.*, **4**, 13–21.

Koetswaram, P. and S. Parthasarathy, 1954: The Mean Jet Stream over India in the Pre-Monsoon and Post-Monsoon Seasons and Vertical Motions associated with Subtropical Jet Streams. *Indian J. Meteor. Geophys.*, **5**, 138–156.

Koo, C. C., C. Yung-San, and S. Yu-Fung, 1958: Frontal θ_{se} Chart and its Application to the Analysis of Upper Boundary of Cold-Wave Front in China. *Acta Met. Sinica*, **29**.

Krishnamurti, T. N., 1961: On the Role of the Subtropical Jet Stream of Winter in the Atmospheric General Circulation. *J. Meteor*, **18**, 657–670.

Lee, Y.-Y., G.-H. Lim, and J.-S. Kug, 2010: Influence of the East Asian Winter Monsoon on the Storm Track Activity over the North Pacific. *J. Geophys. Res.*, **115**, D09 102.

Loewe, F. and V. Radok, 1950a: A Meridional Aerological Cross Section in the Southwest Pacific. *J. Meteor*, **7**, 58–65.

Loewe, F. and V. Radok, 1950b: Some Amendments to "A Meridional Aerological Cross-Section in the Southwest Pacific. *J. Meteor*, **7**, 305–306.

Lorenz, D. J. and E. T. DeWeaver, 2007: Tropopause Height and Zonal Wind Response to Global Warming in the IPCC Scenario Integrations. *J. Geophys. Res.*, **112**, D10 119, doi: 10.1029/2006JD008087.

Lu, A., 1930: On the Movements of the Cold and Warm Air Masses and the Shifting of the Line-Squall in June 1938. *Philosophical Transactions*, **11**.

Lu, A., 1954: The Cold Waves of China. *Collected Scientific Papers, Meteorology 1919-1949*, C.-W. Tu and A. Lu, Eds., Academia Sinica, Peking, 137–161.

Martin, J. E., 2014: Quasi-Geostrophic Diagnosis of the Influence of Vorticity Advection on the Development of Upper Level Jet-Front Systems. *Q. J. R. Meteorol. Soc.*, **140**, 2658–2671.

Mohri, K., 1953: On the Fields of Wind and Temperature over Japan and Adjacent Waters during Winter of 1950–1951. *Tellus*, **5**, 340–358.

Morrice, A. M., 1973: Quantitative Forecasting of the Winter Monsoon in Hong Kong. Tech. rep., Tech. Note No. 35, Royal Observatory Hong Kong, 41 pp.

Newton, C. W., 1954: Frontogenesis and Frontolysis as a Three-Dimensional Process. *J. Meteor.*, **11**, 449–461.

Otkin, J. A. and J. E. Martin, 2004: The Large-Scale Modulation of Subtropical Cyclogenesis in the Central and Eastern Pacific Ocean. *Mon. Wea. Rev.*, **132**, 1813–1828.

Palmén, E. and C. W. Newton, 1969: *Atmospheric Circulation Systems: Their Structure and Physical Interpretation.* Academic Press, 603 pp.

Reiter, E. R., 1961: *Meteorologie der Strahlströme (Meteorology of the Jet Streams)*. Springer-Verlag, Vienna, 473 pp.

Reiter, E. R., 1963: *Jet Stream Meteorology*. University of Chicago Press, 515 pp.

Reiter, E. R. and L. F. Whitney, 1969: Interaction between Subtropical and Polar-Front Jet Stream. *Mon. Wea. Rev.*, **97**, 432–438.

Riehl, H., 1962: Jet Streams of the Atmosphere. Tech. rep., Dept. of Atmospheric Science, Colorado State University Tech. Rep. 32, 117 pp., Fort Collins, Colorado.

Rolph, G. D., 2015: Real-time Environmental Applications and Display sYstem (READY) Website (http://ready.arl.noaa.gov). NOAA Air Resources Laboratory, Silver Spring, MD.

Rowe, S. M. and M. H. Hitchman, 2015: On the Role of Inertial Instability in Stratosphere-Troposphere Exchange near Midlatitude Cyclones. *J. Atmos. Sci.*, **72**, 2131–2151.

Rowe, S. M. and M. H. Hitchman, 2016: On the Relationship between Inertial Instability, Poleward Momentum Surges and Jet Intensifications near Midlatitude Cyclones. *J. Atmos. Sci.*, (in press).

Sawyer, J. S., 1956: The Vertical Circulation at Meteorological Fronts and its Relation to Frontogenesis. *Proc. R. Soc. London*, **234A**, 346–362.

Shapiro, M. A., 1982: Mesoscale Weather Systems of the Central United States. Tech. rep., CIRES Univ. of Colorado/NOAA: Boulder, CO, 78 pp.

Shapiro, M. A., T. Hampel, and A. J. Krueger, 1987: The Arctic Tropopause Fold. *Mon. Wea. Rev.*, **115**, 444–454.

Shapiro, M. A. and D. Keyser, 1990: Fronts, Jet Streams, and the Tropopause. *Extratropical Cyclones: The Erik Palmn Memorial Volume*, C. Newton and E. O. Holopainen, Eds., Amer. Meteor. Soc., 167–191.

Shoji, T., Y. Kanno, T. Iwasaki, and K. Takaya, 2014: An Isentropic Analysis of the Temporal Evolution of East Asian Cold Air Outbreaks. *J. Climate*, **27**, 9337–9348.

Sutcliffe, R. C. and J. K. Bannon, 1954: Seasonal Changes in the Upper-Air Conditions in the Mediterranean Middle East Area. *Scientific Proceedings of the International Association of Meteorology*, Rome, Italy, Int. Union of Geodesy and Geophysics, 322–334.

Takaya, K. and H. Nakamura, 2013: Interannual Variability of the East Asian Winter Monsoon and Related Modulations of the Planetary Waves. *J. Climate*, **26**, 9445–9461.

Trenberth, K. E., 1998: Atmospheric Moisture Residence Times and Cycling: Implications for Rainfall Rates with Climate Change. *Climatic Change*, **39**, 667–694.

Trenberth, K. E., 1999: Conceptual Framework for Changes of Extremes of the Hydrological Cycle with Climate Change. *Climatic Change*, **42**, 327–339.

Wang, L. and W. Chen, 2010: How Well do Existing Indices Measure the Strength of the East Asian Winter Monsoon? *Adv. Atmos. Sci.*, **27**, 855–870.

Wang, L. and W. Chen, 2014: An Intensity Index for the East Asian winter monsoon. *J. Climate*, **27**, 2361–2374.

Wang, L., W. Chen, W. Zhou, and R. Huang, 2009: Interannual Variations of East Asian Trough Axis at 500 hPa and its Association with the East Asian Winter Monsoon Pathway. *J. Climate*, **22**, 600–614.

Watterson, I. G., 2006: The Intensity of Precipitation during Extratropical Cyclones in Global Warming Simulations: A Link to Cyclone Intensity? *Tellus*, **58A**, 82–97.

Winters, A. C. and J. E. Martin, 2014: The Role of a Polar/Subtropical Jet Superposition in the May 2010 Nashville Flood. *Wea. Forecasting*, **29**, 954–974.

Winters, A. C. and J. E. Martin, 2016: Synoptic and Mesoscale Processes Supporting Vertical Superposition of the Polar and Subtropical Jets in Two Contrasting Cases. *Quart. J. Roy. Meteor. Soc.*, **142**, 1133–1149.

Wu, M. C. and J. C. L. Chan, 1995: Surface Features of Winter Monsoon Surges over South China. *Mon. Wea. Rev.*, **123**, 662–680.

Wu, M. C. and J. C. L. Chan, 1997: Upper-level Features associated with Winter Monsoon Surges over South China. *Mon. Wea. Rev.*, **125**, 317–340.

Yang, S., K. M. Lau, and K. M. Kim, 2002: Variations of the East Asian Jet Stream and Asian–Pacific–American Winter Climate Anomalies. *J. Climate*, **15**, 306–325.

Yeh, T. C., 1950: The Circulation of the High Troposphere over China in the Winter of 1945-46. *Tellus*, **2**, 173–183.

Yen, M.-C. and T.-C. Chen, 2002: A Revisit of the Tropical-Midlatitude Interaction in East Asia caused by Cold Surges. *J. Meteor. Soc. Japan*, **80**, 1115–1128.

Yin, J. H., 2005: A Consistent Poleward Shift of the Storm Tracks in Simulations of 21st Century Climate. *Geophys. Res. Lett.*, **32**, L18 701, doi:10.1029/2005GL023684.